

HYDROTHERMAL PROCESSES AT MOUNT RANIER
WASHINGTON

DAVID FRANK

1985

10
B-57
IV
3/2/75

Hydrothermal Processes at Mount Rainier
Washington

by

DAVID GERARD FRANK

A dissertation submitted in partial fulfillment
of the requirements for the degree of

Doctor of Philosophy

University of Washington

1985

Approved by ___

—

—

—

Program Authorized
to Offer Degree _____

Date _____

In presenting this dissertation in partial fulfillment of the requirements for the Doctoral degree at the University of Washington, I agree that the Library shall make its copies freely available for inspection. I further agree that extensive copying of this dissertation is allowable only for scholarly purposes, consistent with "fair use" as prescribed in the U.S. Copyright Law. Requests for copying or reproduction of this dissertation may be referred to University Microfilms, 300 North Zeeb Road, Ann Arbor, Michigan 48106, to whom the author has granted "the right to reproduce and sell (a) copies of the manuscript in microform and/or (b) printed copies of the manuscript made from microform."

Signature_

Date _____

UNIVERSITY OF WASHINGTON

Date: May 28, 1985

We have carefully read the dissertation entitled Hydrothermal Processes at Mount Rainier, Washington

David Gerard Frank submitted by
in partial fulfillment of
the requirements of the degree of Doctor of Philosophy
and recommend its acceptance. In support of this recommendation we present the following joint statement of evaluation to be filed with the dissertation.

This dissertation provides a detailed study of the hydrothermal system presently active within the Mount Rainier volcanic cone. It also documents the extent of such hydrothermal activity over the past 5,000 years. The importance of this work is threefold. Firstly, this study documents that the source of heat that drives hydrothermal circulation within the volcano cannot be accounted for by simple cooling of recently erupted materials. Secondly, this dissertation presents field evidence and geochemical modelling which suggests that an acid sulfate-chloride fluid is responsible for hydrothermal alteration in the interior of the cone. This is important, in that such fluids are thought to be involved in the formation of porphyry-copper ore deposits which are often associated with dissected andesitic volcanoes. Thirdly, this dissertation provides considerable insight into the volcanic hazards present at Mount Rainier and their relationship to the hydrothermal activity.

The dissertation is well organized, carefully thought out, and clearly written. We anticipate its publication will make a significant contribution to the geochemical literature.

DISSERTATION READING COMMITTEE:

University of Washington

Abstract

HYDROTHERMAL PROCESSES AT MOUNT RAINIER
WASHINGTON

by David Gerard Frank

Chairperson of Supervisory Committee:
Assistant Professor Mark S. Ghiorso
Department of Geological Sciences

Field studies and thermal-infrared mapping at Mount Rainier indicate areas of active hydrothermal alteration where excess surface heat flux is about 9 megawatts. Three representative settings include:

1. An extensive area (greater than 12,000 m²) of heated ground and slightly acidic boiling-point fumaroles at 76-82°C at East and West Craters on the volcano's summit, where alteration products include smectite, halloysite and disordered kaolinite, cristobalite, tridymite, opal, alunite, gibbsite, and calcite;
2. A small area (less than 500 m²) of heated ground and sub-boiling-point fumaroles at 55-60°C on the upper flank at Disappointment Cleaver, and other probably similar areas at Willis Wall, Sunset Amphitheater, and the South Tahoma and Kautz headwalls;

3. Sulfate and carbon dioxide enriched thermal springs at 9-24⁰C on the lower flank of the volcano in valley walls beside the Winthrop and Paradise Glaciers, where calcite, opal-A, and gypsum are being deposited.

In addition, chloride- and carbon dioxide-enriched thermal springs issue from thin sediments that overlie Tertiary rocks at, or somewhat beyond, the base of the volcanic edifice in valley bottoms of the Nisqually and Ohanapecosh Rivers where maximum spring temperatures are 19-25⁰C and 38-50⁰C respectively and where extensive travertine deposits have developed.

The heat flow, distribution of thermal activity, and nature of alteration products indicate that a narrow, central hydrothermal system exists within Mount Rainier forming steam-heated snowmelt at the summit craters and localized leakage of steam-heated fluids within 2 kilometers of the summit. The lateral extent of the hydrothermal system is limited in that only sparse, neutral sulfate-enriched thermal water issues from the lower flank of the cone. Simulations of geochemical mass transfer suggest that the thermal springs may be derived from an acid sulfate-chloride parent fluid which has been neutralized by reaction with andesite and highly diluted with shallow ground water.

Present heat flow from Mount Rainier is substantial relative to other Cascade Range volcanoes and does not appear to have diminished since at least the late 19th century. Evidence of older hydrothermal processes found in Holocene lithic tephra and debris avalanches record activity more extensive but similar in chemical composition to that of today.

TABLE OF CONTENTS

	Page
List of Figures.....	iv
List of Tables.....	vi
List of Plates.....	viii
List of Symbols.....	ix
Introduction.....	1
Chapter 1: Geologic setting.....	4
Chapter 2: Thermal activity.....	11
Summit area.....	13
Historical observations.....	13
1981-1983 observations and inferred crater structure.....	21
Heat flow.....	33
Upper flank.....	48
Disappointment Cleaver.....	53
Other headwall thermal areas.....	59
Structural implications.....	60
Lower flank.....	66
Winthrop Springs.....	66
Paradise Springs.....	70
Adjacent to cone.....	74
Longmire Springs.....	74
Ohanapecosh Springs.....	78
Chapter 3: Gas and spring compositions.....	82

Major constituents.....	82
Summit fumaroles.....	82
Flank fumaroles.....	88
Thermal springs.....	90
Stable isotopes.....	103
Rock-water interaction and evaporation.....	103
Recharge altitude.....	105
Summit fumarole condensate.....	113
Chapter 4: Alteration mineralogy.....	115
Analytical methods.....	115
Surficial alteration.....	116
Fumarolic areas.....	116
Thermal springs.....	124
Subsurface alteration.....	126
Discussion of secondary mineral assemblages.....	140
Variation in character and extent of alteration...140	
Mineralogic constraints on hydrothermal system...143	
Chapter 5: Conceptual hydrothermal model.....	146
Significance of thermal springs.....	147
Cooling process.....	148
Possible parent fluid.....	152
Reaction-path simulation.....	160
Flow path.....	173
General discussion.....	175
Hazard implications.....	178
Bibliography.....	182

LIST OF FIGURES

	Page
1. Map of regional tectonic setting.....	5
2. Map of thermal areas.....	14
3. Diagrams of thermal-infrared anomaly patterns for the summit fumarole field.....	20
4. Map of 1981 thermal pattern at summit.....	23
5. Profiles of temperature-probe traverses across the summit-crater rims	
A. East Crater.....	27
B. West Crater.....	28
6. Isothermal contour map of summit craters.....	37
7. Map of thermal areas on the upper flank.....	49
8. Diagram of temperature record from Disappointment Cleverer.....	58
9. Cross-sections through upper-flank thermal areas and summit fumarole field.....	65
10. Map of localities for fumarole and firn samples.....	84
11. Diagram of the concentrations of dissolved constituents in the thermal springs.....	96
12. Trilinear diagram of percentage equivalents of major ions in thermal springs.....	97
13. Diagram showing variation of chloride and specific conductance with temperature	
A. Chloride.....	99
B. Specific conductance.....	100
14. Diagram of stable-isotope composition.....	106
15. Diagram of variation in stable-isotope composition with altitude.....	110

16. XRD diagram of secondary minerals at the summit-crater fumarole field	
A. Halloysite-alunite sample.....	120
B. Kaolinite-gibbsite sample.....	121
17. Map showing extent of selected Holocene deposits and sample points.....	135
18. XRD diagram of clay-rich Holocene deposits.....	136
19. Diagram showing distribution of Holocene deposits...	141
20. Diagram of deuterium-enthalpy mixing relations for Paradise and Winthrop springs.....	150
21. Diagram of conductivity, temperature, and concentration in unmixed end members.....	151
22. Trilinear diagram of percentage equivalents of major ions in thermal springs and in simulated waters.....	155
23. Diagram of selected characteristics of chloride-charged acid sulfate water at Sherman Crater, Mount Baker.....	157
24. Diagram of modal mineral and fluid composition during mass-transfer simulation.....	163
25. Activity diagram of mass-transfer simulation in K ₂ O-MgO-Al ₂ O ₃ -H ₂ O system.....	164
26. Activity diagram of mass-transfer simulation in Al ₂ O ₃ -MgO-SiO ₂ -H ₂ O system.....	165
27. Diagram of simplified conceptual model of flow paths that feed flank thermal areas.....	174

LIST OF TABLES

	Page
1. Eruption and large mass-movement events at Mount Rainier.....	8
2. Aerial thermal-infrared surveys at Mount Rainier.....	12
3. Temperature calibration for 1972 thermal-infrared survey.....	36
4. Excess radiant flux from the summit thermal area.....	40
5. Excess evaporative and sensible flux from the summit thermal area.....	42
6. Components of excess heat flow.....	46
7. Comparative energy yield of Mount Rainier with other Cascade-Range volcanoes.....	47
8. Thermal areas on upper flank of Mount Rainier.....	50
9. Physical measurements at Winthrop springs.....	69
10. Physical measurements at Paradise springs.....	73
11. Selected physical measurements at Longmire Springs...	77
12. Selected physical measurements at Ohanapecosh Springs.....	80
13. Gas samples from Mount Rainier, 1981-1983.....	83
14. Composition of two fumaroles in East Crater.....	86
15. Helium concentrations in fumaroles at Mount Rainier..	87
16. Composition of thermal springs at Mount Rainier during 1982-1983	
A. Winthrop Springs.....	91
B. Paradise Springs.....	91
C. Longmire Springs.....	92
D. Ohanapecosh Springs.....	92

17. Methods of water analysis.....	94
18. A variety of computed aquifer temperatures based on aqueous geothermometers.....	102
19. Stable isotope composition of springs, snow, and firn.....	107
20. Secondary minerals at fumarolic areas.....	118
21. Secondary minerals at thermal springs.....	125
22. Holocene tephra and large mass movement deposits examined in this study.....	127
23. Secondary minerals in Holocene deposits.....	132-134
24. Composition of unmixed end members at Paradise and Winthrop springs.....	152
25. Localities of acid sulfate-chloride waters shown in figure 31.....	156
26. Fluid compositions for mass-transfer simulation.....	159

LIST OF PLATES

	Page
I. Aerial photograph of summit craters.....	15
II. Aerial infrared image of the summit thermal area...	22
III. Photograph of Mossy fumarole at West Crater.....	25
IV. Photograph of East Crater rim.....	29
V. Photograph of crevasse near subglacial lake at West Crater.....	32
VI. Aerial photograph of Disappointment Cleaver.....	54
VII. Aerial infrared image of Disappointment Cleaver....	55
VIII. Photograph of Disappointment Cleaver thermal area..	57
IX. Aerial photograph of Sunset Amphitheater.....	61
X. Aerial infrared image of Sunset Amphitheater.....	62
XI. Close-up aerial photograph of Sunset Amphitheater..	63
XII. Photograph of main spring, WS1, near Winthrop Glacier.....	68
XIII. Photograph of main spring, PS5, near Paradise Glacier.....	72

LIST OF SYMBOLS

A	area
Å	angstrom
BP	before the present (expressed in years)
°C	degrees Celsius
cm	centimeter
D_w	coefficient of water-vapor diffusion
e_a	atmospheric water-vapor pressure
e_s	saturated atmospheric water-vapor pressure
f	relative humidity
ft	foot
g	gram
H	enthalpy
\bar{H}_v	enthalpy of saturated water vapor
IS	ionic strength
J	joule
K	kelvin
k	von Karman constant, 0.36
kg	kilogram
km	kilometer
L	liter
M	local earthquake magnitude approximated by coda length
m	meter
mbar	millibar
meq	milliequivalent
mg	milligram
mm	millimeter
mol	mole
MW	megawatt
nd	not determined
P_a	air pressure
ppm	parts per million
Q	water discharge
Q_v	vapor discharge
R	isotopic ratio, $^{18}\text{O}/^{16}\text{O}$ or D/H
s	second
T	ground surface temperature
T_a	air temperature
T_c	cold-spring temperature

T_Hunmixed, hot end-member water temperature
 T_0cold reference temperature of
 non-geothermally heated ground
 T_Ssaturated air temperature
 T_Tthermal-spring temperature
 uwind speed
 vvapor discharge
 Wwatts
 ΔWexcess radiant exitance
 W/Rwater/rock ratio
 Xmixing fraction of cold water in thermal spring
 zheight above ground surface
 z_0roughness height of ground surface
 ZImass-transfer reaction progress

 βBowen Ratio of sensible to evaporative flux,
 H/LE
 ΔAexcess advective heat flux
 ΔGexcess heat flow
 ΔHexcess heat flux from eddy diffusion and molecular
 conduction
 $\Delta H_{\underline{}}$enthalpy of thermal water less nearby cold
 groundwater
 ΔLEexcess evaporative flux
 ΔRexcess radiant exitance
 $\delta^{18}O$oxygen isotope composition, in parts per mil
 δDhydrogen isotope composition in parts per mil
 ϵemissivity of ground surface
 2θin X-ray diffractometry, the angle between the
 incident and the diffracted beam
 μmmicrometer
 μSmicrosiemen
 ρdensity
 ρ_aair density
 σStefan-Boltzmann constant, $5.67 \times 10^{-8} \text{ Wm}^{-2}\text{K}^{-4}$

 $\%$percent
 ‰parts per mil; parts per thousand

ACKNOWLEDGEMENTS

I thank the members of my Supervisory Committee, Professors J.A. Vance, C.R.B. Lister, and F.C. Ugolini, for their guidance in this project. I especially benefitted from the undaunted energy and optimism of the Chairperson of my Committee, Professor Mark S. Ghiorso. Many of the aerial photographs which enabled efficient planning of fieldwork and which so clearly showed structural features in poorly accessible parts of the volcano were taken by A. Post and R.M. Krimmel. J.D. Friedman and H.H. Kieffer kindly provided thermal-infrared images, allowing a synoptic and quantitative view of the distribution of thermal activity. Fumarole-gas analyses and sampling equipment were provided by T.J. Casadevall and I. Friedman. I greatly appreciate the field companionship and efforts of L. Borrie-Bakewell, A.S. Eash, C. Fabiani, B.S. Frank, W. Frank, M.S. Ghiorso, S.M. Hodge, A. Horstman, P. H. Mills, L. Muir, F. Pessl, S.A. Safioles, and M.A. Spiers. Numerous rangers with the National Park Service provided assistance in working within Mount Rainier National Park. Access to private land was given by the St. Regis Paper Company. Financial support for this project was received from the Geothermal Program and the Water Resources Division of the U.S. Geological Survey.

DEDICATION

This dissertation is dedicated to Austin Post who introduced the author to the summit fumarole field at Mount Rainier and to other volcanic delights in the Cascade Range.

INTRODUCTION

Mount Rainier, Washington, like many of the other large stratovolcanoes in the Cascade Range, contains a presently active hydrothermal system that produces a distinctive set of mineralogical alteration products from primary volcanic rocks. Concurrently, the hydrothermal system overlays a chemical imprint on the composition of circulating ground water. Surface leakage of these fluids produces thermal activity in the form of fumaroles and heated ground on the volcano's upper slopes, and thermal springs at lower elevations.

Hydrothermal processes may aid in evaluation of hazards associated with a volcano. For example the history and extent of hydrothermal activity provide clues about pathways for fluid transport to the surface, and about the longevity and intensity of the heat source for the hydrothermal system. Permeable areas of hydrothermal leakage in turn indicate likely localities for early recognition of future increases in thermal activity that could precede or accompany magmatic intrusion into the cone. Furthermore,

some types of hydrothermal activity, particularly that of an acid-sulfate nature, degrade the structural stability of volcanic rock. Hence knowledge of hydrothermal pathways may allow evaluation of potential source regions for hazardous structural failures in the form of rapid mass movement such as debris avalanches.

This study of hydrothermal processes at Mount Rainier was undertaken both to determine the nature of the present hydrothermal system as well as to evaluate the corresponding implications for volcanic hazards. Ideally drillhole data provide the best basis for placing surficial processes into perspective relative to the main part of the hydrothermal system. However in many areas, particularly at stratovolcanoes or in places not intended for industrial development such as national parks, alternative approaches are needed because acquisition of drillhole data is impractical. Such restrictions apply to Mount Rainier. An alternative approach developed in this study is to combine information from surficial thermal activity with subsurface data from deposits that originated at depth in a hydrothermal system. Appropriate deposits are those which, following subsurface alteration, were subsequently transported to more accessible locations at the land surface. Examples are debris avalanches and lithic tephras that are laden with hydrothermal minerals.

The first four chapters of the dissertation present a description of the physical characteristics of present-day hydrothermal activity, the composition of fluids, and the mineralogy of past and present alteration products. Chapter Five discusses a theoretical analysis of possible physical and chemical reaction paths between minerals and heated fluids, and addresses implications concerning volcanic processes and hazards.

Chapter 1

GEOLOGIC SETTING

Mount Rainier is the largest North American stratovolcano, south of Alaska, that contains an active hydrothermal system. The present cone rises from about 1000 m up to 4392 m above sea level; it is situated just west of the crest of the Cascade Range (fig. 1), a volcanic arc that stretches from northern California to southern British Columbia. The volcano occurs in a region of North-South compression (Crosson, 1972; Crosson and Frank, 1975). The compression is consistent with a model of active subduction resulting from oblique convergence 300 km seaward between the Juan de Fuca and America Plates (Riddihough and Hyndman, 1976; Riddihough, 1977).

Geologic studies by Coombs (1936) and Fiske and others (1963) show that Mount Rainier is built upon a 5000-m-thick pile of volcanic flows and detritus that accumulated since the Early Oligocene through much of Tertiary time. The volcanic rocks range from basalt to rhyolite, with andesite predominant. These Tertiary volcanics were intruded, mainly

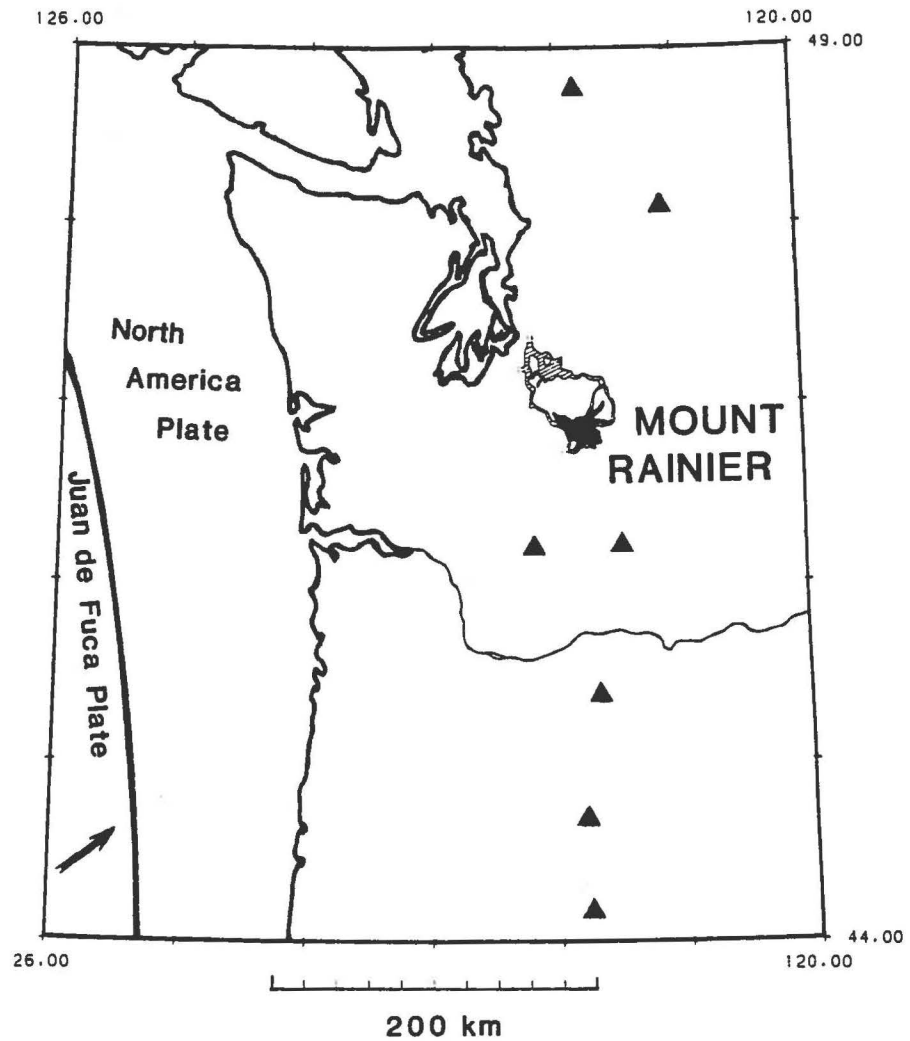


Figure 1. Regional tectonic setting of Mount Rainier. Mount Rainier lies just west of the Cascade Range and 300 km inland from a zone of oblique convergence (arrow) between the Juan de Fuca Plate and North America Plate. Solid - areal extent of Mount Rainier lava; hatched - extent of Holocene lahars; cones - other Quaternary stratovolcanoes.

during the Miocene, by numerous dykes and sills and a major plutonic complex of primarily granodiorite (Mattinson, 1977).

Early Pleistocene volcanic sediments of hornblende-hypersthene andesite (Lily Creek Formation) west of Mount Rainier may represent the earliest eruptions from a Rainier vent that has since been buried (Crandell, 1963, p. A21-22; Mattinson, 1977, p. 1512). The oldest unequivocal flows from Mount Rainier are hypersthene-augite andesite with normal magnetic orientation. The amount of erosion in the oldest Rainier flows suggests that they are no younger than early Pleistocene (Fiske and others, 1963, p. 82), and normal magnetism indicates an age no older than 700,000 years. Thus Mount Rainier probably began its development somewhat less than 700,000 years ago.

The bulk of Mount Rainier is built of lava flows and brecciated lava flows, with lesser amounts of interlayered tephra and other pyroclastic deposits. These products vary little in composition, consisting mainly of hypersthene-augite andesite. However two small satellitic vents which produced olivine andesite occur on the north flank (Fiske and others, 1963, p. 75-79).

Mount Rainier has been one of the more active Cascade volcanoes during Holocene time. Evidence of 11 eruptions

can be found in Holocene tephra deposits (Mullineaux, 1974). Lava flows, brecciated flows, and explosion rubble that form a young summit cone at least 400 m thick are no more than 2200 years old (Crandell, 1971, p. 11). Table 1, based on the work of Crandell (1971) and Mullineaux (1974) indicates that during the last 10,000 years major eruptive episodes occurred between 6500 and 4000 years ago and again between 2500 and 2000 years ago. Lesser eruptions also occurred, the most recent of which was during the early to middle 19th century (Mullineaux and others, 1969).

In addition to eruptive deposits, at least 55 large Holocene mass-movement deposits from Mount Rainier (fig. 1), including debris avalanches and mudflows as large as $2 \times 10^9 \text{ m}^3$, have been identified by Crandell (1971). Many of these apparently accompanied eruptions and may have been triggered by eruptions. However, some of the larger mass-movement deposits represent events that occurred during time periods for which no eruptive deposits have been recognized (Crandell, 1971, p. 57). These events may have resulted from non-eruptive phenomena such as hydrothermal explosions, earthquakes, or oversteepening from long-term erosive processes. The most recent episode of large avalanches occurred in December 1963 when $11 \times 10^6 \text{ m}^3$ of rock debris fell from Little Tahoma Peak onto the lower Emmons Glacier (Crandell and Fahnestock, 1965). Smaller debris avalanches

Table 1. Holocene eruption and large mass-movement events at Mount Rainier. Data are from Mullineaux (1974) and Crandell (1971). BP-before present. Age-dates are from tree-rings or are in radiocarbon years and are not corrected for variations in atmospheric CO₂. *-contains hydrothermal alteration products.

ERUPTIVE DEPOSIT	APPROXIMATE AGE	ESTIMATED VOLUME, 10^6 m^3	MASS-MOVEMENT DEPOSIT	APPROXIMATE AGE	MINIMUM DISTANCE TRAVELED, km	ESTIMATED VOLUME, 10^6 m^3	DRAINAGE BASIN
Layer X, pumice tephra	AD 1820-1854	1	Lahar	AD 1967	5		South Tahoma
			Avalanches	AD 1963	7	11	Emmons
			Lahars	AD 1947	11		Kautz
Layer C, pumice, scoria, lithic tephra	2200 BP	300	4 Lahars	AD 1932-1955	--		Nisqually
Summit cone lava	1000-2200 BP	1200	Avalanche*	AD 1910-1930	7		South Puyallup
Block and ash flow	2400 BP	--	Lahar	<450 BP	29		West Fork White
			2 Lahars	<450 BP	8		Nisqually
			2 Lahars	<450 BP	5		Kautz
Layer B, scoria, lithic tephra	4500 BP	5	Lahar*	440 BP	5		South Tahoma
Layer H, pumice, lithic tephra	4700 BP	1	2 Lahars*	<450 BP	--		South Puyallup
			2 Lahars	<450 BP	--		South Puyallup
Layer F, lithic, pumice, crystal tephra*	5000 BP	25	Lahar	<450 BP	3		South Mowich
Layer S, lithic tephra	5200 BP	20	Lahar	2200-3400	29		West Fork White
Layer N, lithic, pumice tephra	5500 BP	2	5 Lahars	450-2200 BP	6-24		White
Layer D, scoria lithic tephra	6000 BP	75	Lahar	450-3400 BP	5		Cowlitz
Layer L, pumice tephra	6400 BP	50	7 Lahars	800-3400	7-14		Nisqually
Layer A, pumice, lithic tephra	6500 BP	5	3 Lahars	450-3400	5		Kautz
Layer R, pumice, lithic tephra	>8750 BP	25	2 Lahars*	450-2600	3		South Tahoma
			Electron				Tahoma
			Mudflow	530 BP	50	150	Puyallup
			Lahar*	1000 BP	5-22		South Puyallup
			Lahar	2500 BP	5-22		South Puyallup
			2 Lahars	>400 BP	--		North Puyallup
			Lahar	450-3400 BP	5-11		South Mowich
			Lahar	450-3400 BP	9		Ohanapecosh
			Round Pass				Tahoma
			Mudflow	2600 BP	30	150	Puyallup
			2 Lahars	3400-5000 BP	17-29		West Fork White
			Lahar	3400-6600 BP	9		Ohanapecosh
			4 Lahars	3400-6600 BP	24-40		Nisqually
			Lahar	>3400 BP	6		Kautz
			Lahar	>3400 BP	--		South Puyallup
			Lahar	>3400 BP	11		South Mowich
			Lahar	3400-6600 BP	8		Carbon
			Osceola				West Fork White
			Mudflow*	5000 BP	110	2000	White
			5 Lahars	5000-6600 BP	4-14		White
			Greenwater				
			Lahar*	5000-6600 BP	45	600	White
			Paradise				
			Lahar*	5500-6600 BP	30	50-100	Nisqually
			Lahar	>6600 BP	2		Ohanapecosh
			Avalanche*	>5500 BP	7		Paradise
			Avalanche*	>6600 BP	6		Van Trump

up to about 50,000 m³ occur each winter from headwall areas around the mountain; whereas glacier-outburst floods (Richardson, 1968) occur every few years from some of the larger glaciers, most notably the South Tahoma and Nisqually Glaciers (for example, Hodge, 1972). A particularly large succession of outburst floods deposited about 40×10^6 m³ of rock debris below the Kautz Glacier in 1947 (Crandell, 1971, p. 46-48).

Moderately frequent microseismicity as well as sporadic larger earthquakes up to magnitude 4.8 have also occurred in recent years at Mount Rainier. Early studies using temporary seismometer arrays (Unger and Decker, 1970; Unger and Mills, 1972) revealed common low-frequency seismicity at the cone and suggested that these events were similar to Type-B volcanic earthquakes as classified by Minikami (1960). Later studies by Weaver and Malone (1976, 1979) show, however, that low-frequency events result from ice movement within the mountain's glacier cover. The portable arrays and two nearby permanent stations have also detected many high-frequency microearthquakes up to a magnitude of about 2. These are thought to have a tectonic origin (Weaver and Malone, 1976) although their source mechanisms are not well known.

A few larger earthquakes up to Intensity V have

occurred each decade at Mount Rainier since the 1890's (Rasmussen, 1967). The three most recent of these events (1969, magnitude 4.0; 1973, 3.9; and 1975, 4.8) have been interpreted as the result of regional North-South compression rather than of volcanic processes within the cone (Crosson and Frank, 1975; Crosson and Lin, 1975). No earthquakes greater than magnitude 3, however, have occurred at the volcano since 1977. Weaver and Smith (1983) consequently include Mount Rainier in a region of southwestern Washington that is currently undergoing unusual seismic quiescence at the greater-than-magnitude-3 level.

In summary, seismicity at a low to moderate level is apparently tectonic in origin and only equivocally, if at all, indicates the presence of volcanic processes underway within the cone. Less equivocal evidence of ongoing volcanic processes lies in hydrothermal activity and attendant alteration, the subject of the remainder of this dissertation.

Chapter 2

THERMAL ACTIVITY

Aerial thermal-infrared surveys and field investigations, combined with a search of historical reports of visual observations provide the basis for mapping active thermal areas at Mount Rainier. Moxham and others (1965; see also Moxham, 1970, 1972) first used infrared surveys to delineate the pattern of heat emission in the summit area during the middle and late 1960's. Continued thermal-infrared surveillance of Cascade Range volcanoes during the early 1970's (Friedman and others, 1973) indicated little variability in activity at the summit and detected previously unrecognized thermal activity at lower elevations. A 1981 aerial survey (Kieffer and others, 1982) completes a 17-year span of synoptic thermal data (table 2) - the longest record available for any Cascade Range volcano. Subsequent field investigations and ground-based infrared measurements, coupled with historical field observations, provide a data base to aid in calibration of airborne measurements.

Table 2. Aerial thermal-infrared surveys of Mount Rainier, made with imaging systems. Spectral band is 8-14 μm except where noted.

DATE	LOCAL TIME	SURVEYING AGENCY	INSTRUMENT	REF ¹
9/4/64	0630-0700	USFS-M ²	AAS/5 ³	5
9/4/66	0620	USGS	RECON IX	3
7/27/69	0645	USGS	RECON IX	4
7/15/70	1243	USMC	AAS/18	7
	1510-1515			
	2120-2156			
4/3/71	2018-2035	USFS-B	RECON XI	7
8/7/71	0314-0323	USFS-B	RECON XI	7
8/17/71	1600-1640	USMC	AAS/18	7
8/18/71	0435-0520	USMC	AAS/18	7
4/18/72	2127-2157	USFS-M	RS-7	1
11/15/72	0512-0549	NASA	RS-14	7
4/26/73	0255-0303	USFS-M	RS-7	1
4/29/73	0532-0556	USFS-M	RS-7	1
12/13/75	1850-1910	OANG	AAS/14A	6
7/21/81	0423-0519	EG&G	DS-1260	2

¹References: 1-Friedman and Frank (1974); 2-Kieffer and others (1981); 3-Moxham (1970); 4-Moxham (1972); 5-Moxham and others 1965; 6-C.A. Rosenfeld (unpub. comm.); 7-unpublished.

²USFS-M, U.S. Forest Service, Missoula; USFS-B, Boise; USGS, U.S. Geological Survey, Denver; USMC, U.S. Marine Corps; OANG-Oregon Army National Guard, Salem; NASA, National Aeronautics and Space Administration, Houston; EG&G Corp., Las Vegas, U.S. Dept. of Energy, U.S. Geological Survey.

³AAS/5, 4.5-5.5 μm , polaroid record; AAS/14A, film record; AAS/18, film record; RS-7, Texas Instruments, film record; RS-14, Texas Instruments, film and video record; Recon IX, HRB Singer, film record; Recon XI, HRB Singer, Polaroid record; DS-1260, Daedalus, 8-12 and 3-5 μm , film and digital record.

The complete record of data on thermal activity at Mount Rainier can be conveniently discussed with reference to four representative settings (fig. 2), three of which are on the cone:

1. The summit cone, above 4000 m altitude;
2. The upper flank, 3000-4000 m altitude;
3. The lower flank;
4. Adjacent to the base of the cone.

Summit Area

Historical Observations

Boiling-point fumaroles and adjacent heated ground cover an exposed area of 12,000 m² along the rims of two overlapping craters at the volcano's summit (plate I). Additional fumarolic activity occurs beneath the ice cover that fills the basins of both craters. Observations over more than 100 years suggest little change in this activity. The first recorded visit to the summit in about 1855 and many more from 1870 on through the late 19th century noted the presence of fumaroles, some with sulfurous odor, within

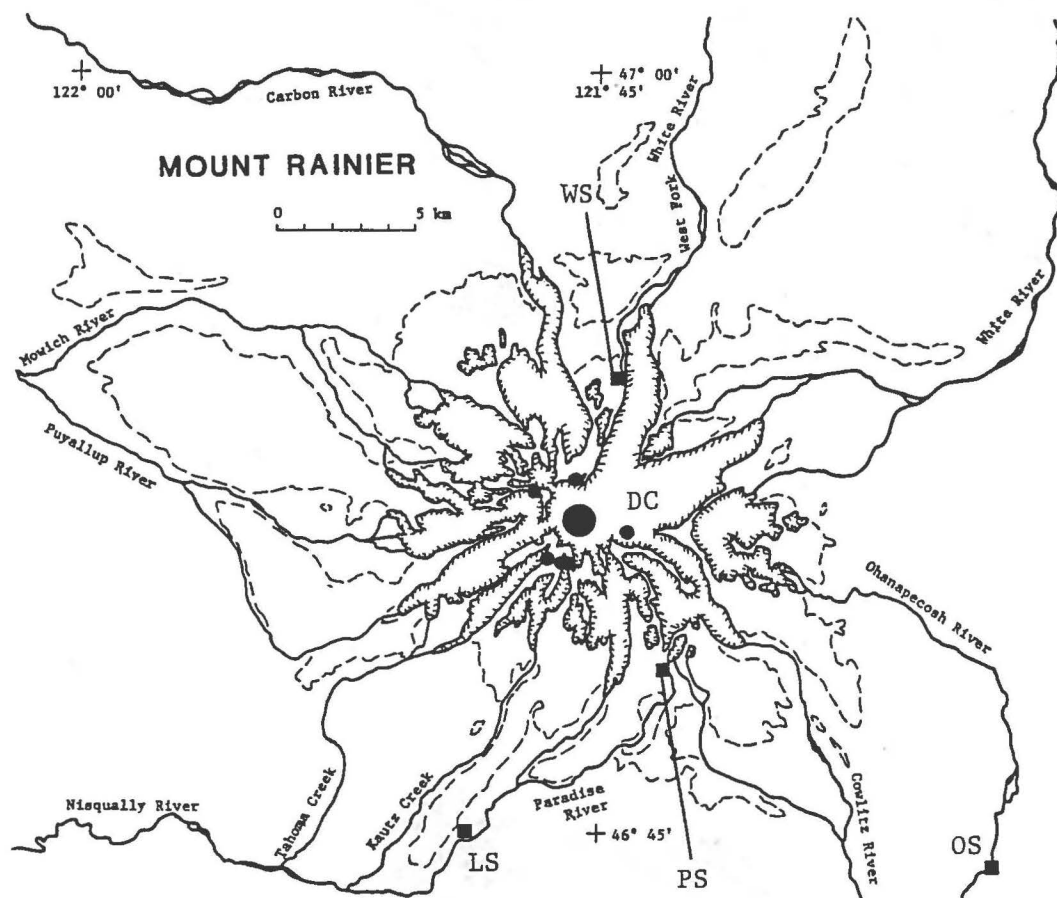


Figure 2. Localities of thermal activity at Mount Rainier. A large fumarole field occurs at the top of the young summit cone (large dot); fumaroles and heated ground occur at Disappointment Cleaver (DC) and, in some cases ephemerally, at 5 other similar but poorly accessible areas on the upper flank (small dots). Thermal springs (squares) occur on the lower flank of the volcano near Paradise (PS) and Winthrop (WS) Glaciers and beyond the volcanic edifice at Longmire (LS) and Ohanapecoh (OS). Dashed - present extent of Mount Rainier lava flows; hachured - glacier margins.



Plate I. View looking northeast at the summit fumarole field. Fumaroles and heated ground keep about 12,000 m² of the rims of East and West Craters free of snow during summer months. The craters span about 700 m. Aerial photograph 69R1-61 by Austin Post, USGS, August 22, 1969.

the crater rims (Molenaar, 1979, p. 33-49). The earliest report is that of the Indian guide, Saluskin, who maintained that two of his clients in 1855 observed a crater lake and steam vents (Haines, 1962, p. 17). Later, Stevens (1876) reported the occurrence of sulfurous fumes and steam vents along the north part of the West Crater rim in 1870. A veteran Rainier climber, E.S. Ingraham (1895, p. 21), noted that as late as 1894 abundant sulfurous vapor issued from the West Crater while the East Crater produced only steam that lacked sulfurous fume. Shortly thereafter, I.C. Russell (1898) and others of the U.S. Geological Survey described fumarolic activity in 1896 on the inner slope of the East Crater rim much as can be seen today. Coombs, (1936, p. 202-203) gave similar descriptions, and added that no traces of sulfur were detected in the steam emanations from the East Crater.

Saluskin's second-hand report of an exposed crater lake in the mid-19th century appears credible, since the most recent verifiable eruption, as represented by a sparse tephra deposit, occurred not more than a few decades earlier (1820-1840, Mullineaux and others, 1969). The heat released from the cooling products of that eruptive episode could have provided the energy to maintain a crater lake for a few years, however no exposed crater lake has been seen since. Later observers have long suspected the presence of a

subglacial lake based on audible splashing noises as rocks are rolled downslope through ice caves, for example in 1911 (Flett, 1912) and in 1954 (Molenaar, 1979, p. 186). As noted below, these suspicions were eventually confirmed.

In a detailed compilation of historical reports and newspaper accounts, Majors and McCollum (1981a, b) make a case for a tephra eruption in 1894 from the summit area based on observations of apparent smoke emission as seen by residents in the Puget Lowland in November and by a climbing party on the lower flank of the volcano in December. The descriptions, however, indicate only small amounts of "smoke" were seen; this and the small number of observers suggest that, more likely, increased fumarolic activity may have occurred in 1894, perhaps accompanied by ejecta entrained in the fumarole plumes. Close-range climbers' descriptions of fumaroles in subsequent years do not indicate any lasting change in fumarolic activity.

A number of more detailed field studies have been made over the last three decades. Field observations over a period of several weeks in 1959 as part of a human-endurance experiment called Project Crater (Molenaar, 1979, p. 179) provided the first repetitive set of temperature measurements. Reported values include maximum temperatures of 77⁰ C for West Crater fumaroles (Miller, 1970, p. 1).

Molenaar (1979, p. 176) made a suite of temperature measurements around both crater rims in August 1970 and found that both fumarole and near-surface ground temperatures (8-15 cm deep) ranged up to 72⁰ C. The following month, Moxham and others (1972) installed a temperature-monitoring platform with satellite telemetry on the northern part of the West Crater rim. The instrument operated for five weeks and provided the only continuous thermal measurements available for an extended period of time. Three probes in small fumaroles on the West Crater rim recorded maximum near-surface temperatures of 70-72⁰ C, accompanied by several decreases in temperature that were probably caused by meltwater entering the vents (Moxham and others, 1972, p. 197).

Further Project Crater efforts during 1969-1972 (Lokey and others, 1972; Lokey, 1973) led to increased exploration of the geothermally formed ice caves within the crater basins (Kiver and Mumma, 1971). Highlights of these studies were the production of a plane-table map of the crater rims and adjacent glacier surface (Lokey and others 1972), and the discovery of a cold subglacial lake in West Crater along with topographic evidence (a depression in the snow surface) for an additional subglacial lake in East Crater (Kiver and Steele, 1972).

Such ground studies yielded a number of spot thermal measurements at various localities near Mount Rainier's summit. The first synoptic display of heat emission in the crater area, however, is the result of a series of aerial infrared surveys in 1964, 1966, and 1969 by Moxham (1970, 1972). His results, coupled with the ground investigations of others, demonstrated that widespread fumarolic activity and heated ground not only lined the inner rims of the craters but also extended partway down the outer west slope of the West Crater. Furthermore, Moxham's (1970, 1972) data clearly showed that the highest level of infrared emission, as well as the greatest areal extent, occurred in the west and northwest parts of each crater rim.

Aerial infrared surveys (table 2) during 1970-1973 and most recently in 1981 show a thermal pattern for the crater area that is very similar (fig. 3) to earlier data acquired by Moxham (1972). Small variations in 1969, interpreted by Moxham (1972, p. 121) as real changes in geothermal emission, are more easily explained by simple seasonal variation in snow cover adjacent to the thermal areas. Much of the warmer ground is bridged over by snow in the winter and thus masked from infrared sensors.

For example, figure 3 allows comparison of surveys made during different seasons. The early spring survey of April

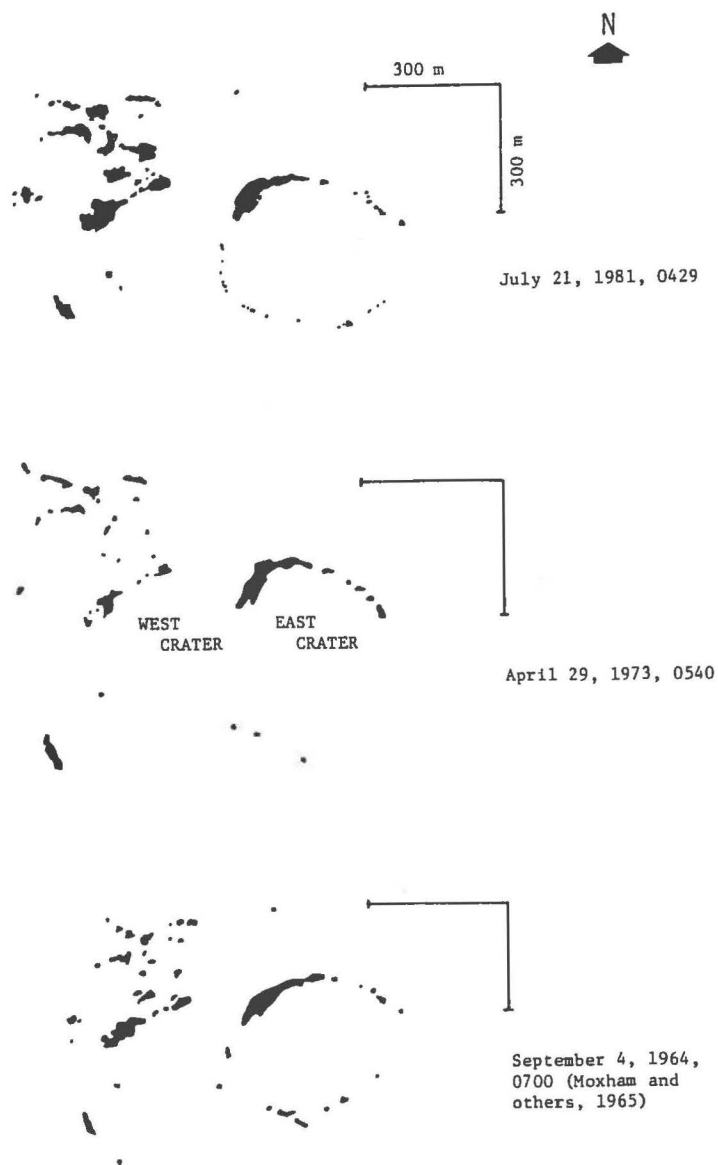


Figure 3. Representative thermal-infrared anomaly patterns for the summit fumarole field at East and West Craters during the past 20 years, as shown by aircraft-based line-scan images. The thermal patterns represent areas of fumaroles and heated ground that line the inner slopes of both crater rims and that cover a large area extending down the outer southwest to northwest slope of the West Crater. Scale bars indicate image distortion.

1973 failed to detect many of the small thermal areas in the southwest part of the East Crater rim (fig. 3) because in April, a time normally near the peak of the snowpack, these areas were covered by snow. Field observations during this same time period in the mid-1970's, did not verify any unusual changes in thermal activity.

1981-1983 Observations and Inferred Crater Structure

The most recent infrared images acquired through joint Department of Energy and Geological Survey efforts (Kieffer and others, 1982) show a representative pattern of heat emission from the summit area (plate II). Plate II and figure 4 indicate that the greatest heat emission is concentrated in four clusters of activity:

1. The inner slope (A and B) of the northwest quadrant of the East Crater rim;
2. The inner and outer slope (C) of the northwest quadrant of the West Crater rim; and
3. An isolated outcrop (D) on the outer southwest slope of the West Crater.

Lesser amounts of activity occur elsewhere along the inner slopes of both crater rims and far down the outer northwest

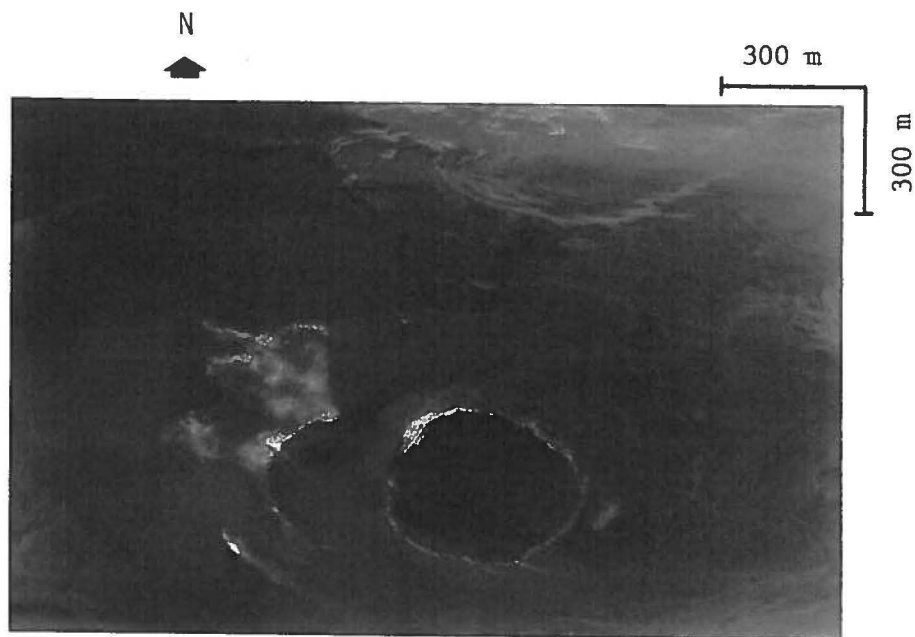


Plate II. Thermal-infrared image of summit, July 21, 1981, 0429 PST. Polarity is white - warm, black - cool. Scale bars show limited distortion. Digitally recorded image is by EG&G Corporation using a Daedalus DS-1260 scanner recording in the 8-12 μm spectral band. Image courtesy of H.H. Kieffer, USGS.

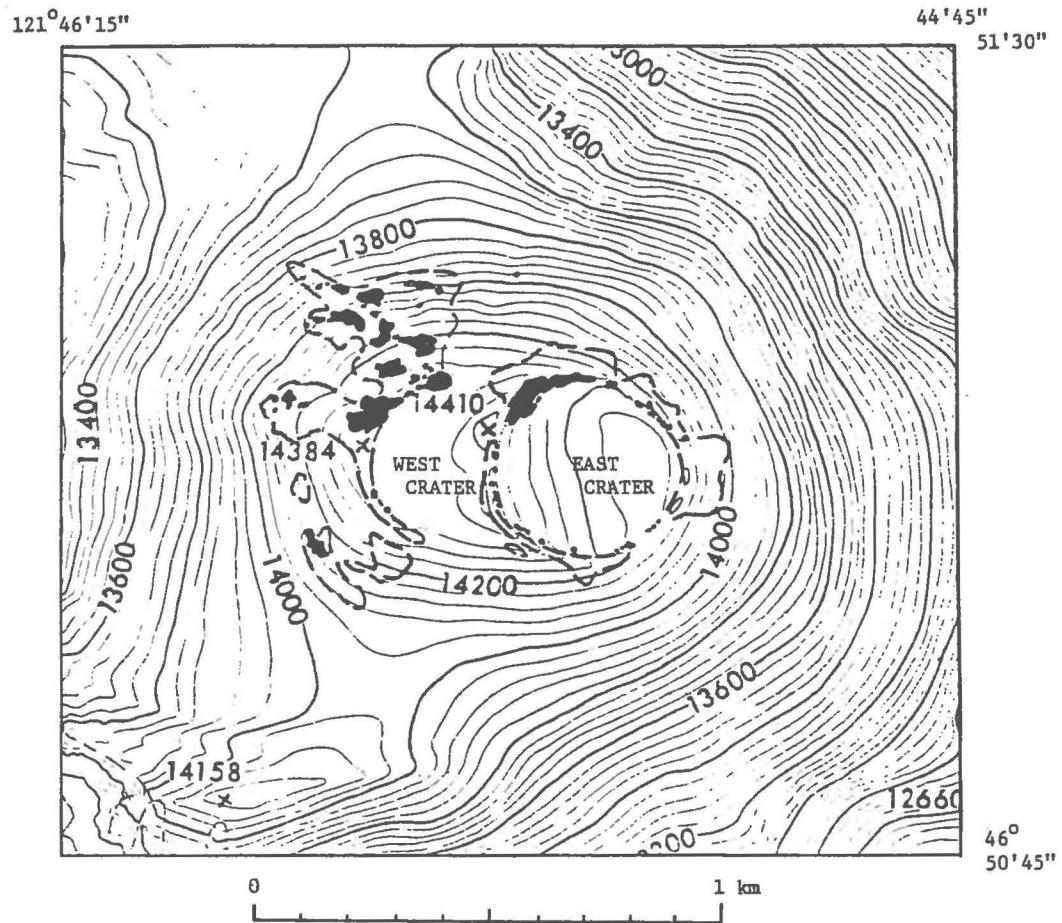


Figure 4. Planimetric display of 1981 thermal pattern (solid). Letters denote areas of greatest thermal activity including A - inner northwest slope of East Crater rim, B - inner north slope of East Crater, C - crest and outer northwest slope of West Crater rim, D - outer southwest slope of West Crater, E - thermal area at slump scarp on outer northwest slope of West Crater. Base from USGS advance sheet, Mount Rainier West, 40 ft, Mount Rainier East, 40 ft, compiled Menlo Park Base Map Section. Dashed - late summer snowline.

and west slope of the West Crater.

Field investigations in September 1982 and August 1983 recorded typical vapor temperatures of 72⁰ C for West Crater fumaroles and 80⁰ C for East Crater fumaroles. The maximum fumarole temperatures in each respective area were 74⁰ and 81⁰ C. Heated ground temperatures in unvented areas, on the other hand, ranged up to 72⁰ and 76⁰ C respectively. For comparison, the boiling point of pure water at the crater altitude is about 86⁰ C. Three temperature-probe traverses shown in figure 5 illustrate representative shallow temperatures of the hottest parts of the summit fumarole field.

Fumaroles are typically small, mostly a few centimeters across, but some are up to 20 cm. The vents with the greatest discharge make an audible hissing sound but are not highly pressured. The warmest fumaroles are easily found as most have sparse patches of moss and liverwort around their orifices. Fumaroles are most commonly situated along margins and joints of isolated andesite blocks embedded in the clayey to sandy matrix of the explosion rubble (plate III), or in joints at the top of the highly fractured lava flows that crop out at the crest and inner slopes of the crater rims.

The inner northwest quadrant of the East Crater rim



Plate III. Typical fumarole (Mossy fumarole) on the outer northwest slope of West Crater along temperature-probe traverse C-C'. Fumarole vent occurs in joints of andesite block embedded in clay-rich explosion rubble. View looking northeast toward crest of rim, August 21, 1983.

provides a good example of the role of jointed lava in localizing fumaroles. In the East Crater, the largest and most noticeable fumaroles occur near the top of a single andesite flow that intermittently crops out on the inner slope of the crater rim (fig. 5A, plate IV). Typically, these fumaroles are at or near the contact of the jointed lava with overlying clayey rubble which effectively seals off the flow path for vapor. This cluster of activity produces the long thermal lineament noted by Moxham (1970, p. 86) in his infrared images and visible in the northwest quadrant of East Crater in plate II.

Adjacent to this area, concentric thermal patterns occur both above and below the andesite flow as seen in plate II. In contrast to the fumarole clusters, these patterns result from hot unvented ground that is easily spotted in the field by the presence of damp patches of ground several meters across (plate IV), sometimes having a dry baked region in the middle. Also, in contrast to areas of fumaroles, unvented thermal ground occurs where rubble is particularly fine-grained, and large jointed blocks are absent at the surface. These relations suggest that, at the surface, jointed blocks provide the principal means of egress for heated vapor.

Factors which localize fumarolic activity near the

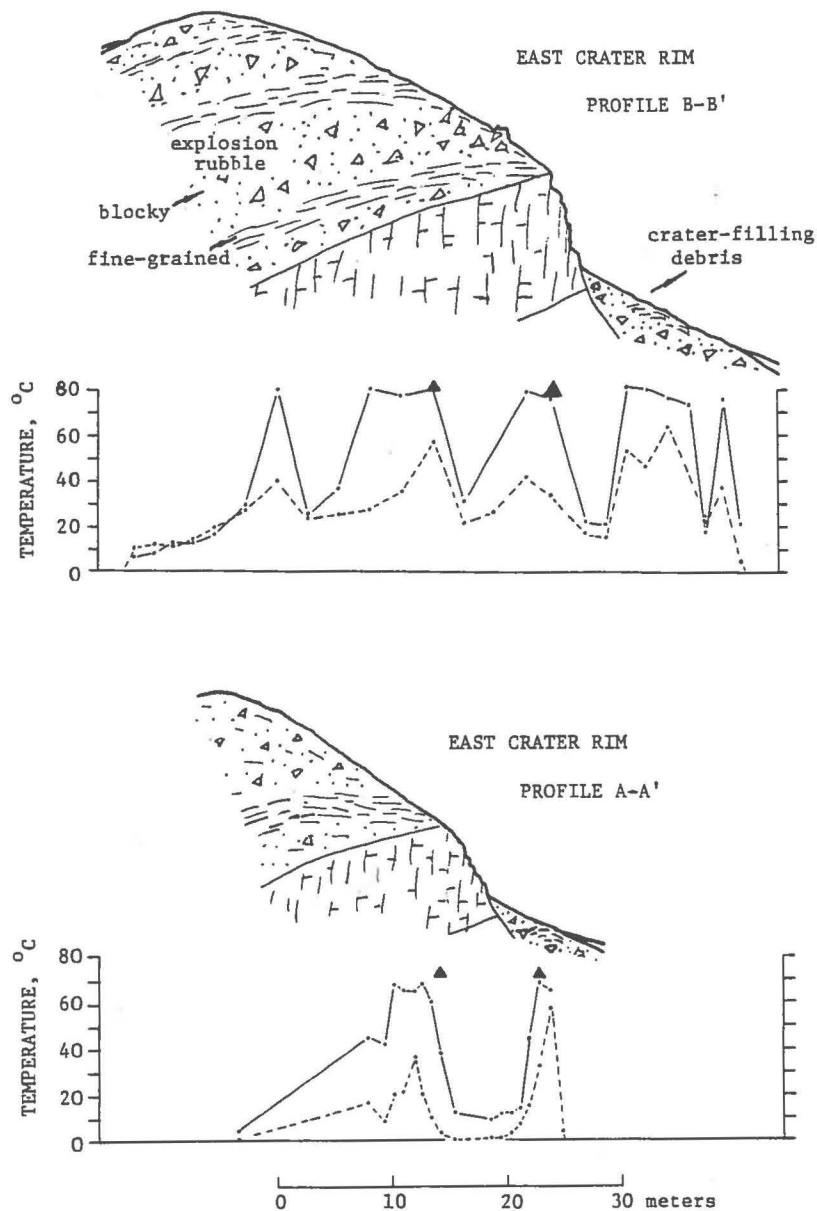
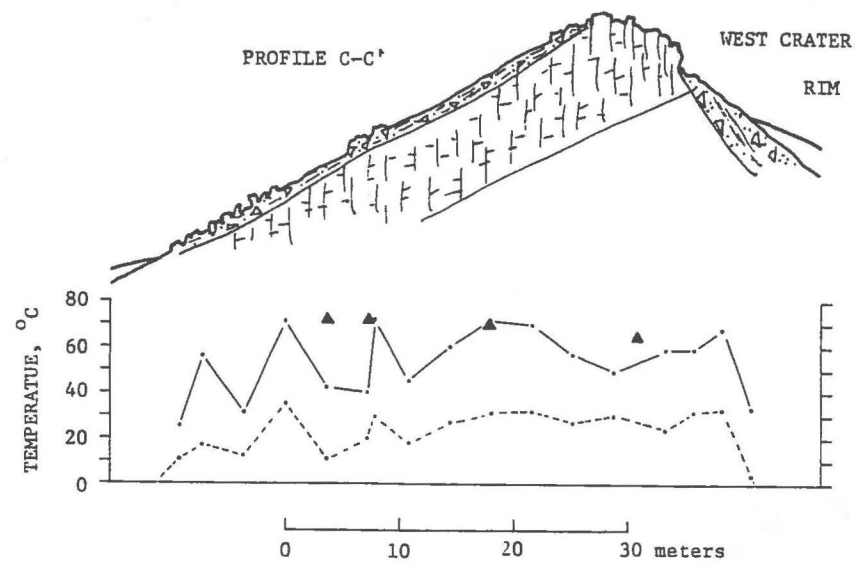


Figure 5. Profiles of temperature-probe traverses across the crater rims. Surface (dashed) and 15-cm-deep (solid) ground temperatures and fumarole (triangles) temperatures are shown in relation to three schematic profiles.

5A. Profiles A-A' and B-B' across the northwest slope of East Crater. See figure 6 for location of profiles.



5B. Profile C-C' across the northwest slope of West Crater. See figure 6 for location of profiles.



Plate IV. Inner northwest slope of East Crater rim. Main fumarolic activity occurs in damp (dark) ground along top of prominent lava flow extending from upper left to center right. Additional concentric damp patches of heated ground with sparse fumaroles can be seen above and below the flow. Letters denote location of temperature-probe traverses. Hikers provide scale. View looking west across East Crater. August 22, 1983.

crest and inner slope of the West Crater rim are similar to those at the East Crater (fig. 5B). Processes farther down the outer slope, on the other hand, are less apparent. The northern part of the thermal area on the outer north slope of West Crater (E in fig. 4) occurs where outward slumping has formed a scarp in the sheath of layered flows that make up the bulk of the summit cone. The scarp has exposed jointed lava allowing egress of heated fluids moving outward and downward from the crater within jointed flows or along permeable contacts between flows. However, the overall concentric pattern of thermal activity on the outer southwest to north slope of the West Crater (D-E in fig. 4) indicates the presence of an arcuate fracture zone which dips inward toward the crater heat source (Moxham, 1970, p. 87).

Subglacial clusters of thermal activity also extend down the inner slopes of both crater rims and, in combination with rivulets of meltwater and circulating air currents, form caves within the glacier cover of the crater basins (Kiver and Mumma, 1971). Mapping by Kiver and Mumma (1971, p. 321) shows a concentric pattern of ice-cave development 50-80 m inside the crater rim. The pattern suggests localization of thermal activity along a concentric zone of relatively high permeability, perhaps either inward-dipping faults or more likely the contact of

clay-rich, vent-filling breccia with truncated, jointed flows of the enclosing rim.

Kiver and Mumma (1971, p. 321) measured subglacial ground temperatures as high as 86° and vapor temperatures at 56° C in East Crater caves, while Kiver and Steele (1972) measured vapor temperatures up to 76° C in West Crater caves; these measurements are $4-5^{\circ}$ C higher than maximum reported vapor temperatures at the surface and reach the boiling point of pure water at the crater altitude. The existence of a lake in the West Crater, though only 0.5° C (Lokey, 1973) suggests significant thermal activity beneath the ice cover when compared to the subfreezing temperature of the ice, for which reported values include -10° in 1959 (Miller, 1970, p. 195) and -4° C in 1971 (Kiver and Steele, 1972). In this regard, Kiver and Mumma (1971, p. 320) suggest using observations of ice-cave dimensions as sensitive indicators of changes in hydrothermal activity. Subglacial thermal activity was not examined during the course of this study. However a thin crevasse was observed above the margin of the subglacial lake (plate V) during late summer 1983. Surficial monitoring of changes in this or similar crevasses could indicate enlargement or shrinkage of the lake in response to variations in subglacial melting around the lake.



Plate V. Snow-covered crevasse along north margin of subglacial lake in West Crater, August 20, 1983. Tent lies over approximate position of lake. Ice cave in foreground leads to subglacial passages formed by thermal activity. Monitoring of selected crevasse and snowmelt patterns provides a method to detect changes in thermal activity. View looking east toward East Crater rim and summit.

Heat Flow

The level of thermal activity in the upper part of the hydrothermal system can be quantitatively assessed through calculation of heat flow and comparison of the results with those of other volcanoes. Available Mount Rainier data are particularly suited to surficial heat-flow calculations whereby excess heat flow (ΔG) from the thermal-ground surface is that part of the total heat flow which is greater than that from nearby non-volcanogenic areas. Consequently, the excess heat flow is due to the hydrothermal system. Using the concept of heat balance at the earth's surface (Budyko, 1956), excess heat flow can be partitioned into four components of heat-flux density by

$$\Delta G = \Delta R + \Delta H + \Delta LE + \Delta A$$

where positive flux is upward; ΔR is excess net radiation; ΔH is excess flux due to eddy diffusion and molecular conduction; ΔLE is excess evaporative flux; and ΔA is advective flux due to ice melt, surface-water runoff, ground-water infiltration, and fumarolic mass transfer by means of vapor discharge.

Thermal-infrared images, ground measurements, and approximate micrometeorological values allow estimates to be

made of most of these heat-flow components. Nighttime net radiation is often expressed as the difference between upward exitance, or radiant flux density, from the earth's surface and downward counter radiation from the atmosphere. Previous applications (Sekioka and Yuhara, 1974; Friedman and Frank, 1980) of the heat balance method for heat-flow determinations at volcanoes have used an empirical term devised by Brunt (1934) for counter radiation; this term is not used here. In alpine environments, the effective counter radiation results from a relatively thick air column above the ground surface because of low air temperature and water vapor (LeDrew, 1975b, p. 228-229). Field observations at Mount Rainier indicate that high temperature gradients commonly exist near the ground surface such that, even above thermal ground, subfreezing temperatures are normal at screen level (about 1 m). Thus air temperature and water vapor quickly approach ambient above the ground. It may be assumed, therefore, that closely spaced areas above both thermal and non-thermal ground at the top of Mount Rainier are subject to similar effective counter radiation irregardless of the ground temperature. Hence excess net radiation, under the conditions discussed here, should not include the empirical Brunt-type term for counter radiation. Instead, excess net radiation simply results from ground-surface temperatures, and may be expressed as

the excess exitance, ΔW .

Ground-surface temperatures, T , may be determined from airborne-acquired infrared data that have been corrected for atmospheric absorption and ground emissivity. Excess radiant exitance is then calculated through the Stefan-Boltzmann relation

$$\Delta W = \sigma \epsilon (T^4 - T_0^4)$$

where ΔW as W/m^2 is approximated by radiation in the atmospheric spectral window of 8-14 μm ; ϵ is emissivity, 0.98; σ is the Stefan-Boltzmann constant, $5.67 \times 10^{-8} Wm^{-2}K^{-4}$; T is surface temperature of warm ground in Kelvins; and T_0 is cold reference temperature of adjacent non-geothermally heated ground. The 8-14 μm window coincides with peak infrared emission at temperatures from freezing up to about $130^{\circ} C$ and thus justifies the use of the fourth power relation.

Two aerial infrared surveys to date (table 2) are sufficiently well calibrated to allow calculation of ground temperatures. The most recent in July 1981 (Kieffer and others, 1982) produced digital tapes of thermal emission calibrated by two blackbody reference temperatures inside the scanner housing; computer processing of these data is not yet complete. The earlier survey (November 1972)

produced a calibrated photographic film by means of an onboard analog image processor. A ten-step gray scale calibrated by two blackbody reference temperatures was attached to the film. Original film images were acquired for the analysis below.

Figure 6 shows an isothermal contour map of the summit area produced from an isodensity scan of the 1972 film image by a Photometrics EDP scanning microscope densitometer with 200 μm scanning aperture. Radiometric temperatures as seen by the scanner are converted in table 3 to true ground temperatures, T, shown on figure 6, by correction for atmospheric absorbance and emissivity.

Table 3. Calibrated temperature ranges of November 1972 thermal-infrared survey. In Kelvins, K.

UNCORRECTED RADIOMETRIC TEMPERATURE	CORRECTED FOR 4% ATMOSPHERIC ABSORPTION	CORRECTED FOR 98% EMISSIVITY	AVERAGE SURFACE TEMPERATURE
259-293	262-296	263-297	280 7 ⁰ C
293-299	296-302	297-303	300 27 ⁰ C
299-305	302-308	303-309	306 33 ⁰ C

Cold non-hydrothermally heated ground surface = 263 K
(-10⁰ C).

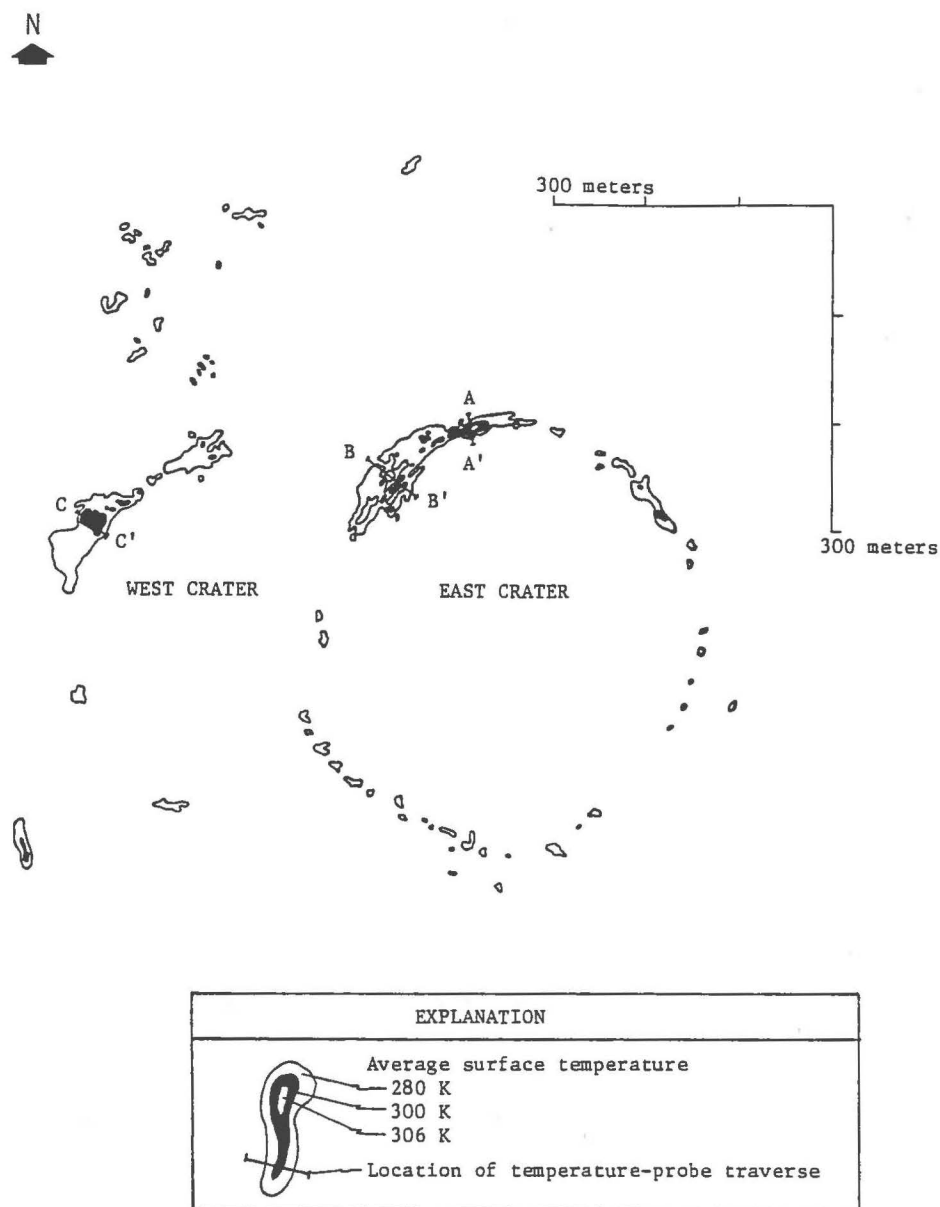


Figure 6. Isothermal contour map of summit fumarole field. Contours are drawn from microdensity scan of thermal-infrared image of November 15, 1972, 0520 PST. Radiometric temperatures were calibrated by internal blackbody reference in the scanner housing and were corrected for atmospheric absorption and ground emissivity by methods described in the text. About 2% of 280 K thermal ground is missing northwest of West Crater. Image by NASA for USGS Landsat 1 experiment SR251.

Absorbance from water vapor mixed with other gases was calculated using microclimatic conditions at the time of the survey as approximated by radiosonde data from Quiyallute, Washington (National Climatic Center, 1972) and by standard-atmosphere data (McClatchey and others, 1972). Parameter values necessary for these corrections are:

Scanner altitude, 5180 m (17,000 ft)
Mean altitude of crater thermal area, 4360 m (14,300 ft)
Scanner angle of rotation, 80°
Mean length of atmospheric path, 880 m
Mean path humidity, 40%
Mean path temperature, -18° C
Mean path air pressure, 550 mbar
Mean water concentration in path, 0.044 g/cm^2
Mean path length for mixed gases (CO_2 , N_2O , CO , CH_4), 0.35 km

From these data, atmospheric-path absorbance to 8-14 μm radiation is estimated at 4%.

Daniels (1968, p. 74-78) found that emissivities for a variety of polished volcanic rocks ranged from 0.868 to 0.985, whereas Saunders (1970) reported 0.99 for water

surfaces. An average value of 0.95 should be appropriate for dry volcanic rock surfaces at Mount Rainier. However field observations during the present study showed that more than half the area of heated ground maintained a moist surface. Therefore, an average value of 0.98 is used here.

A reasonable approximation for the cold reference temperature, T_0 , is the mean annual air temperature at the crater. This value is determined by applying a lapse rate of temperature decrease with altitude to mean annual temperatures from nearby meteorological stations. Data from four stations (Stampede Pass, Greenwater, Electron, and Paradise Ranger Station) within 8-55 km of the summit during the period 1951-1980 (National Climatic Center, 1983) indicate a lower-atmosphere lapse rate of about 5 K/km. A more extensive compilation of meteorological data from 1931-1960 using 18 stations throughout the Washington Cascade Range (Porter, 1977, p. 109) indicated a lapse rate of 4.7 K/km. The latter value is used for calculations in the present study and yields a mean annual air temperature of -10° C for the crater area at 4350 m altitude. Therefore the cold reference temperature is approximated at -10° C, a value considered conservative on the high side. For comparison, summer air temperatures at West Crater have ranged as low as -62° C (Miller, 1970, p. 193).

The sum of radiant flux over each of the isothermally contoured areas (table 4) yields 1.03 MW for total excess radiant flux for the summit fumarole field in November 1972, with almost equal flux attributed to each crater. An average of about 86 W/m^2 of excess radiant exitance occurred over the total thermal area of $12,000 \text{ m}^2$. Partition factors, $\Delta R/\Delta G$, of excess radiant exitance typically range from 0.04 to 0.1 for a variety of geothermal areas (Friedman and others, 1981, p. 289). Applying this range to the measured radiant exitance suggests the total excess flux (ΔG) should be on the order of 10-26 MW for the thermal areas.

Table 4. Excess radiant flux from East Crater, EC, and West Crater, WC.

T, K	R, W/m^2	AREA, m^2			FLUX, MW		
		EC	WC	TOTAL	EC	WC	TOTAL
280	73	5400	5490	10,890	.411	.417	.828
300	172	560	480	1,040	.103	.089	.192
306	209	50		50	.011		.011
TOTAL		6010	5970	11,980	.525	.506	1.031

RADIANT EXITANCE AVERAGED OVER THERMAL AREA = 86 W/m^2

Evaporative flux density can be estimated following Sellers (1965, p. 145) using

$$LE = 0.622 \rho L D_w (e_s - e_a) / P$$

where 0.622 is the ratio of the specific gravity of water vapor to dry air; ρ is air density, 0.786 kg/m^3 ; L is latent heat of vaporization in J/kg ; P is air pressure, 580 mbar; D_w is coefficient of water-vapor diffusion in cm/s ; e_s is saturated water vapor pressure at ground-surface temperature in mbar; and e_a is water vapor pressure, in mbar, at atmospheric temperature, T_a .

The transfer coefficient for water vapor is here assumed equal to that for momentum (Sellers, 1965, p. 158), so that

$$D_w = k^2 u (\ln z / z_0)^{-2}$$

where k is von Karman constant, 0.36; u is wind speed in m/s ; z is height of wind speed and z_0 is roughness, both in m .

The roughness, or effective height where wind speed equals zero, has been experimentally determined by LeDrew (1975a) for a rubble-strewn alpine field in Colorado which is similar in size of debris cover to that of the crater rim. LeDrew's (1975a, p. 308) average value of 1 cm is

used here. Since most of the thermal area is exposed to the wind, wind speed is taken to be that at Quiyallute at the time of the infrared survey, 3 m/s (National Climatic Center, 1972). Latent heat and water-vapor pressures are calculated for each ground temperature under consideration. Excess evaporative flux density is calculated by subtracting the flux for the cold reference surface at -10° C from that of the hydrothermal surface. Table 5 lists values of excess evaporative flux and appropriate parameters for each isothermal area mapped on figure 6. Total excess evaporative flux is 4.3 MW.

Table 5. Excess evaporative and sensible flux density for each isothermal area.

AVERAGE SURFACE TEMPERATURE, K	EVAPORATIVE FLUX DENSITY, W/m ²	SENSIBLE FLUX DENSITY, W/m ²	BOWEN RATIO β
280	270	230	0.87
300	1200	480	0.43
306	1800	570	0.35

Sensible heat due to molecular conduction and eddy diffusion is calculated via the Bowen ratio of sensible heat to evaporative flux, $\beta = H/LE$. Following Barry (1981, p. 224), the Bowen ratio may be approximated by

$$\beta = 0.61 \times 10^{-3} (T - T_a) (e_s - e_a)^{-1} P$$

where the parameters are the same as described previously. Total excess sensible heat flux is 3.0 MW.

Advective heat flux comprises several components - snow- and icemelt, runoff, infiltration, and vapor discharge - all difficult to estimate. Snowmelt occurs over the exposed thermal area whereas icemelt occurs beneath the crater ice cover. If geothermally induced melting did not occur, the amount of snowfall accumulation over exposed thermal area would be about 6000 m³ based on the area of thermal ground of 12,000 m² and an average annual snow thickness of 0.5 m. For comparison, the depth to firn was measured at 0.7 m in the wall of an ice cave in the East Crater in September 1982; snow accumulation on the rim should be somewhat less because of its greater exposure to wind. Using a snow density of 500 kg/m³ and a latent heat of melting of 336 x 10³ J/kg, the amount of heat required to melt, in one month, the annual snowfall over exposed thermal areas is only about 32 W/m² and should already be accounted

for in other heat-flow components.

Heat required to melt ice caves, however, is additive and can be estimated from measurements made during ice-cave explorations by Kiver and Mumma (1971), Kiver and Steele (1972), and Lokey (1973). These studies revealed about 1900 m of passageways ranging up to 10.5 m high and 3.5 m wide. Approximate values derived from their data yield a tunnel volume of about 49,000 m³ and an additional volume of 26,000 m³ for a large subglacial room near the center of each crater. In all, a total of about 75,000 m³ of icemelt accounts for the cave system, 83% of which is in the East Crater. Kiver and Steele (1972) estimated a downward movement of ice at 6-10 ft/yr (about 8×10^{-8} m/s) which, combined with a total area of ice-cave coverage of 16,000 m² produces a total ice flux of 0.0013 m³/s and an equivalent heat flow of 0.26 MW. Here, Kiver and Steele's (1972) firn density of 600 kg/m³ is used.

Heat flux from runoff and infiltration is not estimated, but it is probably not a major component as all meltwater streams that were measured had temperatures close to freezing. Furthermore, much of this heat flux is probably already accounted for in other components. For example, some of the ice-cave entrances are probably initiated by meltwater runoff from hotter areas upslope.

Also, the crater lake in West Crater had a temperature of 0.5° C (Lokey, 1973) indicating a heat flux value there just sufficient to melt ice.

Heat flux from the larger fumaroles is not included in the previous estimates and may be a significant additive component, particularly if the fumaroles are pressurized. Fumarolic discharge measurements are not available, but visual comparison with other fumarolic areas where measurements have been made (for example at Mount Baker by Kiver and Steele, 1976) indicates the typical weakly pressurized discharge of the largest Rainier fumaroles of about 40 cm^2 is on the order of $0.001 \text{ m}^3/\text{s}$. If a fumarole of this type represents about 1% of the largest fumaroles, then an average fumarolic heat flux of 0.06 MW can be obtained from

$$F = v f \rho \underline{H}_v$$

where v is discharge, $0.01 \text{ m}^3/\text{s}$; f is relative humidity, 0.95; ρ is density of saturated water vapor at 72° and 80° C, $0.217\text{-}0.293 \times 10^{-3} \text{ kg/m}^3$; and \underline{H}_v is enthalpy of saturated water vapor, $2.64 \times 10^6 \text{ J/kg}$. Such a low flux for fumarolic discharge is almost insignificant compared to other heat-flux components.

Table 6 lists values of the various heat-flow

components. From these values, total geothermal flux is estimated at 8.3 MW with a flow of 300 W/m^2 averaged over the thermal area of $28,000 \text{ m}^2$ (rim plus ice cave) and 16 W/m^2 averaged over the crater area of $520,000 \text{ m}^2$.

Table 6. Components of excess heat flow.

COMPONENT	FLUX, MW	FLUX DENSITY AVERAGED OVER THERMAL AREA, W/m^2
Radiant exitance, ΔR	1.03	86
Evaporation, ΔLE	4.3	360
Molecular conduction and eddy diffusion, ΔH	3.0	250
Advective flux, ΔA snow and icemelt, 0.26 fumarole discharge, 0.06	0.32	20
TOTAL, ΔG	8.6	700^1

¹Not counting area of subglacial activity.

Comparison with flux estimates at other Cascade Range volcanoes (table 7), suggests that Mount Rainier has a modest repose-period discharge through its central vent comparable to that at Mount Hood but spread over three times the vent area of Hood. The large area of heat emission

Table 7. Heat-flux at Mount Rainier compared to estimates for other Cascade Range volcanoes. Values are rounded to one or two significant figures.

VOLCANO	HYDROTHERMAL ENERGY YIELD	AREA OF THERMAL FEATURES ¹	AVERAGE EXCESS HEAT FLOW	REF ²
	MW	m ²	W/m ²	
Rainier				
Summit craters	8.6 ³	12,000 ¹	700	8
Upper flank fumaroles	1.0 ³	3,000	300	8
Lower flank springs	0.9			8
Baker				
Sherman Crater, 1972	11	8,800	1,300	3
Sherman Crater, 1975	81	35,200	2,300	3
Dorr Field, 1972	1.2	3,000	400	3
Hood, 1972, 1977				
Crater Rock/Steele Cliff	9.8	9,700	1,000	5
St. Helens				
Old dome, 1972	0.2	1,000	200	1
New crater and bulge, May 16, 1980	30- 75	30,000	1,000- 2,500	6,7
New crater and dome, August 13, 1980	4,000- 10,000	800,000	5,000- 13,000	4,7
Lassen Volcanic National Park				
Lassen Peak, 1972	0.3	900	300	7
Bumpass Hell, 1972	55	45,000	1,200	2
Devils Kitchen, 1972	47	41,000	1,100	2
Boiling Springs Lake, 1972	31	16,000	2,000	2

¹Not counting areas of subglacial activity.

²References: 1-Friedman and Frank (1977); 2-(1978); 3-(1980); 4-Friedman and others (1981); 5-(1982); 6-Kieffer and others (1981); 7-Frank (unpublished); 8-This study.

³Probable maximum value.

relative to that at other Cascade volcanoes indicates the presence of a permeable cap over a large area, in other words an open top on the hydrothermal system.

Upper Flank

Several small areas of thermal activity have been observed on the upper flank of Mount Rainier (fig. 7). These occurrences are in marked contrast to those on the edifices of other Cascade Range volcanoes where most activity is confined to sites of old eruptive vents, primarily the central crater or dome margins. Table 8 lists selected references to reported areas of flank thermal activity and makes note of the type and number of observations. Close attention to the source of such data is important, particularly for Mount Rainier, because of several reports each year of "steam vents" that are in fact non-volcanic, such as wind-blown snow or dust columns. Nonetheless, some observations, especially those repeated for the same site or corroborated by different types of data may be valid indications of thermal activity.

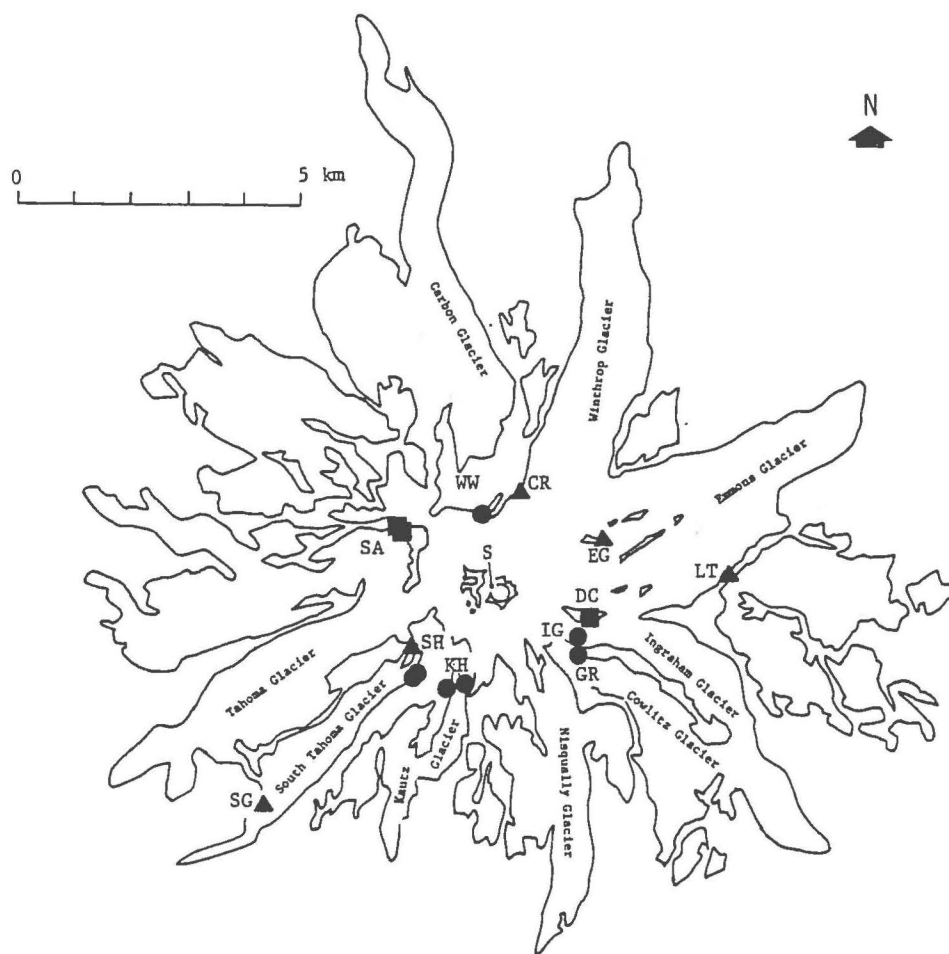


Figure 7. Areas of reported thermal activity on the flank of Mount Rainier. Continuous hydrothermal emission (squares) probably occurs in those areas which have been detected more than once by instrumental observations over a span of several years at Disappointment Cleaver (DC) and Sunset Amphitheater (SA). Possibly discontinuous or ephemeral activity (circles) occurs in those areas which were detected by isolated instrumental or short-range visual observations at Willis Wall (WW), South Tahoma headwall (SH), Kautz headwall (KH), Gibraltar Rock (GR), and Ingraham Glacier (IG). Unverified thermal activity (triangles) has been reported in several source areas of debris avalanches at Curtis Ridge (CR), Gibraltar Rock, South Tahoma headwall, South Tahoma Glacier (SG), and Little Tahoma Peak (LT). S - summit.

Table 8. Thermal areas on the upper flank of Mount Rainier.

LOCALITY	ALTITUDE, m/ft	DATE	TYPE OF OBSERVATION	REF ¹
Disappointment Cleaver, DC	3630	11/15/72	Aerial IR survey	2
	/11,900	4/29/73	Aerial IR survey	2
		12/13/75	Aerial IR survey	4
		1974-1982	Field observation	6
Ingraham Glacier, IG	3630 /11,900	7/23/56	Ranger report of strong sulfur fume from ice pit, 9 m across, 30 m deep, no noise	3
Gibraltar Rock, GR	3410 /11,200	8/61	Guide report of steam fissure at NE end of Gib shooting 20-30 m for several days	3
Kautz Headwall, KH	3570	3/7/65	Climber report of steam vent	1
	/11,700 3570- 3600 /11,700- 11,800	4/29/73	Aerial IR survey, 2 sites	2
South Tahoma Headwall, SH	3350- 3410 /11,000- 11,200	4/29/73	Aerial IR survey, 2 sites	2
Sunset Amphitheater, SA	3930	4/29/73	Aerial IR survey	2
	/12,900 3900 /12,700	7/21/81	Aerial IR survey	6
Willis Wall, WW	3780	4/29/73	Aerial IR survey,	2
	/12,400	12/13/75	Aerial IR survey	4

¹References: 1-Danes (1965); 2-Frank and Friedman (1974);
3-Moxham and others (1965); 4-Rosenfeld (unpublished);
5-Unpublished; 6-This study.

Table 8 includes events that were visually observed at close range, within 1 km, or were observed by instrumental means, primarily thermal-infrared surveys. An infrared survey of April 29, 1973, is the only source of information for several of the flank thermal areas. This survey was designed for detailed coverage of the upper flank of the mountain and was flown at low altitude (4720 msl), thus providing data of exceptionally high spatial resolution. Initial analysis revealed more than 80 previously undetected infrared anomalies of unknown origin (Frank and Friedman, 1974) in both upper and lower flank areas; subsequent field study shows that many of the anomalies were caused by hydrothermal emission. Of the upper flank localities, only those seven that produced a film density (infrared brightness) equal to or greater than that of the Disappointment Cleaver fumarole field are listed in table 8. The lower brightness, inaccessibility, and lack of repetitive observation of the remaining infrared anomalies prevent unequivocal interpretation of their cause.

The localities noted in a number of other references to thermal activity on the flanks of Mount Rainier are also shown in figure 7, but are not included in table 8 because they were based on visual observations made at great distance (more than 5 km) and were not verified by

instrumental means. Of particular note are common late-summer observations of dust plumes and perhaps water vapor in erosional alcoves at about the 3570 m level of the South Tahoma headwall, and the 3440 m level of Curtis Ridge (SH and CR in figure 7); both of these localities are the source of frequent small- to moderate-size (10,000-100,000 m³) debris avalanches. Observations of the South Tahoma headwall are discussed in detail by Crandell (1971, p. 60-63) who concluded that small steam explosions during late summer 1969 could have occurred in that area. Other sites where short-lived thermal activity or steam explosions have been considered as possible causes for rock-fall include the north slope of Little Tahoma Peak (LT, fig. 7) at 3000 m in December 1963 (Crandell and Fahnestock, 1965, p. A25-A29), the icefall at 1980-2130 m on the lower South Tahoma Glacier (SG) in February 1969 (Crandell, 1971, p. 62), and cliffs in the middle of the Emmons Glacier (EG) at 3,000 m also in 1969. Additional data are required to determine if these have ever been sites of either continuing or intermittent thermal activity.

Weak anomalies recorded by ground-based thermal-infrared surveys (Lange and Avent, 1973, 1975) are also not included in table 8 because of difficulties in interpretation that arise from the small radiant temperature differences (less than 3 K) and great distances (6-12 km)

involved in these surveys. It is noted however that one of Lange and Avent's (1973, fig. 2) anomalies coincides with an avalanche-source area in the South Tahoma headwall (SH, fig. 7).

Disappointment Cleaver

The only thermal area on the upper flank that has been studied in any detail is that on Disappointment Cleaver (plate VI). Though not reported in previous geological studies of Mount Rainier, some Park rangers and climbers had been familiar with the existence of the thermal area for many years (L. Henkle, unpublished communication, 1981). That so little information has been available concerning Disappointment Cleaver is quite remarkable considering the thermal area lies within only 30 m of the most heavily used climbing route on the mountain.

Good quality geographic information from the April 1973 infrared survey (plate VII) enabled accurate location of the site. Observations made over the period from May 1973 to June 1982 indicate little variability in activity. Two clusters of small, weak fumaroles occur along the ridge of Disappointment Cleaver at about 3630 m altitude; 320 m² of heated ground surrounds the fumaroles and extends 30 m along



Plate VI. Disappointment Cleaver (DC) on the upper east flank. GB - Gibraltar Rock, IG - Ingraham Glacier, EG - Emmons Glacier. Small fumarolic area (arrow) occurs at 3630 m altitude halfway up the crest of the 700-m-long cleaver. Aerial photography looking west, July 12, 1980.

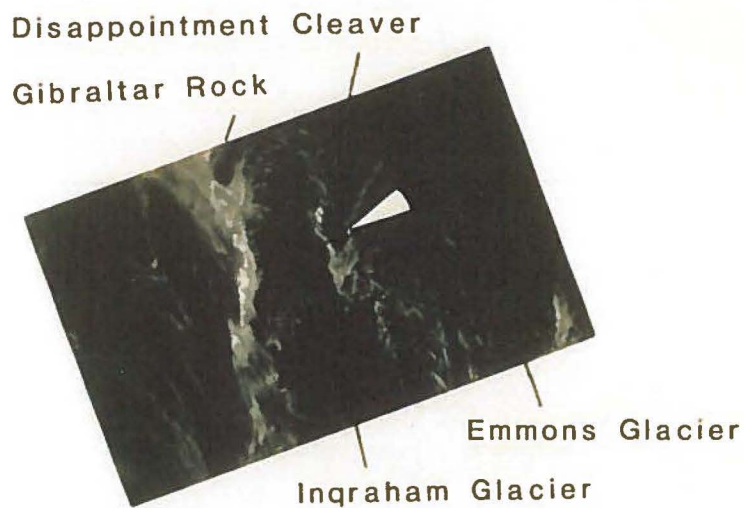


Plate VII. Aerial thermal-infrared image showing anomaly from 300 m² of thermal ground on Disappointment Cleaver, April 29, 1973, 0535 PST. Polarity is white - warm, black - cool. Other light features are slightly warmer than the exposed snow-covered surfaces, and include snow-free ridges and crevasse walls. Film-recorded image by U.S. Forest Service using Texas Instruments RS-7 scanner recording in 8-14 μ m spectral band.

the ridge crest and 15 m down the south facing slope of the cleaver. The thermal activity occurs at and below the contact between a grey andesite flow and an overlying red brecciated flow. The contact zone contains a mixture of poorly consolidated block and cinder breccia (plate VIII) which is variably cemented by opal and calcite.

A spring-driven Foxboro recorder with a vapor-liquid temperature probe was installed at the largest, hottest fumarole on Disappointment Cleaver in July 1974 and run intermittently for 159 days during the next two years. Recorder data for a 50-cm depth (fig. 8) show a range of 35-62^o C. Consistent temperature peaks of 54-62^o C suggest a stable heat flow at shallow depth within the cleaver. Maximum temperatures show a decreasing trend from July to November which is probably a seasonal effect resulting from cooler weather and perhaps changes in ground-water recharge from snowmelt. Several short-term downward fluctuations superimposed on this seasonal trend are likely caused by storms that flood the shallow hydrothermal system with cool air and precipitation. Recent field measurements in August 1981 and June 1982 showed similar temperatures with a maximum of 58^o C for the vapor and 57-60^o C for nearby heated ground.

To arrive at an estimated heat-flow value for



Plate VIII. Disappointment Cleaver thermal area. Fumarole vapor (arrow) can be seen wafting off crest of cleaver from contact zone where basal rubble of a grey andesite flow is overlain by a reddened brecciated flow. Cemented scoriaceous debris makes up the prominent spire near the fumarole. All of the foreground is heated to near-surface temperatures as high as 60^o C. Instrument box and cable provide scale. View looking east, August 5, 1981.

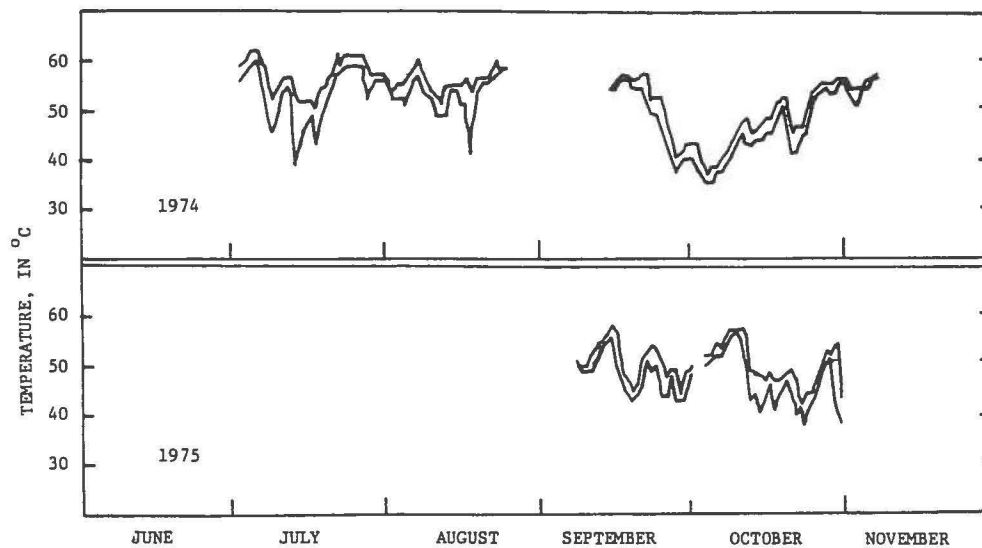


Figure 8. Temperature variation at 50-cm-depth in Disappointment Cleaver thermal area. Daily maximum and minimum temperatures taken from a continuous record produced by a Foxboro recorder show thermal peaks at 54-62^o C. Downward fluctuations probably result from cooling by shallow infiltration of snowmelt.

Disappointment Cleaver, ground temperatures and observed activity may be matched with a similar-sized area at the summit for which infrared-based calculations of heat flow were made. The indicated excess heat flow is on the order of 300 W/m^2 , resulting in a heat discharge of about 0.1 MW for the Disappointment Cleaver thermal area. This level of heat emission has not appreciably varied over the last decade of observation and probably has had little change for a much longer period.

Other Headwall Thermal Areas

Evidence ^{of} from thermal activity elsewhere on the upper flank of Mount Rainier suggests that such activity in some areas may be ephemeral or may undergo significant variations. For example, observations of apparent fumarole emission in the Ingraham Glacier in 1959, at Gibraltar Rock in 1963, and on the Kautz headwall in 1965 (table 8) have not been repeated even though all of these areas occur within 1 km of popular climbing routes. Subsequent infrared surveys have detected an anomaly at only one of these sites, the Kautz headwall in 1973.

No known visual observations of thermal activity have been made at any of the remaining sites in table 8 including

those on the South Tahoma headwall, Sunset Amphitheater, and Willis Wall. This is not surprising because of poor accessibility to the headwalls. In addition to Disappointment Cleaver, many of the other upper-flank thermal areas may have continuing activity. However, only two have been detected more than once in infrared surveys (table 8). These include sites at Willis Wall and on Sunset Amphitheater (plates IX, X, XI). Only the latter was detected by the most recent infrared survey in 1981.

Considering the size of the upper-flank thermal areas and their relatively weak activity, excess heat flux for each area is assumed to be comparable to that estimated for Disappointment Cleaver, 0.1 MW. Depending on how many upper-flank sites (2 to 10) may have continuing activity, excess heat flux from the upper flank would range from 0.2 to 1 MW, or 2-10% of the heat discharge from the summit. Undiscovered thermal activity or possible activity in the more frequent avalanche-source areas (triangles in figure 7) would increase the heat-flux estimate by a small amount.

Structural Implications

The upper-flank thermal areas in table 8 all lie within a remarkably restricted range in altitude of 3350-3950 m

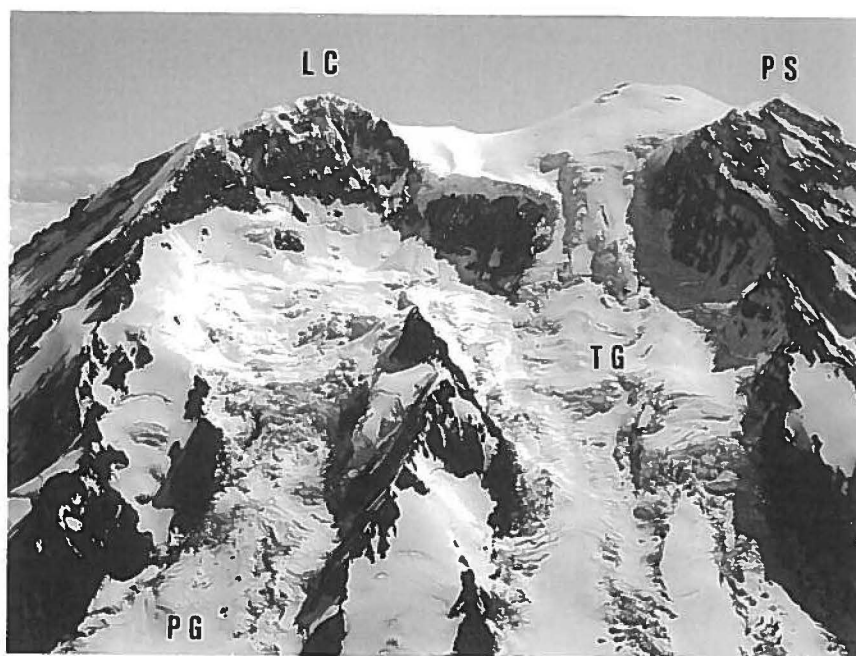


Plate IX. Location of thermal-infrared anomalies in Sunset Amphitheater, the prominent headwall northwest of Mount Rainier's young summit cone. PG - Puyallup Glacier, TG - Tahoma Glacier, LC - Liberty Cap, PS - Point Success. Circle and oval mark the 1973 and 1981 anomaly locations at about 3930 m altitude. Aerial photograph looking northeast, July 12, 1980.

Liberty Cap



Puyallup Glacier

Tahoma Glacier

Plate X. Aerial thermal-infrared image showing anomalies (arrows) from probable thermal activity on headwall of Sunset Amphitheater, April 29, 1973, 0540 PST. Polarity is white - warm, black - cool. Other light features are crevasses and snow-free ridges and cliffs. Film-recorded image is by U.S. Forest Service using Texas Instruments RS-7 scanner recording in 8-14 μm spectral band.

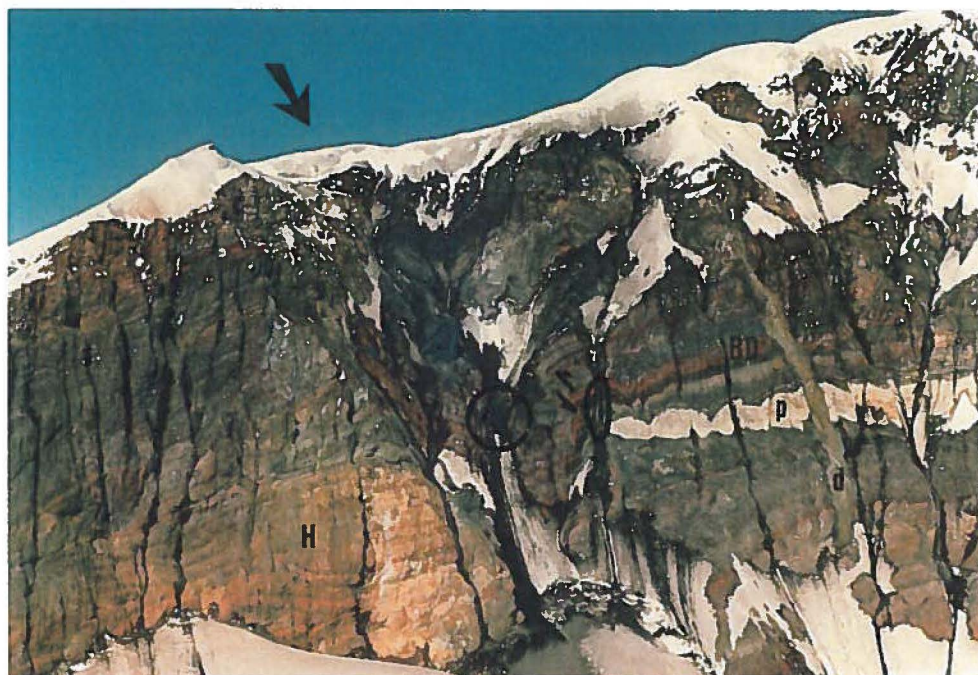


Plate XI. Detail of 1973 (circle) and 1981 (oval) infrared-anomaly locations in Sunset Amphitheater. Thermal areas occur in buried collapse pit formed in bedded deposits (BD) that are banked up against an old crater wall of hydrothermally altered rock (HA). Evidence of fracturing that would enhance vertical permeability include dykes that feed overlying lava flows, the contact zone with the crater wall (arrows), and several faults (half-arrows) marked by offset pumice and scoria layers especially in the collapse pit. Aerial photograph looking northwest, September 23, 1976.

(11,000-13,000 ft). Such a relationship suggests localization of fluid emission in these areas by common structural or hydraulic controls. All of the upper-flank thermal areas occur where outward dipping flows, or flow breccias, have been truncated by headwall erosion. Permeable contacts between these layers, such as that observed at Disappointment Cleaver, would provide opportune paths for fluid transport. Other possible permeable structures such as flank eruptive vents, dome margins, dykes, cone sheets, or inward-dipping faults are absent at most of the flank thermal areas, except for Sunset Amphitheater.

Cross sections (fig. 9) through the flank thermal areas indicate that, with the exception of Sunset Amphitheater, the loci of activity occupy comparable positions relative to the central vent of the volcano. These relations are consistent with migration of upper-flank thermal fluids downward and outward from the central vent along permeable contacts between flows. As discussed below, helium concentrations in fumarole vapor at Disappointment Cleaver support this conclusion.

Sunset Amphitheater differs from other upper-flank localities in that it contains a number of vertical structures adjacent to the thermal areas. Dykes, buried

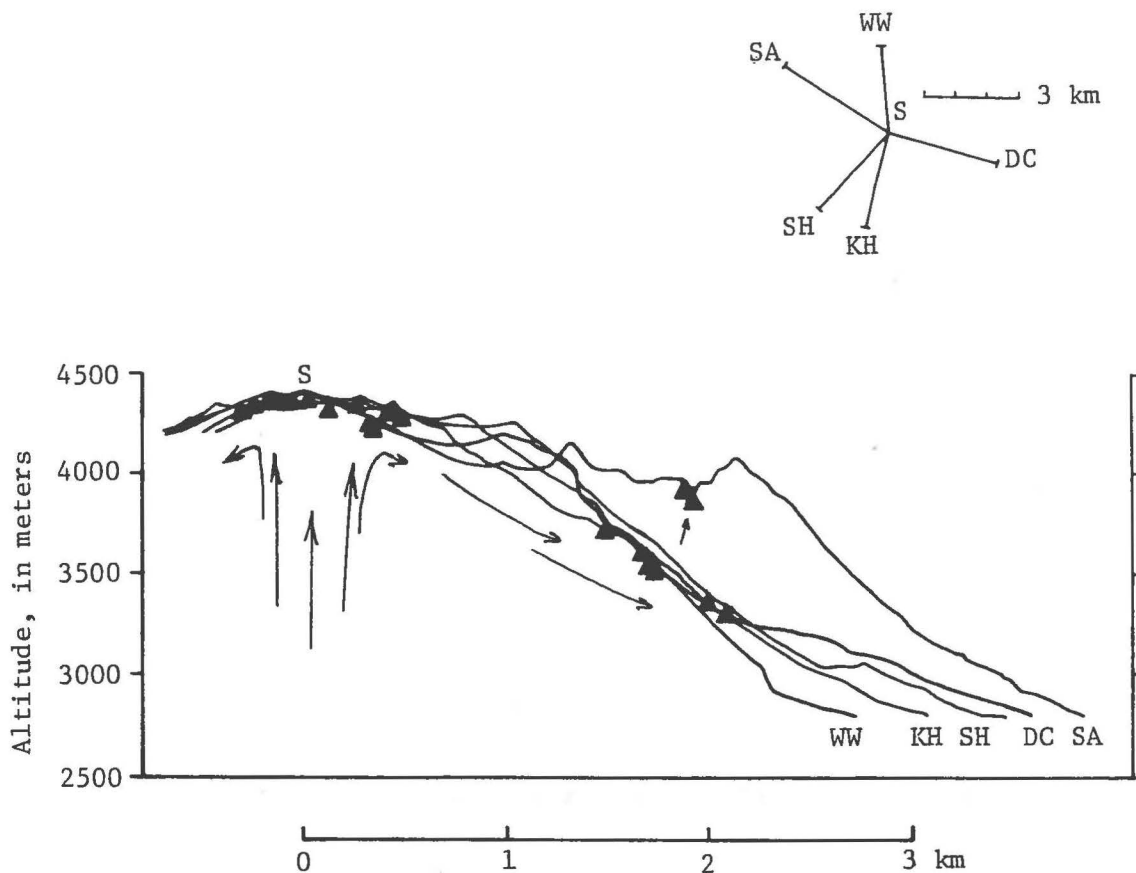


Figure 9. Overlaid cross-sections through the upper part of Mount Rainier showing spatial relationship of thermal activity (triangles) near the summit (S) and on the upper flank at Disappointment Cleaver (DC), Willis Wall (WW), Sunset Amphitheater (SA), South Tahoma headwall (SH), and Kautz headwall (KH). Upper flank thermal areas lie within a restricted region between 3350-3950 m altitude and 1.4-2.1 km from the summit. Arrows show possible paths of subsurface thermal fluids, with most upper flank thermal areas fed by downward and outward transport from beneath the summit fumarole field along permeable zones in or between outward-dipping flows and breccias. Only Sunset Amphitheater, clearly anomalous in position, contains numerous vertical structures capable of providing significant upward transport of fluid. Inset shows position of sections.

crater-wall contacts, and faults, as shown by prominent offset tephra beds (plate XI), occur in the headwall. Layered pumice and scoria (BD in plate XI) lie within an old crater formed in unbedded masses of vent-filling, hydrothermally altered rock (HA). The thermal area occurs in a buried collapse pit next to the old crater wall. Thermal fluids at Sunset Amphitheater are probably preferentially channelled through the vertical structures and may therefore arise from a greater depth than those at other upper-flank thermal areas (fig. 9).

Lower Flank

Two clusters of low-temperature thermal springs occur on the lower flank of Mount Rainier at about 2,000 m altitude. Although these springs are not of common knowledge, a few references to their activity may be found extending back many decades. Available evidence indicates little variation in spring activity during this century.

Winthrop Springs

Thermal-infrared surveys in 1972, 1973, and 1981 recorded as many as 18 previously undetected anomalies along

the west valley wall of the Winthrop Glacier. Using the survey data as a guide, field investigations discovered a cluster of at least seven thermal springs that range in temperature up to 17⁰ C and issue from a 900-m stretch of hillslope at 2040-2070 m altitude. A recent compilation of historic newspaper accounts (Majors and McCollum, 1981a, p. 442-443) revealed that in fact these springs had been observed as long ago as 1894 when a winter expedition led by E.S. Ingraham camped at the spring site and reported a maximum temperature of 16⁰ C.

Measurements in 1973, 1982, and 1983 (table 9) show that the higher altitude springs typically range in temperature from 8-17⁰ C. The highest flow is in the easternmost springs. Most of the springs issue from a moss-covered boulder and cobble talus deposit at the base of a lava cliff of olivine andesite. The largest and easternmost spring (plate XII) issues from algae-coated joints in the lava cliff. Streams fed by the springs combine with larger snowmelt streams, flow through talus and meadow below, and eventually discharge into the West Fork White River along the west margin of the Winthrop Glacier terminus. A significant amount of additional seepage also occurs through the talus.

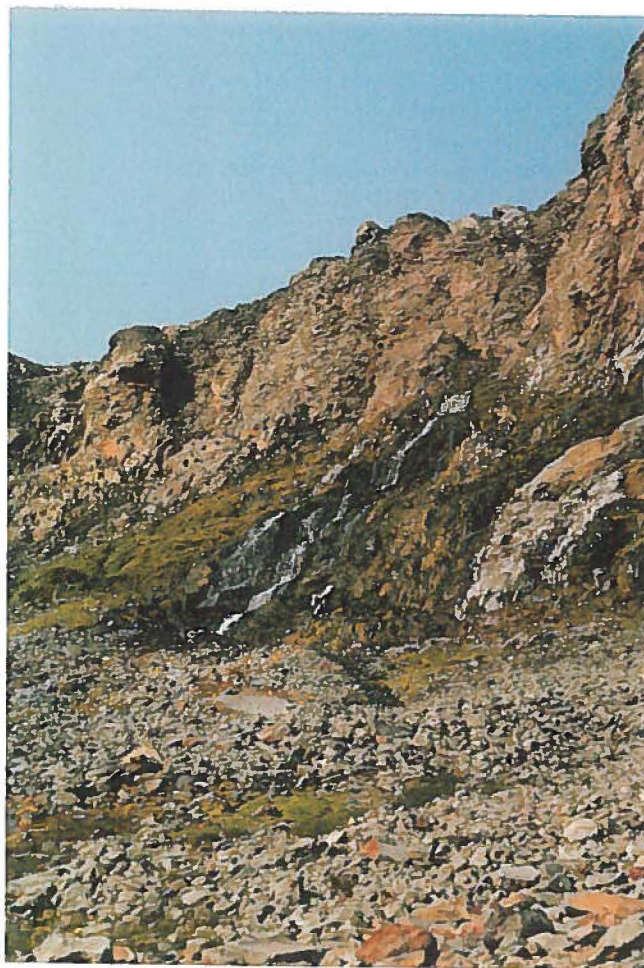


Plate XII. The main Winthrop spring (WS1) issues from algae-coated joints in a 20-m cliff in an andesite flow, and then rapidly mixes with a snow-melt stream that flows over the face of the cliff.

Table 9. Physical measurements at Winthrop Springs.

	WS-1 Main West			WS-2 East	
DATE ¹	73	82	83	82	83
TEMP, °C	11	14	11	12	11
FLOW ³ , L/s	3			0.3	
HEAT FLUX, MW	0.13			0.014	
OTHER SPRINGS					
DATE ¹	94	73	82	83	
TEMP, °C	16 ²	8-17	8-12	--	
FLOW ³ , L/s	0.3 ea				
HEAT FLUX, MW	0.014 ea				
ESTIMATED ADVECTIVE FLUX FOR 7 SPRINGS = 0.24 MW					
ESTIMATED ADVECTIVE FLUX FOR SPRINGS PLUS SEEPAGE = 0.36 MW					

¹94 - December 12, 1894 (Majors and McCollum, 1981, p. 442); 73 - August 10, 1973; 82 - September 6, 1982; 83 - August 11, 1983.

²May have been main spring.

³Estimated.

Heat flow can be determined from estimates of spring discharge and assumed average annual temperature of cold ground water. The excess advective heat flux, ΔA , due to thermal-spring discharge is obtained from

$$\Delta A = \rho Q \Delta H$$

where ρ is water density, Q is spring discharge, and ΔH is enthalpy of thermal water less enthalpy of nearby cold ground water, here assumed to be comparable to the estimated mean annual air temperature of 1° C for 2100 m altitude.

The main, easternmost spring had an estimated flow of 3 L/s, whereas the remaining six springs were about 0.3 L/s each at the time of observation in September 1982. Total spring flow was then about 3 L/s at 14° C and 1.8 L/s at 12° C respectively. Excess heat flux is then estimated at 0.24 MW for major springs. If seepage separate from the major springs provides an additional 50% flow, excess advective flux for the Winthrop Springs thermal area is about 0.4 MW for September 1982.

Paradise Springs

Thermal springs and warm seepage ranging in temperature up to 25° C occurs along a 100-m segment of the west valley

wall of the Paradise River between 1950-1980 m altitude. The main springs issue from joints in thin hypersthene andesite flows that are exposed in the valley wall (plate XIII). The zone of seepage, marked by abundant moss and algae, occurs just above a layer of well-packed interflow rubble near the base of the hillslope and from rock-slide debris and lateral moraine halfway up the slope. Spring discharge flows down the valley wall and enters the Paradise River. During the early part of this century the Paradise Glacier extended downvalley from the springs; their warm effluent may have been a factor in forming tunnels beneath the glacier (Evans, 1930) which then developed into the once spectacular Paradise Ice Caves.

Spring temperatures of 11-25⁰ C were measured during 1982-1983 (table 10). During the same period, the two largest springs were fairly uniform at 24-25⁰ and 16-17⁰ C, respectively. The warmest temperature is comparable to the few available earlier measurements of 24⁰ C in 1930 and 26⁰ C in 1966 (table 10).

Flow measurements of one of the two largest springs are 1.3-1.5 L/s. Calculations using this value, measurements and estimates of flow from other springs, and a mean annual



Plate XIII. The main Paradise spring, PS-5 issues from algae-coated joints in a 5-m cliff in an andesite flow.

Table 10. Physical measurements at Paradise Springs.

	PS1 Main upper spring					PS2 Upper south spring		
DATE ¹	82a	82b	83a	83b	83c	82a	82b	83b
TEMP, °C	16	17	17	17	17	12	24	13
FLOW, L/s		1.3	1.5					

	PS5 Main Lower Spring					PS6 Lower North Spring	
DATE ¹	30	66	82b	83b	83c	83b	83c
TEMP, °C	24	26	24	24	25	25	24
FLOW, L/s				1.7 ²		0.7	

OTHER SPRINGS		
DATE ¹	30	83b
TEMP, °C	17-24	13-16

ESTIMATED ADVECTIVE FLUX FOR 4 SPRINGS = 0.36 MW
ESTIMATED ADVECTIVE FLUX FOR SPRINGS PLUS SEEPAGE = 0.5 MW

¹30-9/1/30 (Evans, 1930); 66-8/15/66 (Crandell, unpub. comm.); 82a-6/18/82; 82b-9/3/82; 83a-6/13/83; 83b-8/8/83; 83c-9/2/83.

²Estimated.

temperature of 1° C for cold ground water at 2000 m altitude, yield an excess advective heat flux of 0.36 MW for the cluster of individual springs. If additional seepage contributes 50% more flux, total excess flux from the Paradise Springs thermal area is about 0.5 MW for September 1982.

Adjacent To Cone

Two clusters of thermal springs occur within Mount Rainier National Park, but off the volcanic edifice. Both areas are easily accessible by road and at one time supported tourist resorts. Comparison of present spring temperatures with data in older reports indicate little change in activity of these springs.

Longmire Springs

James Longmire discovered warm mineral springs in 1883 (Haines, 1962, p. 63) in what is now called Longmire Meadow. He and his family developed the area into a rustic health spa which remained in operation until 1915. Subsequently the meadow was restored to a more natural state.

Longmire Meadow is a shallow, poorly drained basin of 22,000 m² that is bisected by a small cold stream and perforated by numerous small springs with flows and temperatures which range up to 0.1 L/s and 28^o C respectively. Low travertine and tufa mounds built up by the mineralized water are scattered around the meadow. The largest mound is in the west central sector. Water is ponded in some places by travertine and in others, particularly the northern (upstream) part of the meadow, by beaver dams.

The meadow lies on a low terrace at 835 m on the floor of the Nisqually River valley (fig. 2). The terrace was formed by volcanic mudflows which originated on Mount Rainier within the last few hundred years (Crandell, 1971, p. 43). The nearest lava flows from Mount Rainier top Rampart Ridge west of the meadow and are among the oldest flows on the volcano. Bedrock beneath these flows, and probably beneath the meadow, consists of volcaniclastic rocks of the Ohanapecosh Formation (Fiske and others, 1963) of Early Oligocene age, a unit which sparsely crops out around the meadow and in the nearby Nisqually River bed. Additionally, northwest trending sills thought to be of Oligocene or Miocene age cut across Ohanapecosh rocks just north of the meadow (Fiske and others, 1963).

Majors (1962) studied Park Service records and found reference to 50 individual springs which existed in 1919-1920 with temperatures ranging up to 28^o C; on reexamining the area in 1960-1961, he found 23 springs, the remainder having been flooded or covered by travertine. Korosec (1980) measured many of the same springs in 1979 and found similar temperatures ranging up to 29^o C. Data from these studies and observations during 1981-1983 show that the springs in the southeast part of the meadow have moderate gas discharge but very little water flow, whereas those in the western part, particularly around the largest travertine mound, have larger flow and higher temperature. The center of upwelling thermal water is therefore probably beneath the large travertine mound.

This study, accordingly, concentrated on measurements and sampling of two areas in the western part of the meadow. The first is Medicine Spring - LON (#29 of Majors, 1962; LMF of Korosec, 1980; Park Service trail marker 16), which has one of the highest flows among the higher temperature springs. The second is a pool, LOX, on the west edge of the travertine mound which maintains a high temperature from seepage through the mound. A summary (table 11) of temperature measurements from these sites shows only small variation with somewhat lower temperatures in winter when much of the meadow is covered by snow, and

Table 11. Selected temperature measurements at Longmire Springs.

LON Medicine Spring				
DATE	10/4/61 ¹	7/10/79 ²	3/27-9/3/82	6/13-9/2/83
TEMP, °C	19	19	18-21	18-19
LOX Travertine Mound				
DATE	1919-1920 ¹	3/4-12/16/61 ¹	7/10/79 ²	
TEMP, °C	27-28	25-28	24	
DATE		6/24-9/3/82	6/13-9/2/83	
TEMP, °C		21-24	24-25	

¹Majors (1962).
²Korosec(1980)

during storms when increased streamflow enters the meadow.

Excess advective heat flux can be estimated from the increase in temperature (typically 4-6 K) and flow of the main surface-water streams which pass through the meadow, provided there is no change due to stored heat in ponded

water. Late summer flow measurements (table 11) of the two main inflow and outflow streams produced 24 L/s at 8⁰ C of input and 45 L/s at 14⁰ C of output. This yields an advective flux of 1.2 MW. Poned water however probably does mix with the main stream and likely provides output affected to a large degree by both solar-heating and by evaporation making the advective flux as calculated here somewhat large. Hence the flux value simply shows that excess heat discharge from the Longmire Springs is comparable to or perhaps somewhat larger than that from the lower-flank thermal springs.

Ohanapecosh Springs

During the early 20th century a health spa was developed at a small group of springs which range up to 50⁰ C on the valley floor of the Ohanapecosh River (fig. 2). Resort buildings were removed during the 1960's and the hot-spring area returned to a more natural state, though it remains adjacent to a large Park Service campground. The springs occur on the east side of the Ohanapecosh River from river level at 560 m altitude to about 30 m above the river. The springs have formed a lobate fan of travertine and tufa terraces that extend down to the river bed over an area of about 40,000 m², although over half of the fan is

now forested and no longer has any apparent discharge of thermal water. The fan covers talus and river deposits which lie over moderately dipping, bedded volcanoclastic rocks of the Ohanapecosh Formation. The nearest lava flows from Mount Rainier lie on ridgetops 7 km to the northwest of Ohanapecosh Springs.

Springs with the highest flow and temperature occur near the fan's apex, which is probably the center of upwelling thermal water. Other springs are scattered about the fan particularly in old excavations for former resort buildings and an unfinished pool as well as along the river bank where erosion has eaten into the fan's toe. A few additional thermal springs with lower temperatures occur within 400 m to the south and (Korosec, 1980, p. 80) to the northwest. Tephra Layer W (about 450 years old, Hoblitt and others, 1980) from Mount St. Helens is interbedded with the travertine (Crandell, 1969, p. 37), indicating that substantial growth of the deposit has continued during the past several hundred years. Remnants of travertine on the west bank of the Ohanapecosh River near water level attest that a more extensive deposit once extended across the present river bed.

Comparison of older measurements with those from 1982-1983 shows no appreciable change in spring activity

during the past 50 years (table 12). Majors (1962, p. 36) reported that a 1937 map in Park Service files showed 18 thermal springs, while Stearns and others (1937) noted representative temperatures of 43-49⁰ C and a flow of about

Table 12. Selected temperature measurements at Ohanapecosh Springs.

OHA Main Spring				
DATE	1937 ¹	1961 ²	3/30/72	5/22-7/7/73 ³
TEMP, °C	49	46	49	46-50
DATE	8/7/79 ⁴	6/29-9/5/82	7/18-9/4/83	
TEMP, °C	50	46-48	46-50	
OHX Upper Spring				
DATE	1961 ²	3/30/72	8/7/79 ⁴	6/29-9/5/82 7/18-9/4/83
TEMP, °C	39	37	39	38-39 38-39

¹Stearns and others (1937, p. 187).

²Majors (1962)

³Continuous record.

⁴Korosec (1980)

3.8 L/s (60 gpm). A 1961 survey by Majors (1962, p. 36-37) lists 15 springs with temperatures of 22-47⁰ C. In summer 1973, a 45-day continuous temperature record of a small spring adjacent to the warmest main spring was acquired with a Foxboro recorder (the same as described for Disappointment Cleaver). The temperature record shows only slight variations between 48-49⁰ C during the whole period.

During the present study, most measurements and sampling were conducted at the two main springs near the apex of the travertine fan. The highest of these springs, OHX (#1 of Majors, 1962; OHA of Korosec, 1980), has a maximum temperature of 39⁰ C and discharges at about 0.2-0.5 L/s into a shallow, mucky depression on a 10-m-wide travertine terrace. The hottest and largest spring, OHA (#2 of Majors, 1962; OHB of Korosec, 1980), discharges 30 m to the north into a small, algae-rich pool 1 m across and 20-30 cm deep. Runoff from these and numerous other springs produces 2-4 L/s of heated discharge into the Ohanapecosh River.

Upon neglecting the contribution of isolated springs and seepage, an average spring temperature of 50⁰ C at 4 L/s yields an excess advective flux of 0.7 MW. This value is comparable to that at the other thermal-spring areas.

~ 2.5 MW @ 4 L/s

Chapter 3

GAS AND SPRING COMPOSITIONS

Major Constituents

Summit Fumaroles

A few historic observations provide brief mention of sulfurous odor from fumaroles in the West Crater, one of the more recent being that by Kiver (1971, p. 321) in 1970. No verifiable reports of sulfurous gas from the East Crater, however, have been found. During the course of field investigations in 1982-1983, sulfurous vapors were absent in the summit area, although alteration mineralogy, as noted below, indicates that sulfurous emanations were once quite prevalent at the West Crater.

Gas samples were collected in September 1982 and August 1983 to determine the composition of fumarole vapor (table 13, fig. 10). Two samples for major components were collected in duplicate in flow-through, 100 ml glass flasks

with stop-cock seals. The flasks were connected to plastic tubing which was inserted as far as possible into fumarole openings - about 30 cm. Fumarole vapor was then drawn through the flasks by suction pump. Samples were later analyzed by gas chromatography at the USGS Hawaiian Volcano Observatory.

Table 13. Gas samples from Mount Rainier.

SAMPLE	LAT	LONG	CRATER /SECTOR	ALT m	PST TIME	TEMP °C	FUMAROLE
--------	-----	------	-------------------	----------	-------------	------------	----------

Bulk Samples

820902-1,2	465115	1214525	East/N	4346	0930	72	Rib
820902-19,20	465113	1214529	East/NW	4368	1430	79	Slot-1

Helium Samples

820902-3,4	465115	1214525	East/N	4346	0940	72	Rib
820902-21,22	465113	1214529	East/NW	4368	1100	80	Slot-2
820902-23,24	465112	1214530	East/NW	4371	1130	80	Crack
830821-1,2	465112	1214544	West/NW	4368	1305	72	Mossy
830821-9,10	465112	1214542	West/NW	4374	1400	74	Rim
830821-15,16	465113	1214529	East/NW	4368	1550	78	Slot-1
830821-17,18	465112	1214529	East/NW	4359	1700	81	Clay
830821-19,20	465115	1214526	East/N	4353	1715	75	Lip
830821-21,22	465115	1214525	East/N	4346	1730	72	Rib

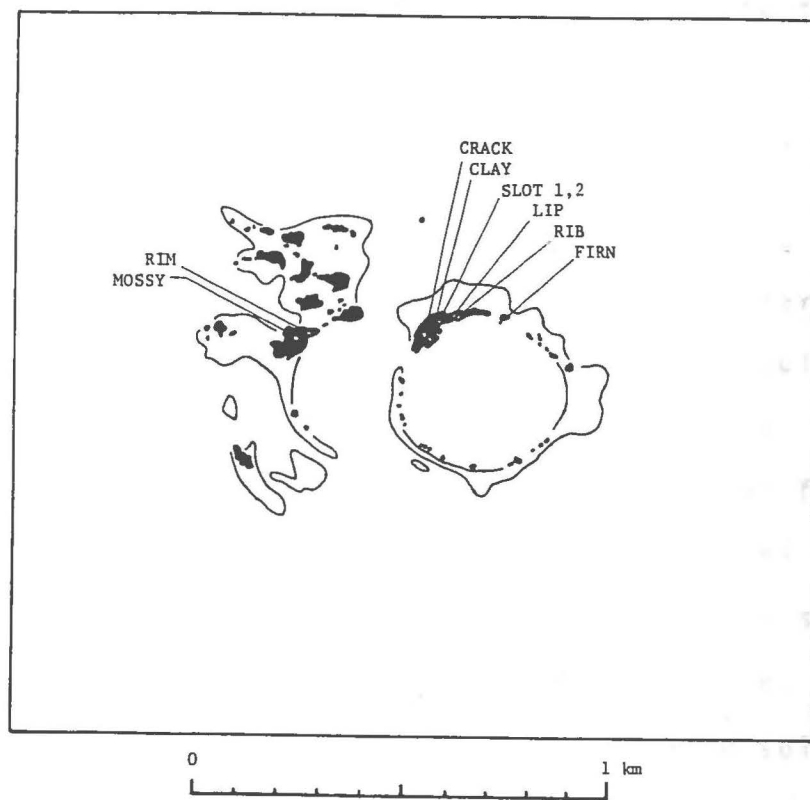


Figure 10. Localities for fumarole and firn samples at the summit craters.

Ten additional samples (table 13) were collected in evacuated test tubes for helium analysis. These samples were also collected through plastic tubing inserted in the fumaroles. Once positive flow through the tubing was achieved, 10 ml samples were withdrawn by hypodermic syringe and then expelled through rubber stoppers into the test tubes. These samples were later analyzed by mass spectrometry at the USGS Isotope Geology laboratory in Denver.

Dry gas compositions (table 14, 15) are similar to air, but with somewhat elevated levels of CO_2 and He. Sulfur gas contents were below detection level in all samples. Measurements of condensate pH were made of several fumaroles by inserting pH paper in the vent openings. Values were typically between pH 5 and 6, which at $70\text{-}80^\circ\text{C}$ is slightly acidic (neutral pH is 6.3 at 80°C). The condensate, though not analyzed, is probably a dilute carbonic acid solution. These relations indicate that fumarole vapor is simply from recycled air plus snow and ice meltwater which has been slightly charged with CO_2 and He. Except for the latter two gases the fluids have probably had little chance to undergo extensive reactions with rock and consequently have probably not traveled to any great depth.

Table 14. Composition of two fumaroles in East Crater.
 Samples collected 9/2/82. Analyzed by gas
 chromatography by L.P. Greenland, USGS, 9/13/82.
 Reported on a water-free basis.

FUMAROLE SAMPLE	RIB		SLOT-1		AVERAGE AIR ¹
	1	2	19	20	
VOL %					
O ₂ +N ₂ +Ar	98.5	98.4	96.1	95.8	99.964
CO ₂	1.50	1.65	3.87	4.23	.0325
PPM VOL					
CO	<.5	<.5	<.5	<.5	.3
CH ₄	2.0	1.9	2.3	1.9	2.0
COS	<.5	<.5	<.5	<.5	-
CS ₂	<.5	<.5	<.5	<.5	-
H ₂ S	<.5	<.5	<.5	<.5	-
SO ₂	<.5	<.5	<.5	<.5	.007
H ₂	<1	<1	<1	<1	.5
He	6	5	9	7	5.24
Ne	21	18	13	19	18.18

¹Butcher and Charlson (1972)

The source of excess CO₂ and He can best be evaluated with future isotopic studies, but some qualitative inferences may be derived from just their bulk abundances. The carbon dioxide content of 1.5-4.2% in fumarole vapor is about 50-100 times that of air (table 14). Much larger CO₂ enrichments can result from a variety of processes that would include decomposition of carbonate minerals in altered zones within the volcano or of carbonaceous sediments

beneath the cone, or degassing of a cooling magma chamber. The lack of other volcanic gases common to cooling magma, particularly H_2S or SO_2 , indicates that the fumarolic CO_2 does not come directly from magma. The relatively low CO_2 enrichment compared with more typical values of 80+% CO_2 in higher temperature fumaroles at other Cascade hydrothermal systems (Mazor and Wasserburg, 1965; Nehring and others,

Table 15. Helium concentrations in fumaroles at Mount Rainier. Analyzed by mass spectrometry by W.P. Doehring, USGS. Reported on a water-free basis.

FUMAROLE	SAMPLE	PPM	FUMAROLE	SAMPLE	PPM
<u>EAST CRATER</u>			<u>WEST CRATER</u>		
Rib	820902-3	7.7	Mossy	830821-1	8.1
	820902-4	7.7		830821-2	8.1
	830821-21	8.9			
Slot-2	820902-21	7.6	Rim	830821-9	8.2
	820902-22	7.5		830821-10	8.6
Crack	820902-23	7.6			
	820902-24	8.2			
Slot-1	830821-15	8.3	<u>DISAPPOINTMENT CLEAVER</u>		
	830821-16	8.1	DC	810805-1	3.3
Clay	830821-17	8.1		810805-2	3.4
	830821-18	8.1		810805-3	3.4
Lip	830821-19	8.3			
	830821-20	8.8			

1981) also suggests little magmatic CO_2 component in Mount Rainier fumaroles. If magmatic gases are present in the Mount Rainier hydrothermal system, they must be going into solution or reacting with minerals at depth. At least at the surface, sparse calcite coatings on explosion rubble indicate near-equilibrium conditions with respect to calcite solubility. Shallow boiling accompanied by precipitation of calcite is the most likely source of excess CO_2 in the fumarole gas.

Excess helium, because of high mobility and low reactivity, can accumulate over time from either radiogenic production in the earth's crust or from primordial sources at the earth's mantle (Ozima and Podosek, 1983, p. 140-142). Helium values in fumaroles at Mount Rainier's summit are around 8-9 ppm in comparison with 5.24 ppm for air (table 15). The lack, at present, of other evidence for deep fluid transport to the surface suggests that helium enrichment in the fumarole vapor may be from radiogenic sources.

Flank Fumaroles

Little is known of vapor composition in flank fumarole areas of Mount Rainier. Ingraham Flats at an altitude of

3400 m is a locality where hydrogen sulfide is frequently detected by climbers, though the source has never been determined. H_2S odor was also noticed in this area during the course of the present study in summer 1981 and 1982. As noted in table 8, climbers during 1956 observed possible subglacial thermal activity nearby beneath the 3600 m level of Ingraham Glacier when they noted sulfurous odor and apparent fume emanating from a large crevasse. It is possible, therefore, that subglacial fumarolic activity with an H_2S component currently exists in the Ingraham Glacier area.

The only fumarolic observations on the upper flank of any detail, however, are limited to those at Disappointment Cleaver. Helium measurements resulting from the same sampling and analytical techniques as used at the summit were acquired in 1981 for the main fumarole at Disappointment Cleaver. In contrast to the helium-enriched fumaroles at the summit, the Disappointment Cleaver samples were all depleted in He relative to air (table 15). Depletion is consistent with a mechanism by which heated fluids beneath the summit thermal field boil, lose helium, and travel downward and outward toward the flank of the cone as suggested by figure 9.

Bulk compositions are not available for Disappointment

Cleaver fumaroles. Sulfur odor was not detected there during this study, nor has it been noted in previous reports. Sulfur-bearing minerals are also absent in the thermal area (see p. 73), so the bulk gas composition is probably largely air and water vapor as it is in East Crater fumaroles.

Thermal Springs

Water samples of the four sets of thermal springs were collected during summer 1982 and 1983 and analytical results are listed in table 16. Data from samples at Winthrop and Paradise springs represent the first compositional information on thermal waters that issue from andesite flows of Mount Rainier. Older analyses for Longmire and Ohanapecosh Springs, on the other hand, can also be found in the following reports: Korosec (1980) for 1978-1979 data, Mariner and others (1982) and Nehring and others (1979) for 1977 data, and Campbell and others (1970) for 1969 data.

In addition to thermal waters, adjacent cold waters from springs or streams were also analyzed during 1982-1983 to provide representative samples of potential shallow diluent water that could mix with and alter the composition of the thermal water. These samples include cold spring and

Table 16. Composition of thermal springs and adjacent cold water during 1982-1983. Dissolved constituents in mg/L; Eh in volts; SP CD in microsiemens; T in degrees Celsius. IS-ionic strength. IB-ionic balance. ALK-titration alkalinity as CaCO₃. HCO₃-ALK as HCO₃ except where noted. *-from CO₂ electrode. ()-estimated value. (ND)-not determined.

16A. Winthrop springs. WS-1, southeastern main spring; WS-2, northwestern spring; WS-3, cold spring southwest of WS-1; WS-4, cold stream southwest of WS-1.

16B. Paradise Springs. PS-1, upper main spring; PS-2, south upper spring; PS-5, lower main spring; PS-3, south cold spring; PS-4, northern cold stream.

SITE	WS-1	WS-1	WS-2	WS-2	WS-3	WS-4
DATE	820906	830811	820906	830811	820906	830811
TIME	1100	0900	1230	1200	1200	1100

K	5.1	3.0	6.9	4.4	.2	<.2
Na	28	20	34	28	.8	<.05
Li	.027	<.05	.028	<.05	.005	<.05
Ca	9.4	6.5	10	8.4	.40	.24
Mg	8.6	6.0	10	8.7	.20	.058
Mn	<.001	<.07	<.001	<.07	<.001	<.07
Fe	<.003	<.009	<.003	<.009	<.003	<.009
Al	<.010	.013	.010	.018	<.010	.021
Cl	2.1	1.5	2.1	1.6	(.40)	.10
F	.4	.4	.3	.3	<.1	<.1
S04	96	65	110	96	(1.6)	<.01
ALK	18	18	44	26	8.0	ND
HCO3	22	22	54	32	9.8	.24*
SiO2	49	43	46	44	4.8	<2.5
B	.12	.14	.15	.18	<.010	<.06
NH4,N	ND	<.01	ND	.02	ND	<.01
NO2,N	ND	<.02	ND	<.02	ND	<.02
NO3,N	ND	<.1	ND	<.1	ND	<.1
PO4,P	ND	.06	ND	.04	ND	.01
Ba	ND	<.03	ND	.062	ND	<.03
PH	7.1	7.3	(6.6)	6.6	5.3	5.4
EH	ND	.44	ND	ND	ND	.56
SP CD	310	190	360	280	9.2	1.7
T	14.0	10.8	12.0	10.8	9.0	.1
IS	.0030	.0028	.0047	.0039	.00018	.000025
IB	1.9%	-0.4%	-4.5%	-2.3%	-45%	

SITE	PS-1	PS-1	PS-1	PS-2	PS-5	PS-5	PS-3	PS-4
DATE	820618	820904	830808	820618	820904	830808	820904	830808
TIME	1840	1450	1200	1900	1540	1400	1630	1700

K	11	9.6	8.9	6.9	16	18	.9	<.2
Na	56	57	49	34	100	90	2.8	.43
Li	ND	.086	.064	ND	.15	.116	.011	<.05
Ca	28	28	23	15	49	44	1.7	.41
Mg	20	20	17	11	36	33	.81	.104
Mn	<.001	.003	.073	<.001	.001	.071	<.001	<.07
Fe	<.003	<.003	.009	<.003	<.003	.013	<.003	<.009
Al	.010	.030	.018	<.010	<.010	.011	.010	<.03
CL	42	40	36	24	72	71	1.4	.2
F	.2	.3	.3	.2	.4	.4	<.1	<.1
S04	120	120	100	65	210	200	4.8	.019
ALK	114	107	103	68	195	191	17	ND
HCO3	139	130	126	83	238	233	21	4.2*
SiO2	78	86	80	51	130	130	13	2.5
B	.53	.54	.52	.32	.94	.90	.020	.068
NH4,N	ND	ND	<.01	ND	ND	.03	ND	.02
NO2,N	ND	ND	<.02	ND	ND	<.02	ND	<.02
NO3,N	ND	ND	<.1	ND	ND	<.1	ND	<.1
PO3,P	ND	ND	.04	ND	ND	.10	ND	.02
Ba	ND	ND	ND	ND	ND	ND	ND	ND
PH	5.6	6.0	6.2	6.0	6.2	6.2	5.7	7.0
EH	ND	ND	.46	ND	ND	.35	ND	.49
SP CD	590	650	570	380	980	1000	33	3.8
T	16.0	16.5	17.0	12.0	24.0	24.0	2.0	7.2
IS	.0081	.0080	.0069	.0047	.014	.013	.00052	.00008
IB	-1.9%	0.1%	-2.7%	-1.4%	-0.7%	-3.9%	-64%	-39%

Table 16. Continued.

16C. Longmire Springs. LON, main southwestern spring; LOX, pool west side of travertine mound; LOT, main outflow stream; LIN, main inflow stream.

16D. Ohanapecosh Springs. OHA, main spring; OHX, upper southeastern spring; OHC, eastern cold stream.

SITE DATE TIME	LON-15 820904 0930	LON-15 830902 1400	LOX 820904 1000	LOX 830902 1500	LON-OUT 820904 0900	LON-OUT 830901 1700	LON-IN 820904 0830	LON-IN 830901 1540
K	46	40	52	40	11	7.6	.80	.76
Na	640	530	710	540	140	86	2.9	2.4
Li	2.2	2.0	2.5	2.1	.53	.29	.011	<.03
Ca	550	510	500	420	110	69	4.6	4.0
Mg	170	140	190	140	38	25	.79	.84
Mn	2.0	1.8	1.4	1.2	.50	.31	.011	.071
Fe	(13.0)	13.0	(13.0)	11.5	2.6	1.10	.15	.24
Al	<.010	<.01	ND	<.01	<.010	.050	.010	.034
Cl	870	540	1000	940	210	140	1.7	1.6
F	.4	.4	.4	.4	.1	.1	<.1	<.1
S04	46	46	36	30	11	7.3	(5.2)	4.7
ALK	2170	2240	2100	2050	443	306	18	18
HCO3	2650	2730	2560	2500	540	373	22	22
SiO2	120	130	120	130	44	38	26	21
8	3.8	3.2	4.3	3.6	.82	.59	<.010	.076
NH4,N	ND	.51	ND	.37	ND	ND	ND	.02
NO2,N	ND	<.02	ND	<.02	ND	ND	ND	<.02
NO3,N	ND	<.1	ND	<.1	ND	ND	ND	<.1
PO3,P	ND	<.01	ND	<.01	ND	ND	ND	<.01
8a	ND	.34	ND	.32	ND	.073	ND	<.03
PH	6.1	6.2	6.0	5.9	6.2	6.7	5.6	6.4
EH	ND	.17	ND	.12	ND	.19	ND	.39
SP CD	5700	5700	5900	5600	1400	1020	43	39
T	19.5	18.8	24.0	25.4	14.0	12.7	8.0	8.2
IS	.084	.074	.086	.074	.019	.012	.00069	.00063
IB	1.8%	0.8%	2.0%	-8.7%	0.6%	-3.5%	-7.2%	-11.1%

SITE DATE TIME	OHA 820905 1130	OHA 830904 1630	OHX 820905 1100	OHX 830904 1530	OHA-C 820905 1030	OHA-C 830905 1200
K	48	46	51	48	1.6	1.9
Na	950	810	970	790	40	39
Li	3.1	2.8	3.0	2.7	.13	.08
Ca	64	55	68	58	18	18
Mg	5.1	4.5	4.2	4.6	1.8	1.9
Mn	.08	.12	.17	.16	<.001	<.07
Fe	.10	.35	.87	.82	<.003	.015
Al	<.010	.040	<.010	.045	<.010	.025
Cl	920	960	930	910	40	41
F	5.5	5.9	5.4	5.9	.2	.3
S04	170	180	170	170	10	9.0
ALK	834	850	816	852	80	82
HCO3	1020	1040	995	1040	98	100
SiO2	95	98	94	96	12	11
8	12	11	12	11	.55	.56
NH4,N	ND	.18	ND	.19	ND	ND
NO2,N	ND	<.02	ND	<.02	ND	ND
NO3,N	ND	<.1	ND	<.1	ND	ND
PO4,P	ND	.02	ND	<.01	ND	ND
Ba	ND	.13	ND	.11	ND	<.03
PH	6.5	6.6	6.6	6.5	5.5	7.3
EH	ND	.11	ND	.13	ND	.49
SP CD	4400	4400	4400	4400	330	300
T	48.0	45.8	38.0	38.7	6.5	6.8
IS	.049	.046	.049	.045	.0035	.0035
IB	0.1%	-9.5%	1.5%	-8.6%	-1.8	-3.2

snow-melt runoff (WS3, PS3 and WS4, PS4 respectively) near Winthrop and Paradise springs, and cold streamflow resulting from a combination of snowmelt runoff and groundwater discharge (LOI, OHC) at Longmire and Ohanapecosh Springs.

Field measurements were made of pH, Eh, conductivity and titration alkalinity. Samples for later lab analysis of dissolved constituents were passed through 0.45 μm cellulose filters; those for cation analysis were acidified with nitric acid. Samples for nutrient and stable-isotope analysis were left unfiltered but were treated with HgCl_2 to stop biological activity; nutrient samples were kept chilled prior to analysis.

Major and selected minor constituents were analyzed in 1982 at the U.S. Geological Survey Central Laboratory in Denver by methods found in Skougstad and others (1979); 1983 samples were analyzed in part at Denver and at Geological Sciences laboratories at the University of Washington (table 17).

An overview of the spring composition reveals the major features of thermal water, establishes some constraints on important factors that control water composition, and sets the stage for more detailed consideration of aqueous-mineral reactions in Chapter 5. All of the spring waters are near neutral; pH ranges from 5.6 to 7.3. Most dissolved

Table 17. Methods of water analysis. Analyses by USGS laboratory using methods of Skougstad and others (1979), except where noted.

CONSTITUENT	METHOD ¹	
	1982	1983 ²
K	AA	ICP
Na	AA/ICP	ICP
Li	AA/E	ICP
Ca	AA/E	ICP
Mg	AA/ICP	ICP
Mn	AA/ICP	ICP
Fe	AA/ICP	ICP/ thioglycollate ³
Al	AA with chelation- extraction	ICP
Cl	C ferric thiocyanate	C ferric thiocyanate
F	ISE	ISE
S04	C methylthymol blue	C methylthymol blue/ T Dithizonate ³
ALK	T pH	T pH ³
B	C	ICP
Si02	C molybdate blue/ICP	ICP
NH4,N		C indophenol
NO2,N		C cadmium reduction diazotization
NO3,N		C diazotization, calculation
P04,P		C phosphomolybdate
Ba		ICP

¹ AA-atomic absorption spectrophotometry; ICP-inductively coupled plasma spectrophotometry; E-emission spectrophotometry; T-titration with indicator; C-colorimetry with indicator; ISE-ion selective electrode.

² 1983 ICP, C. Cool, analyst.

³ D. Frank, analyst; Fe-Carmichael (1970); S04-White (1959, 1960); ALK-Wood (1976).

constituents increase in concentration with temperature in order from Winthrop, Paradise, Longmire, to Ohanapecosh Springs (fig. 11). Total dissolved solids, as calculated by summation, increases from moderate values of about 270 and 850 mg/L respectively for Winthrop and Paradise Springs up to 3300 and 5200 mg/L for Ohanapecosh and Longmire Springs. Cold water adjacent to the thermal springs contains less than 70 mg/L, except for the cold stream at Ohanapecosh which apparently contains a small component of thermal water.

Gross spring compositions, as summarized in a Piper (1944) diagram (fig. 12), show a distinct grouping for each of the four clusters of springs. The thermal-water types classified according to species greater than 50% abundance include Na-SO₄ water at Winthrop Springs and Na-Cl water at Ohanapecosh Springs. More complicated water types according to species greater than 30% abundance include Na-SO₄-HCO₃ water at Paradise Springs and Na-Ca-HCO₃-Cl water at Longmire Springs. In contrast, cold water adjacent to the thermal springs is a Ca-Na-HCO₃ type at Longmire and Na-HCO₃ at the other areas (table 16). Samples from three wells in the Ohanapecosh Formation outside of the National Park at Ashford, Packwood, and Silver Springs, within 21-29 km of the summit, are all Ca-Na-HCO₃ water (USGS, unpublished data, 1982).

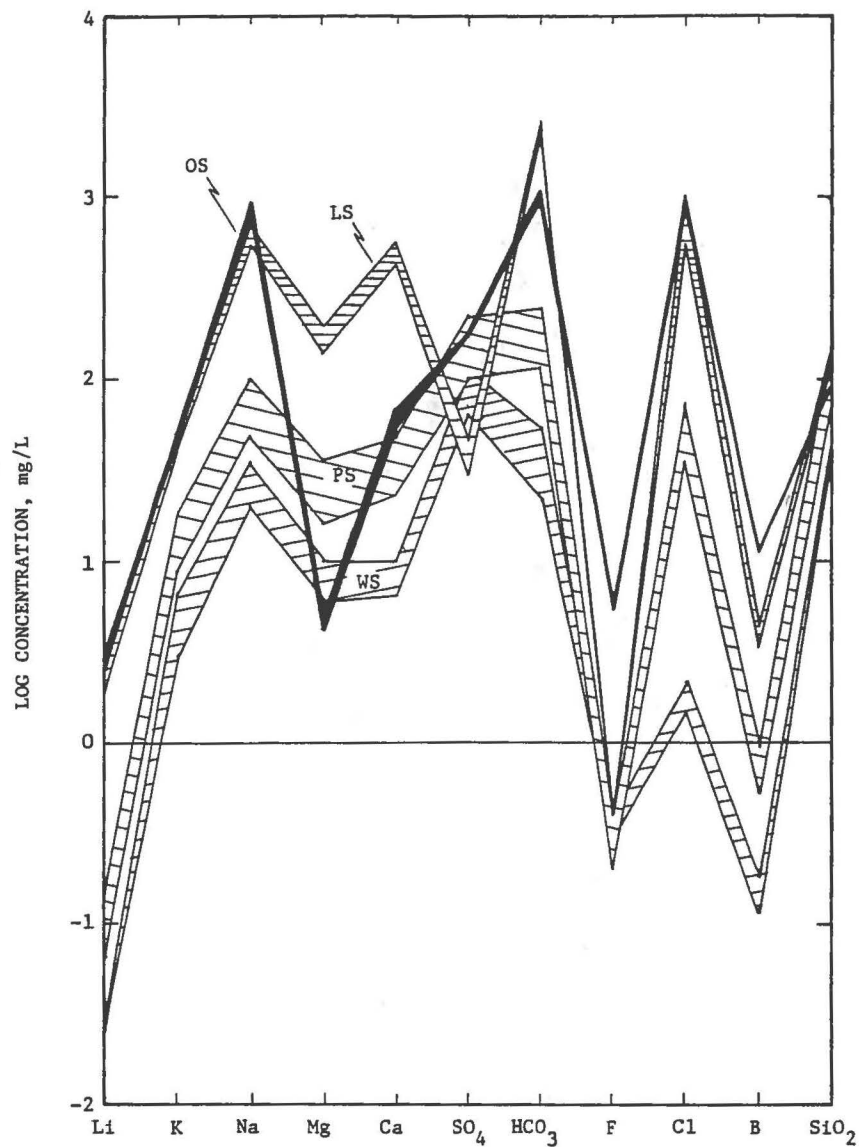


Figure 11. Range of concentration of selected dissolved constituents in the main thermal springs at each site. WS-Winthrop springs, PS-Paradise springs, LS-Longmire Springs, OS-Ohanapecosh Springs.

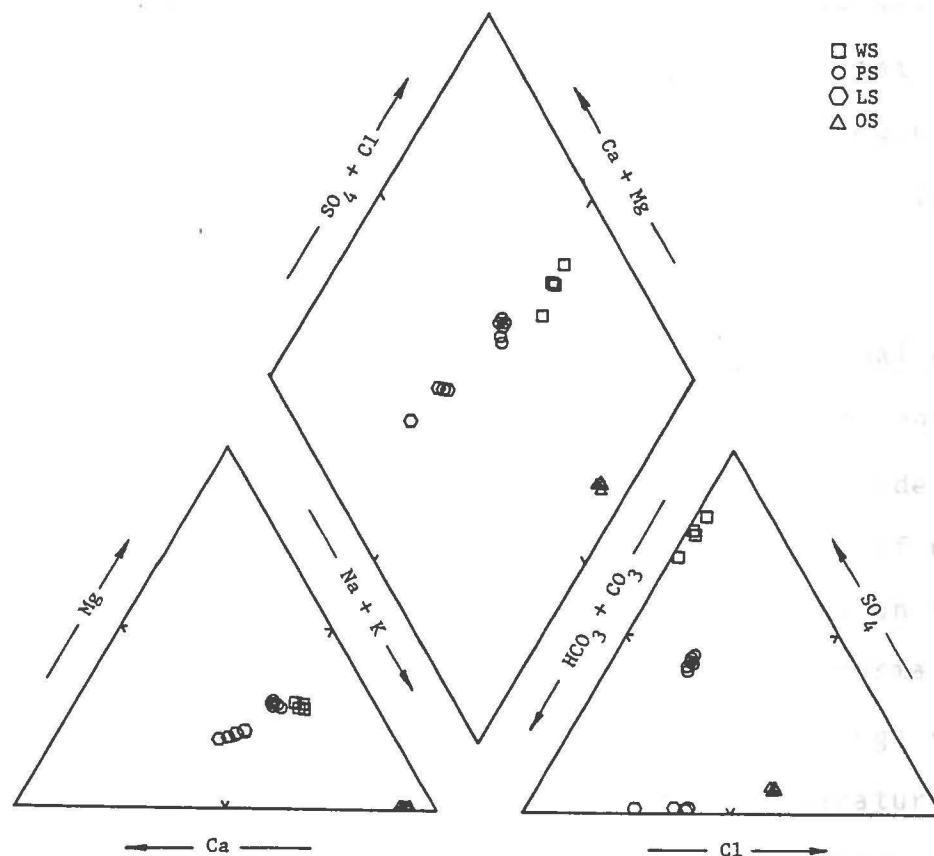


Figure 12. Trilinear diagram of percentage equivalents of major ions in thermal springs. Winthrop (WS) and Paradise (PS) springs contain a large fraction of SO_4 , whereas Ohanapecosh (OS) and Longmire (LS) Springs are primarily Cl and $\text{HCO}_3\text{-Cl}$ waters respectively.

Distinctive features of some of the waters include enrichment of dissolved CO_2 species by a calculated PCO_2 value 3 orders of magnitude greater than atmospheric ($\log \text{PCO}_2 = -3.5$) at Paradise and Ohanapecosh Springs, and by 4 orders at Longmire Springs. Other unusually abundant species include iron (11-13 mg/l) and manganese (1.2-2.0 mg/L) at Longmire, and fluoride (5.4-5.9 mg/L) and boron (11-12 mg/L) at Ohanapecosh Springs.

Evidence of near-surface mixing between thermal water and cold ground water may be found in large variations of conservative dissolved constituents, such as chloride, among the warmest springs. To evaluate the possibility of mixing, figure 13A was constructed to show available data on the variation of chloride with temperature for the thermal springs. Values from 7 sites at Ohanapecosh Springs show at most a 170 mg/L range (17% of mean) over a temperature interval of 20°C . Chloride variations in the other spring areas are, in contrast, much greater and indicate significant mixing. Field measurements of conductivity are much more plentiful than chloride analyses and can be used as a surrogate for dissolved species. The conductivity measurements display similar trends (fig. 13B) with a variation at Ohanapecosh of only $800 \mu\text{S}$ over a 38° interval indicating cooling primarily by conduction rather than by

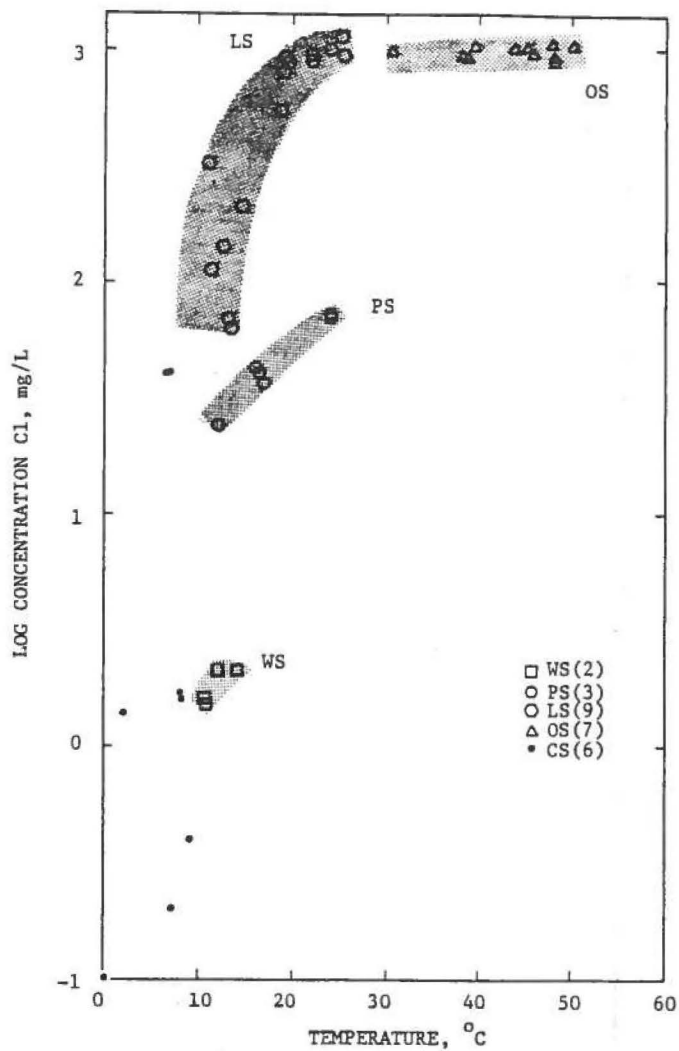
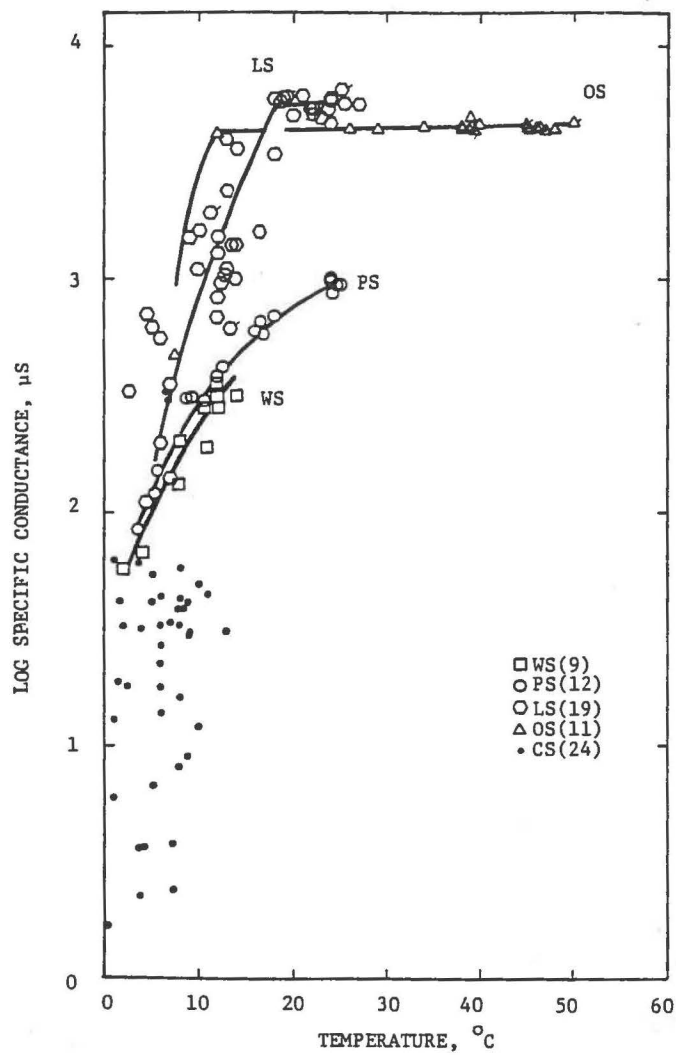


Figure 13. Variation of Cl and specific conductance with temperature. WS-Winthrop springs, PS-Paradise springs, LS-Longmire Springs, OS-Ohanapecosh Springs, CS-adjacent cold and streams. Number of sample sites are indicated in parentheses. Repetitive measurements for several sites are shown.

13A. Chloride concentrations.



13B. Specific conductance.

mixing. Conductivity values also suggest that conductive cooling may take place in the warmest springs at Longmire, though the data there are much less convincing than at Ohanapecosh.

A variety of empirical geothermometers (Fournier, 1981) have been developed during the past 20 years to estimate aquifer temperatures based on the last equilibration between rock and thermal water. Requirements for these estimates to be valid include a temperature-dependant equilibration of water with a particular mineral or mineral assemblage in an aquifer, insignificant reequilibration between the aquifer and the sampling point, and lack of mixing with water of different composition. Among the geothermometers considered here are the silica (quartz, chalcedony, cristobalite, amorphous silica), Na/K, Na-K-Ca, Na-K-Ca with Mg correction, sulfate-oxygen isotope, and lithium geothermometers.

Only Ohanapecosh Springs meets assumptions necessary for strict application of some of these geothermometers. Rough correspondence of the quartz and magnesium-corrected Na-K-Ca geothermometers (table 18) indicate a last subsurface equilibration temperature of about 134-146⁰ C. Somewhat higher temperatures of 150-178⁰ C are suggested by the Na/K and Na/Li geothermometers and these may represent

Table 18. A variety of aquifer temperatures based on various geothermometers. Methods from Fournier (1981) except where noted. Only Ohanapecosh Springs meets the assumptions suitable for application of the Na-K-Ca-Mg and SiO₂-quartz geothermometers. Values in degrees Celsius.

SITE DATE	PS1 6/82	PS1 9/82	PS1 8/83	PS2 6/82	PS5 9/82	PS5 8/83	LON 9/82	LON 9/83	LOX 9/82	LOX 9/83	
OBSERVED TEMP	16	17	17	12	24	24	20	19	24	25	
SiO ₂											
Quartz	124	129	125	103	152	152	148	152	148	152	
Chalcedony	96	101	97	73	127	127	122	127	122	127	
Cristobalite	73	78	74	52	102	102	97	102	97	102	
Amorphous	--	--	--	--	31	31	26	31	26	31	
Na/K	283	266	274	286	261	285	190	194	192	193	
Na-K-Ca ¹	88	84	84	81	95	101	97	92	106	97	
Na-K-Ca-Mg	30	30	30	32	26	27	56	61	48	56	
Na/Li ²	--	100	91	--	99	92	157	165	159	167	
Mg/Li ³	--	25	20	--	30	26	76	76	78	77	
SITE DATE	WS1 9/82	WS1 8/83	WS2 9/82	WS2 8/83			OHA ⁴ 7/77	OHA 9/82	OHA 9/83	OHX 9/82	OHX 9/83
OBSERVED TEMP	14	11	12	11			48	48	46	38	39
SiO ₂											
Quartz	101	95	98	96			137	134	136	134	135
Chalcedony	71	64	68	66			110	107	109	107	108
Cristobalite	50	45	48	46			--	83	85	83	84
Na/K	274	254	286	259			--	165	173	167	178
Na-K-Ca ¹	79	67	90	77			--	165	169	167	172
Na-K-Ca-Mg	28	27	21	26			135	141	141	146	142
Na/Li ²	75	--	67	--				153	158	149	157
Mg/Li ³	10	--	9.6	--				146	145	149	143
S04- ¹⁸ O	--	--	--	--			111	--	--	--	--

¹ =1/3 for Ohanapecosh; =4/3 for all others.

² Fouillac and Michard (1981).

³ Kharaka and others (1985).

⁴ From Nehring and others (1979).

an equilibration temperature prior to mixing with cooler water at depth. The wide variety of temperatures computed from the geothermometers for the other springs results either from water compositions which are controlled by chemical equilibration in more than one aquifer, from lack of equilibration, or from invalid application of a particular geothermometric method. Interpretation of the temperature values in table 18 is therefore fraught with difficulty. Chapter 5 addresses other methods for reconstructing aquifer temperatures.

Stable Isotopes

Hydrogen and oxygen isotopic composition was examined to provide information on the extent of rock-water interaction and evaporation, the recharge altitude of spring water, and the relationship between summit fumarole condensate and summit recharge water.

Rock-Water Interaction and Evaporation

Craig (1961a) showed that stable isotopes in meteoric water follow a linear trend, the Mean Meteoric Water Line (MMWL)

$$\delta D = 8 (\delta^{18}O + 10\text{‰})$$

where

$$\delta = 1000 \left(\frac{R_{\text{sample}}}{R_{\text{standard}}} - 1 \right)$$

and

$$R = {}^{18}O/{}^{16}O \text{ or } D/H.$$

The standard used here is SMOW (Standard Mean Ocean Water, Craig, 1961b).

Craig (1963) further showed that deuterium in many geothermal waters has an abundance similar to nearby meteoric water, whereas oxygen-18 typically displays a distinctive shift toward higher values as a result of reactions with rock at elevated temperatures. Most, but not all, deep waters greater than 90°C in major hot-water or vapor-dominated geothermal systems show an oxygen shift; exceptions occur where either temperatures are relatively low (below 150°C), or the rock in contact with thermal water has low ${}^{18}O$ (Truesdell and Hulston, 1980, p. 180-183). In some geothermal waters where evaporative concentration is the main factor affecting isotopic composition, enrichment of both ${}^{18}O$ and D is observed (Giggenbach and Stewart, 1982).

Samples for stable isotope analyses were collected from

thermal springs and adjacent cold waters at each of the four spring clusters and tightly sealed with a plastic cap overlain by flexible, wax-coated plastic. Bacterial growth was stopped with mercuric chloride prior to sealing. Isotopic compositions (table 19) were determined by mass spectrometry at the USGS Water Resources Division laboratory in Reston, Virginia.

As shown by figure 14, all of the thermal and cold waters closely follow the MMWL within 1% $\delta^{18}\text{O}$ and 10% δD . Hence the stable isotopes show no appreciable oxygen shift as a result of interaction with rock, or hydrogen shift as a result of evaporation.

Recharge Altitude

Stable isotopes in atmospheric water vapor undergo temperature-dependant fractionation when water is removed by precipitation. The amount of fractionation varies with changes in air temperature and, thus, with altitude. Likewise, the mean annual isotopic composition of ground water, whether it be from rainfall or from melting snow, also varies with altitude; under favorable conditions, the general trends may mimic that of precipitation (Fontes, 1980, p. 91-98).

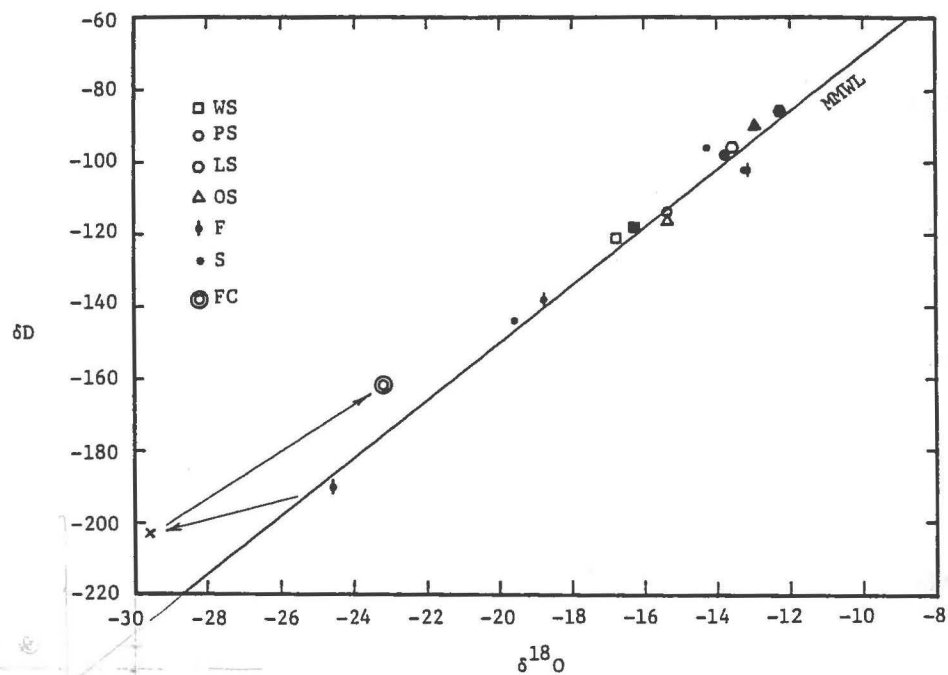


Figure 14. Oxygen and hydrogen isotope composition of thermal springs (open symbols) and adjacent cold springs and streams (closed symbols) at Winthrop (WS), Paradise (PS), Longmire (LS), and Ohanapecosh (OS) Springs; of snow (S) and firn (F) on the upper flank and at the summit; and of fumarole condensate (FC) and vapor (X-calculated) at the summit. Path of fumarole composition (arrows) discussed in text.

Table 19. Stable-isotope compositions of snow (S), firn (F), thermal springs and adjacent coldwater.

LOCALITY	ALTITUDE m	DEPTH TO FIRN cm	$\delta^{18}\text{O}$ ‰	δD ‰	DATE
Muir Peak Snow	2,960	200	-13.3	-102	8/19/82
Firn			-13.2	-102	
Ingraham Flats Snow	3,410	500	-19.6	-144	8/20/82
Firn			-18.8	-138	
East Crater Snow	4,330	77	-14.3	-96	9/02/82
Firn			-24.6	-190	

LOCALITY	ALTITUDE m	ALTITUDE RANGE OF DRAINAGE BASIN m	$\delta^{18}\text{O}$ ‰	D ‰	TEMP °C
Winthrop Springs WS1	2040		-16.8	-121	14.0
WS3	2070	2070-2210	-16.3	-118	9.0
Paradise Springs PS5	1950		-15.4	-114	24.0
PS3	1910	1910-2010	-13.8	-98	2.0
Longmire Springs LON	840		-13.6	-96	19.5
LOC	850	850-1180	-12.3	-86	8.0
Ohanapecosh Springs OHA	590		-15.4	-116	48.0
OHC	610	610-1370	-13.0	-90	6.5

The isotopic data from Mount Rainier may be used to estimate an altitude-composition relationship for cold recharge waters, and from that derive the recharge altitude of thermal waters. A light isotopic composition for thermal water relative to cold water would imply a higher altitude of recharge for the thermal water and hence a longer flow path through the volcanic cone. The Rainier data are particularly applicable to this type of analysis since enrichment effects of rock interaction or evaporation are minimal or absent.

Cold waters that were sampled with thermal springs include nearby springs and surface streams that represent a mixture of snowmelt runoff and ground-water discharge. Isotopic composition of the cold waters then represents recharge values from a range of slightly higher altitudes that are here estimated by the altitude range of the enclosing local drainage basin (table 19).

At altitudes above the firn line where springs and perennial surface waters are absent, samples of snow and firn were collected to estimate the isotopic composition of recharge. These samples (table 19) were collected by excavation at three localities which include a snow pit at Muir Peak, the wall of a freshly formed crevasse at Ingraham

Flats, and the wall of an ice cave at East Crater. The samples were melted by heating in closed containers to prevent vapor exchange with the atmosphere and then bottled in the same manner as the spring samples.

Ideally in this type of study, one would sample a complete firn section to estimate recharge composition at a particular locality. However, practical obstacles limited sampling to above and below the snow-firn contact. Such sites allow an approximate age determination of the samples and an estimate of relative homogenization of isotopes in the snow and firn by sampling within a close distance 3/4-year-old early fall snow and 1 1/4-year-old spring firn.

Figure 15 shows the variations in isotopic composition with altitude for the two groups of samples. The low-altitude samples of the cold surface waters have a variation remarkably close to the average variation of $-3\% / \text{km } \delta^{18}\text{O}$ determined by Burk (1979, p. 69-71; see also Burk and Stuiver, 1981) from analyses of precipitation at 300 to 1,200 m altitude at Pack Forest, Nisqually Entrance, Longmire, and Nisqually Bridge. Higher altitude samples of firn show a variation of about $-9\% / \text{km } \delta^{18}\text{O}$ and $-65\% / \text{km } \delta\text{D}$. The latter compares favorably with $-50\% / \text{km } \delta\text{D}$ for snow and firn from 1400-2200 m at Blue Glacier, Washington (Sharp and

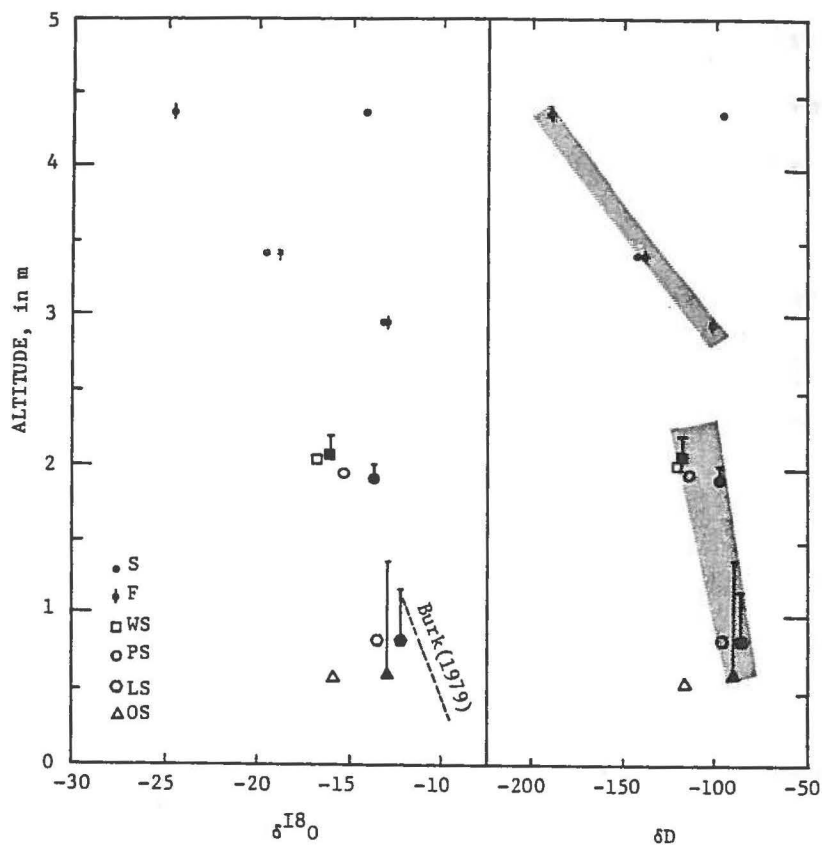


Figure 15. Variation of stable-isotope composition with altitude for thermal (open symbol) and nearby cold (solid symbol) water at Winthrop (WS), Paradise (PS), Longmire (LS), and Ohanapecosh (OS) Springs, and for firn (F) and snow (S). Bars on the top of cold-water symbols indicate range of altitude from which water originated based on respective drainage basins. Burk's (1979) trend based on precipitation on south side of Mount Rainier.

others, 1960, p. 4047), a range of -20 to -40‰/km for snow cores from 1600-3500 m in the Sierra Nevada (Friedman and Smith, 1970), and -20 to -60‰ for fresh snow from 800-3300 m in the Mont Blanc Alps (Moser and Stichler, 1970, p. 46).

In the interpretation of these data it is assumed that the isotopic compositions represent mean annual values. This assumption is tenuous at best in view of the scarcity of data, but is included here for sake of further discussion. As Burk's (1979) low-altitude data are based on an average of many samples during 1976-1978, they are reasonable values for the mean annual composition of precipitation in the Mount Rainier area.

With respect to the higher altitude data, the temperate climate of western Washington keeps buried snow near 0° C and, during firnification, should tend to homogenize the isotopic composition of the snowpack at depth (Dansgaard and others, 1973, p. 12). Below that depth the composition may approximate the eventual groundwater recharge at that altitude, although other factors including evaporation can alter composition. At the highest altitudes in temperate regions, snow and firn may become polar and isotopic compositions may not be homogenized. Isotopic values under polar conditions maintain the well-known records of precipitation events used to interpret paleoclimates (Robin,

1983).

Mount Rainier data indicate that homogenization of stable isotopes in the snow and firn decreases with increasing altitude (table 19) so that the summit snow and firn can be quite different in composition. Nonetheless, the summit firn values are used here to establish an isotope-altitude relationship. Although the seemingly linear trend with respect to lower-altitude firn samples (fig. 15) may be quite fortuitous, it is comparable to that found in other alpine areas.

The variation in isotopic composition of recharge water with altitude should probably not show the abrupt discontinuity seen in figure 15, but instead should vary gradually as the proportion of recharge from snowmelt increases over that from rainwater. Keeping in mind the possible differences between available data and true mean annual isotopic composition, figure 15 suggests that all thermal springs have been recharged at higher altitudes than the cold water, though none are as isotopically light as the summit firn. Furthermore, the isotopic difference between the warm and adjacent cool waters at the thermal sites increases with temperature.

Summit Fumarole Condensate

One sample for stable-isotope analysis of fumarole condensate was collected from Rib fumarole (72°C) in the East Crater (fig. 10) in September 1982. Condensate was dripped from tubing into a 20-ml glass vial. The isotopic composition (fig. 14) was

$$\delta^{18}\text{O} = -23.2 \pm 0.2 \text{ per mil}$$

$$\delta\text{D} = -162 \pm 2 \text{ per mil.}$$

Since the method of collection should yield a fractionated water at 72°C, the vapor composition may be recalculated using fractionation factors compiled by Friedman and O'Neil (1977) to yield

$$\delta^{18}\text{O} = -29.6\%$$

$$\delta\text{D} = -203\% .$$

Mass balance of the deuterium content in the fumarole vapor, in comparison with values discussed above taken from firn (assumed to be representative of recharge water in the East Crater), indicate that about 22% of the recharge is lost by evaporation. The depleted isotopic composition of vapor with respect to firn is consistent with fumarole vapor that originates as secondary steam from a shallow water

table which has been heated by underlying primary steam (Giggenbach and Stewart, 1982). Figure 14 shows a possible fractionation path from summit firn to 86⁰ C vapor to 72⁰ C fumarole condensate.

Chapter 4

ALTERATION MINERALOGY

Hydrothermally formed minerals were examined in 160 samples selected from 70 outcrops at 2 fumarole fields, the four sets of thermal springs, eight debris avalanches and mudflows, and three tephra deposits. The samples represent both surficial alteration near fumaroles and springs, and subsurface alteration at source areas of the avalanches, mudflows, and tephra.

Analytical Methods

About 30 of the samples were studied in thin sections with the petrographic microscope; most of these and the remaining samples were examined by X-ray diffraction (XRD) using a Picker-Nuclear powder diffractometer with nickel-filtered $\text{CuK}\alpha$ radiation. Bulk samples for XRD were ground to $<50\ \mu\text{m}$ and side-packed into aluminum boxes to produce patterns of unoriented material. Oriented mounts were obtained from either smears or sedimentation onto glass

slides. In addition, key samples were split into size fractions by sieving and sedimentation, and then stripped of organic material, soluble carbonates, and free iron oxides (Kittrick and Hope, 1963; Jackson, 1969) for more detailed analysis. Clay fractions were heated to 300^o and 550^o C after potassium saturation of exchangeable ions, and intercalated with ethylene glycol after magnesium saturation. Clay mineral identification was based on criteria of Carroll (1970) and Brindley and Brown (1980).

Surficial Alteration

Fumarolic Areas

Gray, unaltered thin flows, less than 5 m thick, of blocky andesite are exposed in the rim walls of both East and West Craters. These flows are porphyritic with predominantly plagioclase and hypersthene phenocrysts. Less abundant augite occurs both as phenocrysts and as occasional overgrowths on hypersthene. Groundmass is glassy with disseminated microlites of plagioclase and pyroxene. Flow margins are typically black where the percentage of glass is large; flow interiors are medium to light gray where groundmass crystals are abundant.

Coarse explosion rubble that mantles the flows contains mostly angular fragments of the same mineralogical composition as the flows. Additionally, slightly vesicular lava fragments with a greater amount of glass occur throughout the rubble, more commonly on the East Crater rim than the West. Pumice or scoria fragments were not observed on the crater rims.

Detailed descriptions of unaltered rocks from Mount Rainier may be found in Coombs (1936) and Fiske and others (1963). The rocks which make up the cone range from basaltic andesites to dacites. Silica contents span 53-64%, and the upper kilometer of the cone, including the summit-crater lava, is andesite with an average silica content of 61% (Condie and Swenson, (1974).

Secondary minerals at the summit craters (table 20) occur primarily in the core areas of present thermal activity. In adjacent areas of explosion rubble, not now affected by high temperatures, the only secondary minerals found were coatings and vesicle and fracture fillings of white fibrous or saccharoidal calcite, and colorless to white earthy or saccharoidal opal. The opal is X-ray amorphous and is the opal-A of Jones and Segnit (1971) characterized by XRD patterns with a broad hump near the 4 \AA peak of cristobalite.

Table 20. Secondary minerals in fumarolic areas at Mount Rainier. M-major, X-minor, T-trace.

	EAST CRATER		WEST CRATER		DISAPPOINTMENT CLEAVER	
	Bulk	<2 μ m	Bulk	<2 μ m	Bulk	<2 μ m
DIOCTAHEDRAL SMECTITE	M	M	X	M	X	X
TRIOCTAHEDRAL SMECTITE			T	X		
DISORDERED KAOLINITE	X	X	X	M		T
HALLOYSITE	X	X	T	M		
HEMATITE			X		X	
GOETHITE			T	T	T	
AMORPHOUS FE OXIDE		X		X		T
GIBBSITE			M	T		
BOEHMITE	T		T	T		
ALUNITE			M	M		
CALCITE	X				M	
ARAGONITE					M	
CHALECEDONY					M	
TRIDYMITE	X		T		M	
-CRISTOBALITE	X		M			
OPAL-CT				M		
OPAL-A	X		M		M	
CLAY FRACTION	X		X		T	

Toward the centers of thermal activity, calcite and opal coatings are more abundant, andesite fragments are progressively more bleached along alteration rinds, and pink, yellow, red, green, and purple clay-rich patches of altered rubble increase in number and extent. The most clayey deposits coincide with areas of highest temperature as shown on figure 6. In the East Crater, these include the north and northwest inner slope of the rim, both above and especially below the prominent lava flow. At the West Crater, clay-rich alteration occurs mainly at the northwest crest and outer slope of the rim.

Clay minerals occur typically in the once glassy groundmass of flow rock and lithic rubble, and as an alteration product of the fine-grained matrix of unconsolidated surficial debris. Smectite and kaolin are the most common clay-mineral groups in the fumarole areas. Kaolin occurs either as disordered kaolinite or halloysite (fig. 16). XRD patterns of disordered kaolinite show a broad 7.2 \AA $d(001)$ basal peak and poorly differentiated hk reflections which protrude through bands across $20\text{-}30^\circ$ and $35\text{-}40^\circ 2\theta$ (similar to that described by Brindley, 1980, p. 146). Halloysite which is more widespread than disordered kaolinite, shows a hydrated 10.1 \AA peak in a few samples, but is generally observed as $7\text{-}\overset{\circ}{\text{A}}$ -halloysite. The latter form

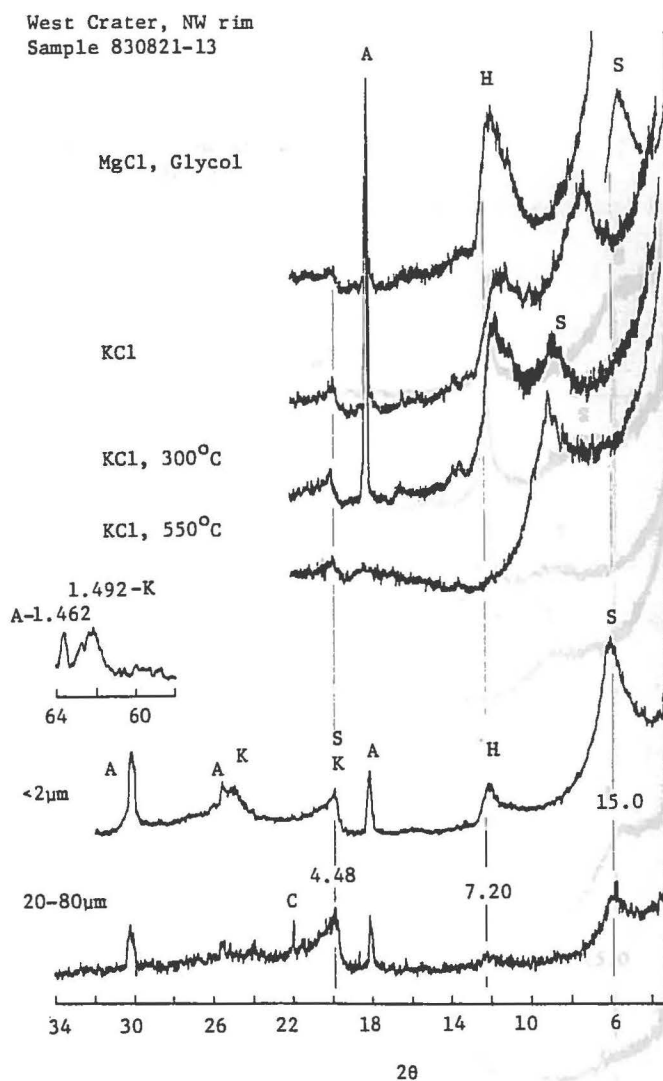
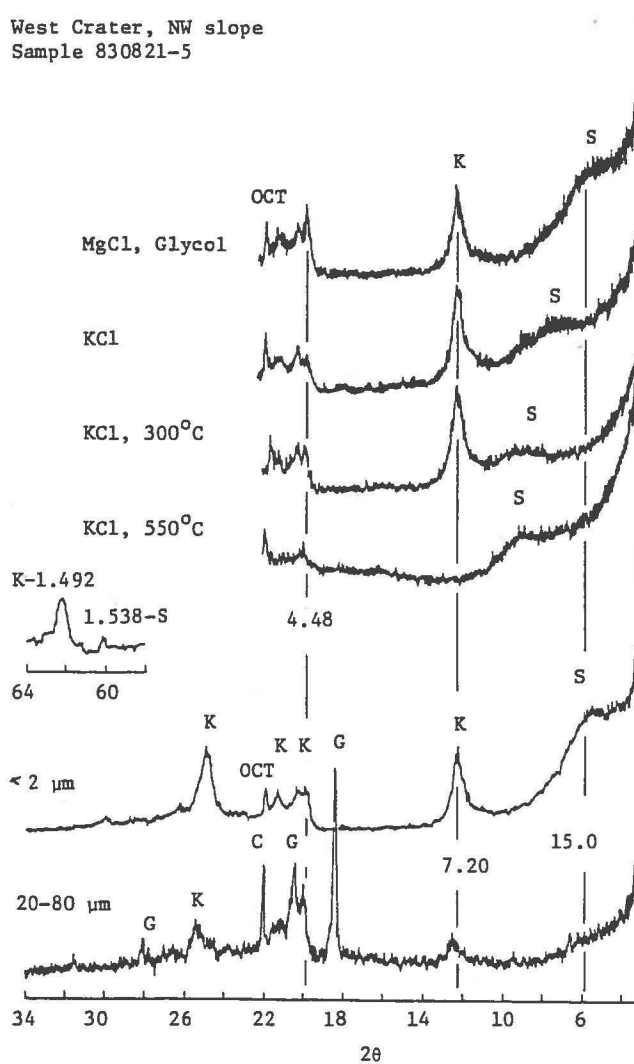


Figure 16. Representative XRD patterns of clay-rich samples from West Crater. Both samples were collected along the temperature-probe traverse shown in figure 5. Top four patterns are oriented; bottom patterns are unoriented and treated as indicated. S-smectite, K-disordered kaolinite, H-halloysite, A-alunite, G-gibbsite, OCT-opal-CT, C--cristobalite.

16A. Sample from excavation near Rim fumarole (72°C) contains abundant Na-rich alunite, halloysite, and dioctahedral smectite.

West Crater, NW slope
Sample 830821-5



16B. Sample from excavation near Mossy fumarole (72^o C, (plate III) contains abundant disordered kaolinite with lesser trioctahedral smectite and opal-CT. Silt fraction contains abundant gibbsite.

has a 7.2 \AA $d(001)$ peak when dried at 50-60% humidity and lacks distinct hk reflections in the high-angle bands. The $d(001)$ peak of K-saturated or ethylene glycol-treated Mg-saturated halloysite expands to about 7.7 \AA (fig. 16A). The low-angle peak persists and intensifies on heating to 300° C as the mineral dehydrates. In contrast, the $d(001)$ peak of disordered kaolinite shows no change in intensity with such heating (fig. 16B). Both phases become amorphous with the 550° C heat treatment.

Both di- and trioctahedral smectite occur with the dioctahedral form more common. Untreated samples of both forms have $d(001)$ peaks at $15.1\text{-}15.5 \text{ \AA}$ indicating the presence of divalent interlayer cations. K-saturation yields $12.0\text{-}12.6 \text{ \AA}$ $d(001)$ peaks, Mg-saturation $14.7\text{-}14.9 \text{ \AA}$ peaks, and ethylene glycol intercalation $16.8\text{-}17.8 \text{ \AA}$ peaks (fig. 16). The two respective forms of smectite show $d(060)$ b -parameter peaks at $1.492\text{-}1.506 \text{ \AA}$ and $1.534\text{-}1.539 \text{ \AA}$.

Trace amounts of possible mixed-layer clays are evident from poorly defined peaks between $20\text{-}25 \text{ \AA}$ but their small size and sporadic occurrence precluded further identification.

A silica phase accompanies clay minerals in the clay fraction of many samples. This is generally opal-CT (Jones and Segnit, 1971) which shows poorly defined cristobalite

and tridymite peaks at 4.1 and 4.3 Å, in some samples superimposed on a broad opal-A hump. Silt-sized fractions of many of the clay-rich samples contain well-ordered α -cristobalite, or in fewer cases, tridymite.

The most conspicuous difference in mineralogy between East and West Craters is the presence of abundant alunite and gibbsite at West Crater thermal areas, particularly in the silt fractions (fig. 16). The main $d(113)$ alunite peak at 2.95-2.97 Å and a very small $d(006)$ peak indicates a high Na content in the alunite. Trace amounts of boehmite at the West Crater probably result from minor alteration of gibbsite. Alunite and gibbsite are commonly associated with one of the kaolin minerals, but all three phases were never found together in the same sample. Gibbsite and alunite were not found in the East Crater.

At Disappointment Cleaver, calcite and opal-A occur throughout the active part of the thermal area as white to beige encrustations and as vesicle and fracture fillings. Chaledony and tridymite, perhaps as a result of aging of opal-A, occurs as encrustations in areas no longer bathed by heated fluids, such as the exposed part of the prominent breccia spire (plate VIII). Rubble in the hottest part of the thermal area contains pockets of clayey debris whose main constituent is dioctahedral smectite.

Thermal Springs

As would be anticipated from the low temperature and high bicarbonate concentration of the thermal springs, secondary minerals include abundant carbonate phases at all four localities (table 21). At Winthrop Springs, white powdery to saccharoidal crusts of calcite, opal-A, and gypsum occur on cobbles downstream from the spring outlets. No alteration of primary minerals was observed.

Similar but more abundant crusts of calcite, aragonite and opal-A occur at Paradise Springs. Opal makes up a greater proportion of the crust here than at Winthrop Springs. Typically the warmer springs produce thicker, more extensive coatings. However, coated cobbles which have been transported to the Paradise River channel eventually lose the minerals by abrasion and by dissolution in the dilute, glacier-fed river. Neither the jointed flows through which the springs discharge, nor a prominent ash layer that forms a barrier of low permeability below the springs show evidence of primary-mineral alteration.

Travertine at Longmire Springs ranges from dark gray to light tan and is composed of fibrous, concretionary, and platy calcite, lesser aragonite, and a small amount of

Table 21. Secondary minerals in thermal-spring areas at Mount Rainier. M-major, X-minor, T-trace.

	WINTHROP SPRINGS	PARADISE SPRINGS	LONGMIRE SPRINGS	OHANAPECOSH SPRINGS
	Bulk	Bulk	Bulk <2 μm	Bulk <2 μm
DIOCTAHEDRAL SMECTITE				T M
TRIOCTAHEDRAL SMECTITE				X
ILLITE				T
AMORPHOUS FE OXIDE			X	X
BOEHMITE		X		
GYPSUM	M			
PYRITE			X	
CALCITE	M	M	M	M
ARAGONITE		T	X X	
RHODOCHROSITE			T	
CHALCEDONY		T		M T
OPAL-CT				X
OPAL-A	T	X		
CLAY FRACTION			X	X

rhodochrosite. Warm, algae-rich pools in and adjacent to the main travertine mound contain a black aragonitic mud with pyrite in the fine-grained fraction. Stream channels that drain Longmire meadow are coated with bright orange amorphous iron oxyhydroxides.

Travertine at Ohanapecosh Springs contains fibrous, concretionary, and granular calcite. In marginal areas, the travertine also contains fragments of breccia derived from the underlying Ohanapecosh Formation. Crandell (1969) reports interbedding of travertine with the 450 BP pumice Layer W from Mount St. Helens. Sediments in the algae-rich pools of the two main springs (OHA and OHX) contain hornblende-bearing pumice grains from Layer W, lithic fragments from the Ohanapecosh Formation, and detrital quartz, plagioclase, and magnetite. Minor amounts of chlorite, random mixed-layer smectite-chlorite, opal-CT, and opal-A occur in the clay-size fraction. The clay minerals are probably also detrital, however opaline phases may be authigenic products of the spring water.

Subsurface Alteration

Lithic eruptive products and mass-movement deposits during the Holocene have incorporated large masses of

hydrothermally altered rocks from Mount Rainier (Crandell, 1971). Hydrothermal minerals in these deposits reflect both surface and subsurface alteration within the cone. Deposits examined in this study (table 22) range in size from 2×10^9 to about $3 \times 10^4 \text{ m}^3$, and in age from more than 6000 BP to the last few decades. In general the larger deposits represent deeper samples of the volcano's interior.

Table 22. Holocene tephra and mass-movement deposits examined in this study. BP-years before present. Age from Crandell (1971) and Mullineaux (1974), except where noted.

TEPHRA DEPOSIT	APPROXIMATE AGE
Lithic layer above Layer W ¹	<450 BP
Lithic layer between Layers W and C ¹	450-2200 BP
Layer F	5000 BP
MASS-MOVEMENT DEPOSIT	
Curtis Ridge avalanche	AD 1974 ²
Gibraltar Rock avalanche	AD 1975 ²
Tahoma Glacier avalanche	AD 1910-1930
South Tahoma avalanche	2200 BP ²
Electron Mudflow	530 BP
Round Pass Mudflow	2600 BP
Osceola Mudflow	5000 BP
Van Trump avalanche	>6600 BP

¹Lithic layers may be partly windblown sand and dust.
²This study.

Crandell (1971) and Mullineaux (1974) used smectite and kaolin group minerals as indicators of a hydrothermally altered component in Holocene volcanic deposits. Numerous studies in recent years support this approach for uncontaminated deposits of known age. At Findley Lake, 52 km north of Mount Rainier, Zachara (1979) found kaolinite in a pre-Fraser weathering surface, but in younger soils on Holocene tephra he found only detrital 2:1 clay; authigenic crystalline clays are absent in these younger soils. In a study of weathering rinds, Colman (1982) found that rinds on Mount Rainier andesite that had been weathered since Evans Creek time (20,000 BP, Crandell and Miller, 1974) contain mainly X-ray amorphous material with minor iron oxides. The youngest Quaternary kaolin-rich soils near Mount Rainier are the glaciofluvial Logan Hill Formation in the Cowlitz River valley, 50 km southeast of the cone (Bethel, 1982), and the Lily Creek Formation in the Cascade foothills northwest of Mount Rainier (Wildrick, 1976). Both of these deposits are several hundred thousand years old (Crandell and Miller, 1974, p. 8). Thus weathering products in soils on deposits less than 10,000 years old in the Cascades should not contain smectite or kaolin minerals unless these minerals are detrital and have a source in older deposits.

Kaolin minerals are common, however, in Holocene

hydrothermal deposits in the Cascade Range. For example, Pevear and others (1982) found poorly crystallized kaolin in an active thermal area in the 400-year-old summit dome at Mount St. Helens, and Frank (1983) reports abundant smectite and kaolinite in active thermal areas at Mount Baker. Smectite minerals at both localities occur in the most recent lithic tephra and in debris-avalanche deposits which originated from the central parts of each cone.

Crandell (1971) and Mullineaux (1974) described clay minerals in Holocene deposits that had previously undergone alteration within Mount Rainier. Here I elaborate on the hydrothermally formed minerals in some of these, and in a few additional deposits (table 22) for later use in geochemical descriptions of the hydrothermal system at Mount Rainier. These deposits were examined in localities where the contamination by older, pre-Holocene material would be unlikely. In the case of large mass-movement deposits, the avalanche facies were studied, where possible, rather than the mudflow facies.

It is apparent from the volumes and hydrothermal mineralogy of deposits mapped by Crandell (1971) and Mullineaux (1974) (table 1) and their source areas in the central part of the volcano that a large part of the hydrothermal system which existed in the upper part of Mount

Rainier during the early Holocene was removed about 5000 years ago. This material was incorporated along with an outer sheath of unaltered rock in the Van Trump, Greenwater, and Paradise Lahars, the Osceola Mudflow, and the lithic part of tephra Layer F. Subsequent rebuilding of the summit, 1000-2000 years ago was accompanied and followed by reestablishment of another hydrothermal system within the upper part of the cone.

Deposits for this study were selected to provide:

1. a picture of the pre-5000 BP hydrothermal system;
2. a sketch of activity during the interval of 2000-3000 BP between removal and rebuilding of the summit cone; and
3. clues to the most recent characteristics of the hydrothermal system within the last 2000 years.

The respective deposits for these time periods (table 22) are:

1. Van Trump lahar, Paradise Lahar, Osceola Mudflow, tephra Layer F;
2. Round Pass Mudflow, avalanche on the South Tahoma moraine; and

3. Electron Mudflow, recent avalanches on the Tahoma Glacier terminus and on Cowlitz and Winthrop Glaciers; two lithic layers less than 2200 years old.

Table 23 lists the secondary minerals in these various deposits, and figure 17 shows the source areas and distribution of the deposits. The extensive degree of hydrothermal alteration that was present in the upper part of the cone 5000 years ago is represented by the alteration assemblage in the Osceola Mudflow. The Osceola contains (fig. 18) dioctahedral smectite, disordered to well-ordered kaolinite, talc, a trace of illite, and several silica phases dominated by chalcedony. Tephra Layer F which was erupted at about the same time that the Osceola Mudflow occurred (Mullineaux, 1974, p. 66-67) contains the same suite of secondary minerals. Smaller deposits of the somewhat older Van Trump and Paradise Lahars which originated on the south side of the cone are generally similar in clay composition to the Osceola (fig. 18), but lack the chalcedony. A major feature of the southern deposits is an abundance of distinctive white clots of sodium-rich alunite.

A somewhat different assemblage of secondary minerals occurs in the two largest of the younger deposits (table 23), the Round Pass and Electron Mudflows which originated

Table 23. Secondary minerals in Holocene deposits of tephra and large mass movements. *-From Crandell (1971, p. 29)
M-major, X-minor, T-trace.

	VAN TRUMP LAHAR	PARADISE LAHAR	OSCEOLA MUDFLOW	LAYER F
	Bulk	Bulk <2 m	Bulk <2 m	Bulk <2 m
SMECTITE				
DIOCTAHEDRAL SMECTITE		T M	M M	X M
TRIOCTAHEDRAL SMECTITE				
MIXED LAYER CHLORITE- SMECTITE				T
CHLORITE				
ILLITE	T	T	T	T
PYROPHYLLITE		T T		T
TALC			X	T X
KAOLINITE	M		M	
DISORDERED KAOLINITE/ HALLOYSITE		T X	X M	T M
HEMATITE				
GOETHITE		T	T	
AMORPHOUS FE OXIDE		X	T	X
GIBBSITE				
GYPSUM				
JAROSITE				
ALUNITE	M	M M		
PYRITE				
CALCITE			M	
CHALCEDONY			M T	M M
TRIDYMITE		M	X	X
-CRISTOBALITE	M	M	M	M
OPAL-CT		M X	X X	X
OPAL-A			X	
CLAY FRACTION		M	M	M

Table 23. Continued.

	ROUND PASS MUDFLOW	SOUTH TAHOMA AVALANCHE	ELECTRON MUDFLOW	LITHIC LAYER ABOVE LAYER C BELOW LAYER W
	Bulk <2 m	Bulk <2 m	Bulk <2 m	Bulk <2 m
SMECTITE			X M	T
DIOCTAHEDRAL SMECTITE	X X	M M		
TRIOCTAHEDRAL SMECTITE				
MIXED LAYER CHLORITE- SMECTITE	X*			
CHLORITE	X*		M	
ILLITE	T*			
PYROPHYLLITE				
TALC				
KAOLINITE				
DISORDERED KAOLINITE/ HALLOYSITE	T*	T	T*	
HEMATITE				
GOETHITE				
AMORPHOUS FE OXIDE	T	X	X	T
GIBBSITE		M X		
GYPNUM				
JAROSITE				
ALUNITE		M M		
PYRITE				
CALCITE				
CHALCEDONY			X M	
TRIDYMIT		T X	M	
-CRISTOBALITE	X		X X	
OPAL-CT				
OPAL-A	X	X		
CLAY FRACTION	X	X	X	T

Table 23. Continued.

	LITHIC LAYER ABOVE <LAYER W	TAHOMA GLACIER AVALANCHE	CURTIS RIDGE AVALANCHE	GIBRALTAR ROCK AVALANCHE
	Bulk <2 m	Bulk <2 m	Bulk <2 m	Bulk <2 m
SMECTITE			X	
DIOCTAHEDRAL SMECTITE	X			T X
TRIOCTAHEDRAL SMECTITE		M M		
MIXED LAYER CHLORITE- SMECTITE				
CHLORITE				
ILLITE		T X		
PYROPHYLLITE				
TALC				
KAOLINITE		X		
DISORDERED KAOLINITE/ HALLOYSITE		X X		
HEMATITE			T	
GOETHITE	T	T		
AMORPHOUS FE OXIDE	T	X	T	T
GIBBSITE				
GYPSUM		X		
JAROSITE		X		
ALUNITE		M		
PYRITE		X		
CALCITE				
CHALCEDONY		X		
TRIDYMITE		M		
-CRISTOBALITE		M		
OPAL-CT			X	
OPAL-A		M		X
CLAY FRACTION	T	M	T	T

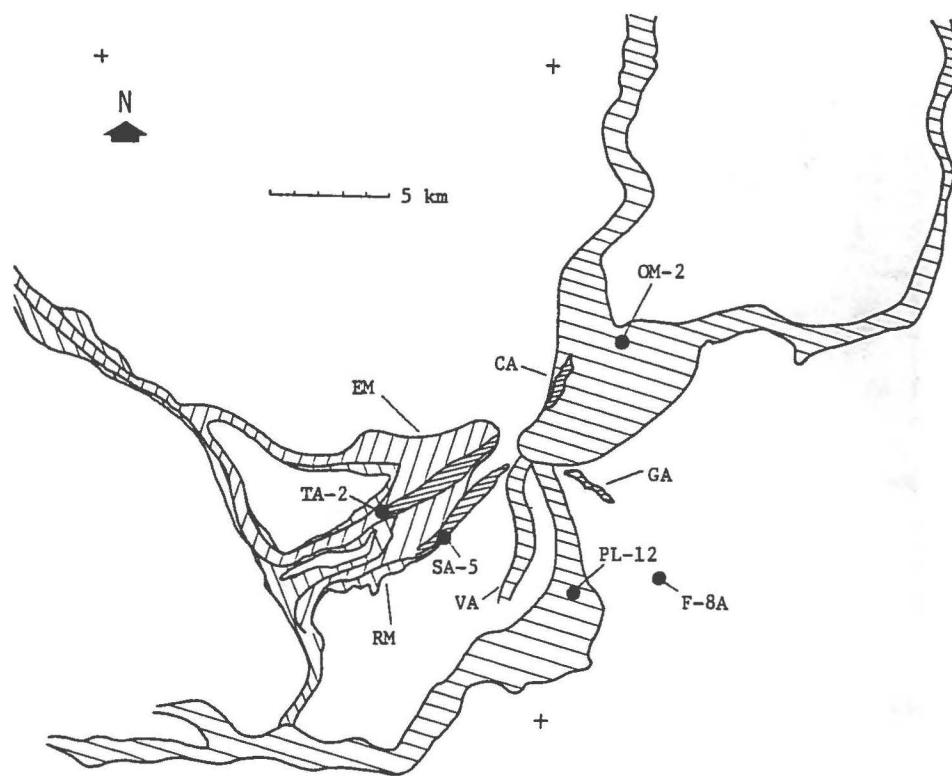


Figure 17. Extent of selected Holocene avalanche and mudflow deposits, and localities for samples shown in figure 18. VA-Van Trump avalanche, PL-Paradise Lahar, OM-Osceola Mudflow, RM-Round Pass Mudflow, EM-Electron Mudflow, SA-South Tahoma avalanche, TA-Tahoma avalanche, GA-Gibraltar Rock avalanche, CA-Curtis Ridge avalanche. Extent of PL, OM, RM, and EM taken from Crandell (1971).

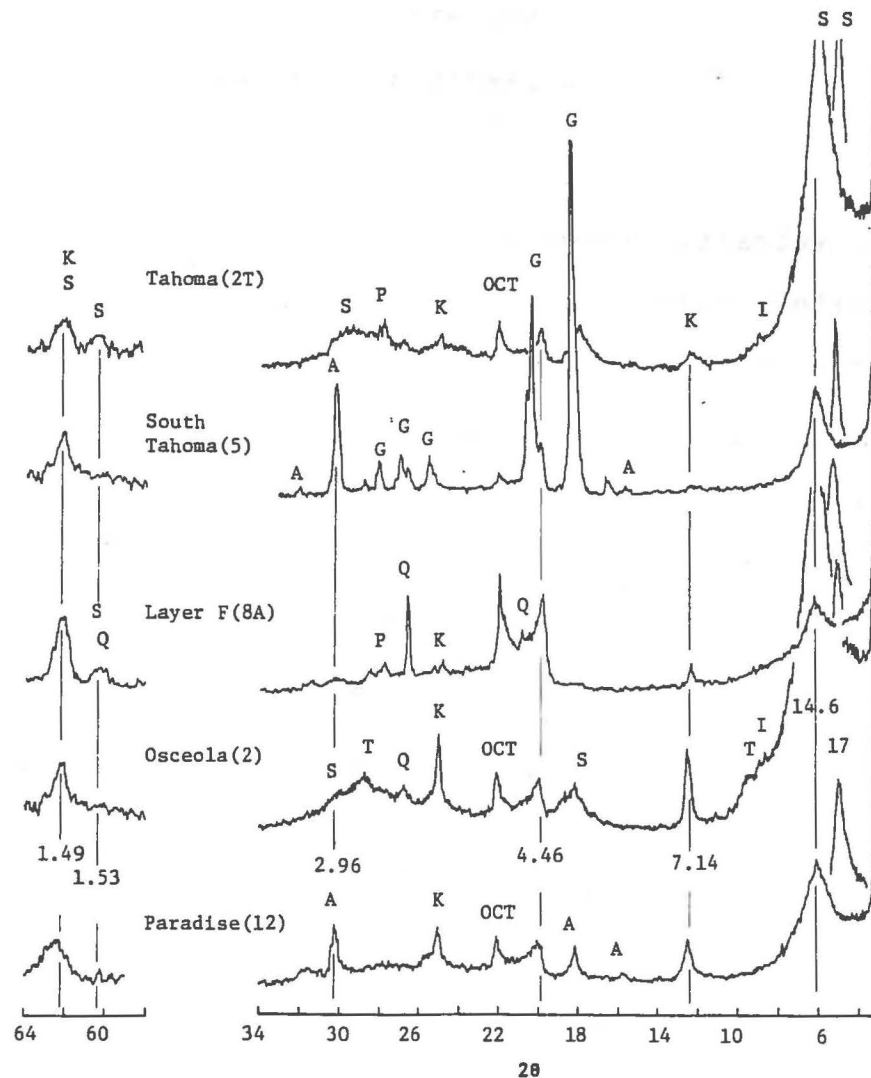


Figure 18. Representative XRD patterns of clay-rich samples of Holocene deposits which contain significant smectite and kaolin or alunite. Long patterns are from unoriented, Mg-saturated clay fractions; superimposed expanded peaks of oriented smectite are also shown. S-smectite, K-kaolinite or halloysite, I-illite, T-talc, P-pyrophyllite, G-gibbsite, A-Na-rich alunite, OCT-opal-CT, P-plagioclase.

on the west part of the summit. The clay fraction is less abundant, though smectite remains the main clay mineral. Chlorite and mixed-layer chlorite-smectite are present in these deposits, whereas kaolin minerals occur only in trace amounts if at all.

Among the younger deposits, two small avalanches from the southwest facing headwalls of Mount Rainier contain a suite of minerals similar to the highly altered deposits older than 5000 BP. A tan to orange, unsorted layer caps a purplish gray moraine on the east side of South Tahoma Glacier at 1950 m altitude. The deposit does not extend eastward beyond the moraine and likely resulted from a small avalanche which traveled down the South Tahoma Glacier when its surface was near the crest of the moraine. The source was apparently the South Tahoma headwall. The deposit contains (fig. 18) abundant dioctahedral smectite, white to tan clots of alunite and gibbsite, and a trace of kaolin. The deposit is younger than the underlying moraine, shown by Crandell (1969) to have formed during the Burroughs Mountain Stade (2500-3000 BP) of the Holocene Winthrop Creek Glaciation. Discontinuous lenses of reddish brown, sand-sized scoria of tephra Layer C are entrained in the deposit and indicate an age of about 2200 BP. The avalanche may correlate with one of two clayey lahars between 450-2600 BP found by Crandell (1971, p. 55-56) downstream in the

Tahoma Creek valley.

A similar avalanche that traveled just beyond the Tahoma Glacier terminus sometime during 1910-1930 (Crandell, 1971, p. 17) originated in the hydrothermally altered plug now exposed in Sunset Amphitheater. This bright yellow to orange deposit contains (fig. 18) abundant trioctahedral smectite, kaolin, jarosite, alunite, and silica phases, with lesser illite, gypsum, and pyrite.

Smaller avalanches usually occur every year from headwall areas of Mount Rainier. Two of the largest to occur during the past 10 years were examined for secondary minerals. A June 1974 avalanche of brecciated lava and scoria fell from the 3300 m level of Curtis Ridge and traveled 2 km down Winthrop Glacier. The source area for this avalanche was a prominent alcove eroded into the ridge from which smaller rock slides frequently occur. Dust plumes commonly issue from the area during late summer and are at times mistaken for steam emission (fig. 97). The deposit consists of blocks as large as 5 m across in a fragmented, sandy matrix.

In March 1975, brecciated lava, scoria, and ash fell from the upper east face of Gibraltar Rock at 3550 m and traveled 1.5 km down Cowlitz Glacier. The source area was near a steam vent observed during the summer of 1961 (fig.

7; table 8). The texture of this deposit was like that of the Curtis Ridge avalanche and contained blocks as large as 3 m across in a sandy matrix. Both avalanche deposits (table 23) contain only trace amounts of clay-size material of which smectite is the main component.

Evidence of secondary minerals was sought in two young lithic layers thought to be wholly or in part lithic tephra from Mount Rainier. These deposits are among many Holocene dark gray or brown, sandy to silty layers that are interspersed between lighter colored vitric or crystal tephra. Such layers are composed of andesite fragments with lesser glass and single crystals. Their source could be either lithic tephra from explosive, magma-poor eruptions, or windblown sand and dust from exposed ground surfaces (Mullineaux, 1974, p. 12).

The two youngest lithic layers were examined for this study. Widespread layers of young lithic material 1-3 cm in thickness occur in many localities on the east slopes of Mount Rainier between tephra Layer C (2200 BP) and Mount St. Helens tephra Layer W (450 BP), and between Layer W and the ground surface. Commonly these layers are mixed near the ground surface with underlying tephra beds or with overlying humus so that the layers are frequently indistinct. However uncontaminated material was found in the two layers at

enough localities to suggest that eruptions were the source of the layers. Only trace amounts of a clay-size component were present in each layer (table 23) and the only identifiable mineral was smectite. If the lithic layers do represent eruptions from Mount Rainier, the sparse amount of secondary minerals in the layers records only minor alteration at the source vent.

Discussion of Secondary Mineral Assemblages

Variation in Character and Extent of Alteration

Holocene deposits reveal marked differences in alteration products, both in their distribution and their content. Figure 19, which is based on table 1 and the work of Crandell (1971), shows how the presence of hydrothermally altered material in avalanches and mudflows has shifted from large early or mid-Holocene deposits on the east side of the cone, to moderate-size or small, younger deposits less than 3400 BP on the west side of the cone.

The older altered deposits originated at a central vent (fig. 17) and are characterized by an abundant clay fraction that includes some combination of smectite, kaolin, and

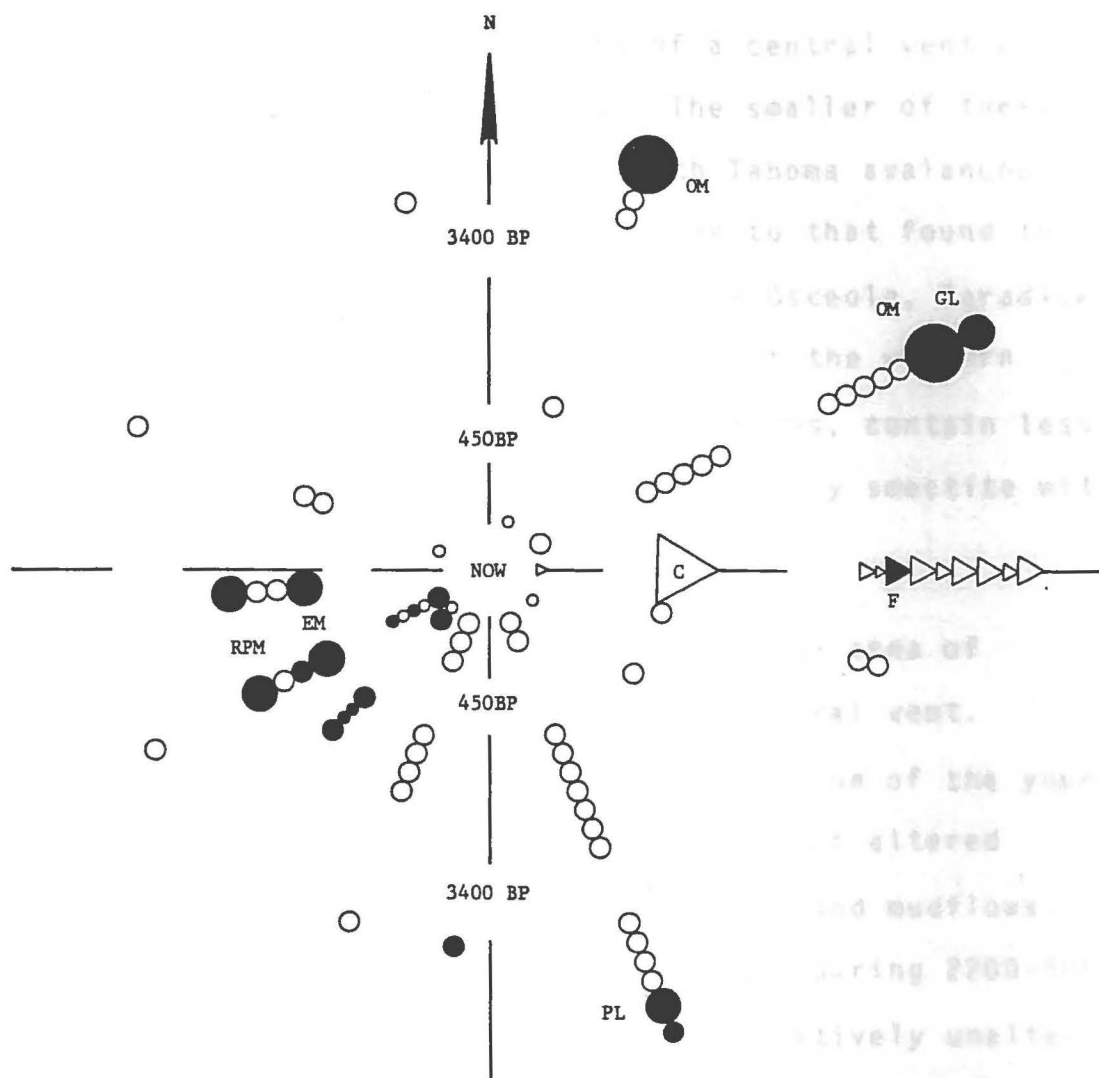


Figure 19. Distribution through time and space of Holocene eruptive (triangle) and large mass-movement (circle) events. Solid symbols depict those events which incorporated appreciable hydrothermally altered material. Larger events are noted as GL-Greenwater Lahar, VA-Van Trump avalanche, PL-Paradise Lahar, OM-Osceola Mudflow, RM-Round Pass Mudflow, EM-Electron Mudflow. Data based on tables 1, 21, and 22.

alunite. Younger altered deposits on the other hand originated either in the west part of a central vent or in a separate vent located to the west. The smaller of these western deposits, the Tahoma and South Tahoma avalanches contain a clay fraction that is similar to that found in much earlier material to the east in the Osceola, Paradise, and Van Trump deposits. But the larger of the western events, the Round Pass and Electron Mudflows, contain less clay and a different composition of primarily smectite with little kaolin or alunite.

This record indicates that an extensive area of alteration existed 5000 years ago at a central vent. Subsequently, but mostly prior to construction of the young summit cone 2200 years ago, lesser amounts of altered material were incorporated into avalanches and mudflows. If extensive areas of alteration were present during 2200-5000 BP, they may have remained sheathed by relatively unaltered rock or they may have been enclosed within a caldera or deep basin such as must have existed following the Osceola Mudflow. The relatively small amounts of those highly altered deposits 2200 years old or younger that do contain the smectite, kaolin, alunite assemblage represent new exposures of old vent material in Sunset Amphitheater and the South Tahoma headwall. The bulk of this material probably remains in place in the upper part of the cone.

In summary, remnants of old altered vent material are best exposed in Sunset Amphitheater. Current alteration of unknown character is taking place at the other small active thermal areas on the upper flank. If such alteration is similar to that at Disappointment Cleaver, it is producing primarily smectite. A variety of alteration products are now forming at the summit fumarole field; predominant among these are smectite, kaolin, and, in the western part, alunite.

Mineralogic Constraints on Hydrothermal System

Secondary minerals reflect chemical and thermal conditions at the time of their formation. The mineralogic data for Mount Rainier provide a number of qualitative constraints on physical and chemical environments. Laboratory experiments (Hemley and others, 1969) and alteration products found in drillholes at a variety of geothermal systems around the world (Browne, 1978) show that the alunite and kaolinite assemblage occurs under acid sulfate conditions (typically pH 0-5; sulfate greater than 100 mg/L) at temperatures up to a few hundred degrees Celsius. In general, higher temperatures within the range of alunite stability favor less acidic conditions. Higher

temperatures also favor more structurally ordered kaolinite. Thus the disordered kaolinite, halloysite, and alunite found at Mount Rainier's summit indicate a relatively low temperature, acidic environment which is appropriate for mineral formation in boiling-point, acid sulfate fluids. Such fluids are easily generated by surficial solution and oxidation of upflowing sulfur-rich gases (Schoen and others, 1974).

In older mass-movement deposits such as the Osceola Mudflow and Van Trump Lahar, kaolinite is well ordered (table 23) and may indicate a temperature of formation above that of surface boiling. Although aging of disordered kaolin may produce ordered kaolinite, the trace illite, pyrophyllite, and talc in these same deposits suggest a higher temperature and hence deeper environment of formation.

The maximum depth of acidic alteration depends on whether upflowing fluids are acidified at depth, or if acidified at the surface, whether subsequent downgoing fluids penetrate very far. Where hydrothermal systems overlie sulfate-rich sediments, such as at El Chichon volcano, Mexico (Casadevall and others, 1984), acidic conditions can extend quite deep. Alternatively, where deep magmatic gases go into solution as at many andesitic

volcanoes (Kiyosu and Kurahashi, 1983), sulfur-bearing sediments are not required for deep acid alteration. Examples of geothermal localities where acid alteration has been found at depth include 900 m deep at Matsukawa, Japan (Sumi, 1969), 700 m at Otake, Japan (Yamasaki and others, 1970), 700 m at Ugusu, Japan (Schoen and others, 1974), and 1100 m at Matsao, Taiwan (Ellis and Mahon, 1977).

At Mount Rainier, the large component of acid alteration in the Osceola Mudflow suggests that the alteration occurred at a depth of as much as 900 m, which is the estimated thickness (Crandell, 1963a, p. B138-B139) for the pre-Osceola summit cone. As discussed in Chapter 5, geochemical simulation of the origin of sulfate-rich thermal springs on the lower flank of Mount Rainier is consistent with the existence of an acid sulfate-chloride fluid at depth in today's summit cone. Therefore, acidic alteration may be taking place now several hundred meters below the summit craters.

Chapter 5

CONCEPTUAL HYDROTHERMAL MODEL

A conceptual model of present processes at work in the hydrothermal system at Mount Rainier, provides a basis for anticipating future events. This model must take into account the following factors:

1. Locations of hydrothermal leakage to the surface;
2. Structures that provide permeable paths of fluid egress to the surface;
3. Amount of excess heat discharge;
4. Composition of surficial thermal fluids;
5. Composition, based on mineralogy, of subsurface thermal fluids.

Data on these factors, as discussed in earlier chapters, point to the existence of a hydrothermal system having a central region of heated upflow which discharges at the summit and produces sparse amounts of lateral leakage at

lower elevations.

Significance of Thermal Springs

Lower-flank thermal springs provide clues of the present composition of fluids in the hydrothermal system.

The origin of the springs can be inferred as follows:

1. Use surface composition and temperatures of the springs to define the most probable means by which the fluids cooled, and then reverse the cooling process to approximate a subsurface end-member;
2. Adjust the end-member composition to define the most geologically reasonable composition of a parent water;
3. Calculate a thermodynamically valid reaction path from the parent composition to the existing thermal spring; and
4. Combine reaction-path results with the previously listed constraints on mineralogy and permeable structures to outline flow paths of hydrothermal fluids.

Cooling Process

The large variation in dissolved chloride and conductivity with temperature at Paradise and Winthrop springs (fig. 13) indicates that these thermal waters cooled by mixing with cold, dilute ground water. Consideration of deuterium values in cold and warm waters allows estimation of the extent of mixing. A hot-water end member, prior to mixing, should have a deuterium concentration no lighter than that found in the lightest recharge water. From figure 15, the lightest recharge is found at the summit and could have a δD as low as -190 ‰ . Taking this value to be the isotopic concentration of the hot end member, one may then construct a pair of equations with two unknowns which allow calculation of the end-member temperature and the cold-water mixing fraction

$$T_T = XT_C + (1-X)T_H$$

$$\delta D_T = X\delta D_C + (1-X)\delta D_H$$

where T is temperature, δD is deuterium concentration, X is mixing fraction, and T , C , and H refer to thermal-spring water, cold diluent, and hot end member, respectively.

Assuming $\delta D_H = -190 \text{ ‰}$, and using data from table 19 for thermal and cold water, the same temperature, 129° C , is found for the hot end member at both Paradise and Winthrop

(fig. 20). The cold-water mixing fractions based on the deuterium limitation are 83% and 96% respectively.

Analogous equations using the deuterium-limited mixing fractions allow calculation of hypothetical end-member compositions for Paradise and Winthrop (table 24). Figure 21 depicts the range of concentration of cold spring, thermal spring and unmixed end-member compositions, in each case using September 1982 analyses (table 16). Interestingly, the unmixed end members are remarkably similar in cation compositions, although they deviate somewhat in anion content. For example, though both waters are fairly high in sulfate, their sulfate-chloride ratios range from 2.9 at Paradise to 46 at Winthrop. Although such simplistic unmixing calculations probably only approximate the composition of the hydrothermal fluids which feed these springs, one may use the general similarity of the unmixed end members as a guide in determining the properties of the present hydrothermal fluids.

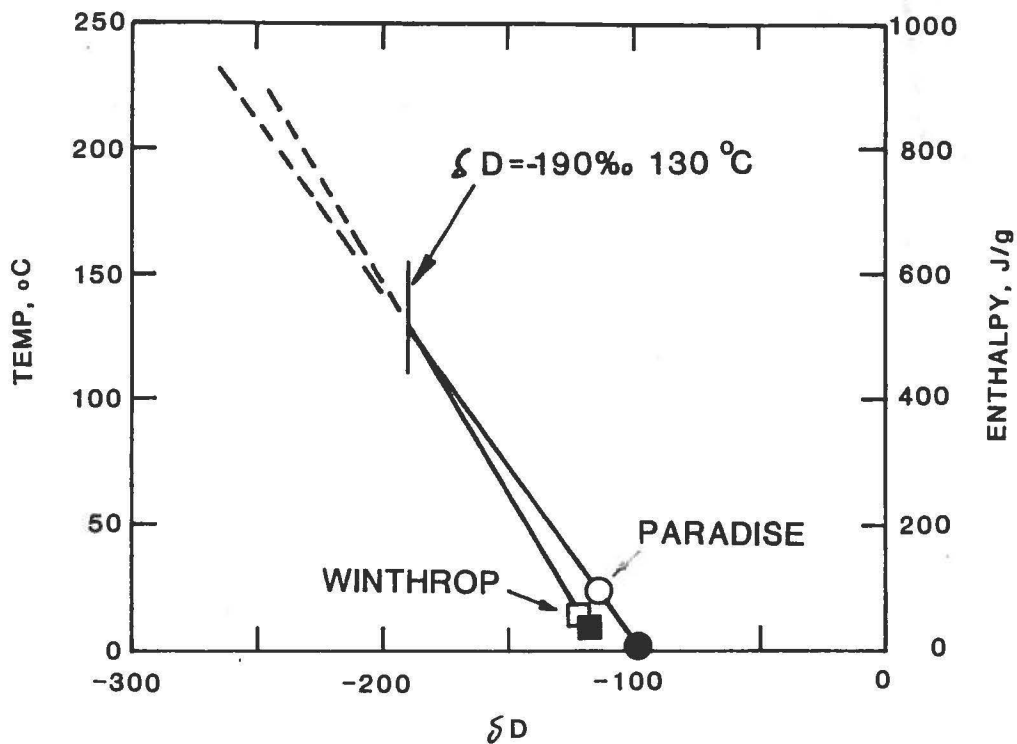


Figure 20. Deuterium-enthalpy mixing relations for Paradise and Winthrop springs. Mixing between cold springs (solid symbols) and a hot end member which is limited by -190‰ δD produces thermal springs (open symbols). Hot end member is 130 C and mixing fractions of cold water are 83% and 96% respectively for Paradise and Winthrop.

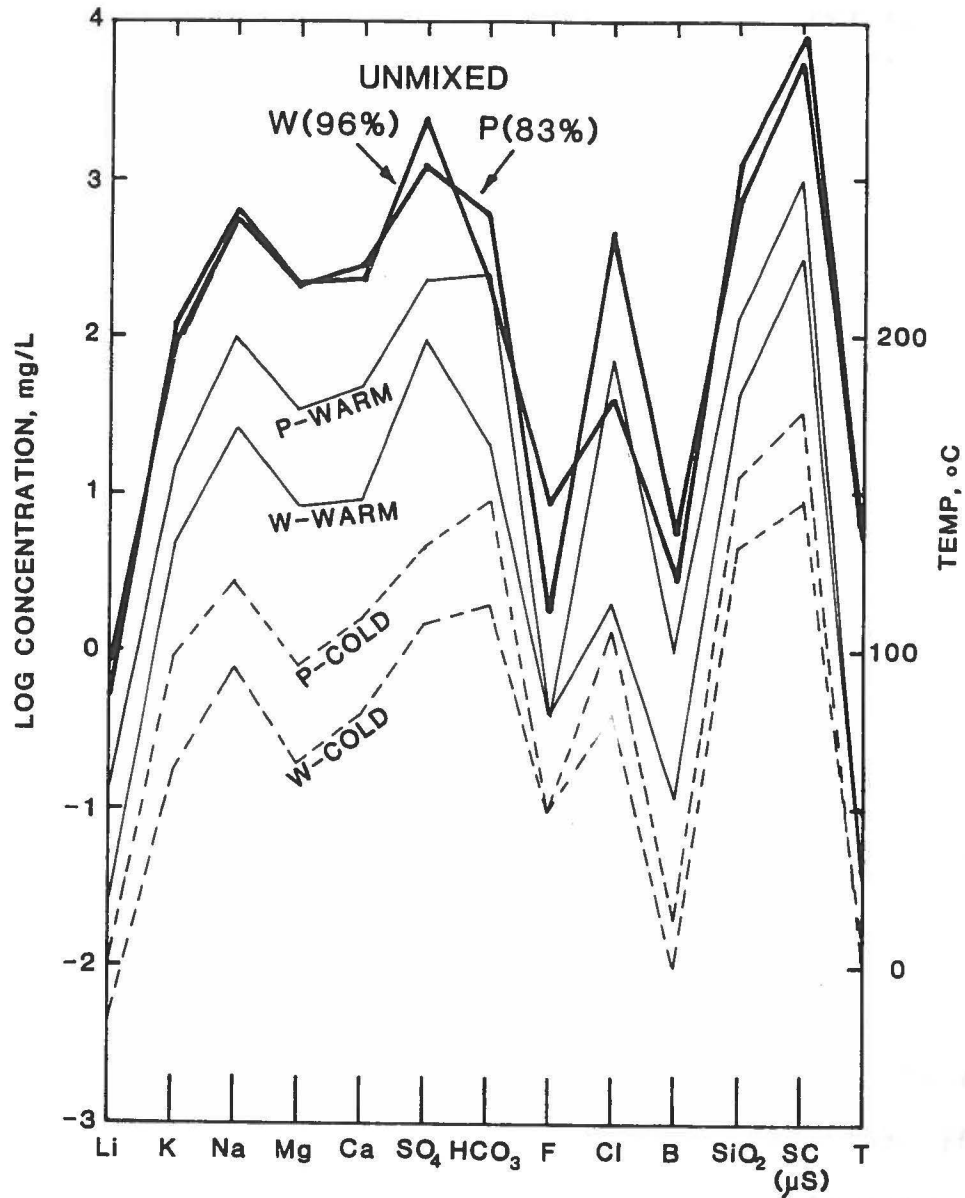


Figure 21. Range of temperature (T), conductivity (SC), and concentration of dissolved constituents in cold springs, warm springs, and unmixed end members at Paradise and Winthrop using September 1982 analyses for PS5, PS3, WS1, and WS3.

Table 24. Unmixed end-member compositions using September 1982 analytical data for PS5, PS3, WS1, WS3, and δD over the deuterium-limitation of -190 ‰. Dissolved constituents in mg/L; SP CD in microsiemens; T in degrees Celsius.

SITE	WINTHROP	PARADISE
K	120	89
Na	660	570
Li	.54	.82
Ca	220	280
Mg	205	205
Cl	42	410
F	7.4-9.8	1.8
SO ₄	2300	1200
CO ₂ TOT	536	1980
SiO ₂	1080	690
B	2.7-2.9	5.4
pH	6.7	6.2
SP CD	7350	5540
T	130	130

Possible Parent Fluid

Two outstanding features of the unmixed end members are their high sulfate (1200-2300 mg/L) and high magnesium (205 mg/L) content. High magnesium water in volcanic terrain typically occurs only at low temperature or under acidic conditions. Neutral waters at high temperatures tend to precipitate out magnesium in magnesium-rich minerals, including primarily smectites, talc, chlorites, or

carbonates. Accordingly, one possible parent water for a hot end member might be an acid sulfate water. However the moderately high chloride at Paradise springs (28 mg/L) and the high chloride in the unmixed end members (42-410 mg/L) preclude a simple surficial, acid sulfate water, as these are typically low in chloride. A more likely parent water is an acid sulfate-chloride water, a type particularly common in andesitic volcanoes.

In a review of volcanic waters, White (1957, p. 1647) suggested a number of ways by which the acid sulfate-chloride type might form, including "... (1) mixing of different sodium-chloride and acid-sulfate waters; (2) near-surface acidification of near-neutral sodium-chloride water by oxidation of H_2S ...; (3) deep condensation of dense vapors that contain alkali halides and oxidized sulfur...; and (4) surficial condensation and oxidation of low-density volcanic gases containing halogen acids and sulfur..." All of White's (1957) methods ultimately rely on condensation of volcanic gases. Ellis and Wilson (1961) suggested additional methods including acidification of a neutral sulfate-chloride water by dissociation of bisulfate during cooling, and reaction of sodium-chloride water with sulfate-rich sediments beneath a volcano. The important role of condensing gases within andesitic volcanoes is supported by the study of Kiyosu and Kurahashi (1983) who

used sulfur isotopes to show that the sulfate in several acid sulfate-chloride waters in Japan is derived from volcanic sulfur-rich gas. The lack of a significant sulfur component in fumaroles at Mount Rainier and the presence of sulfate-chloride springs on the lower flank suggest that an acid sulfate-chloride parent water, if present, is not surficial but occurs at depth and is formed by solution of dense vapors.

Natural examples of acid sulfate-chloride waters reveal a wide range of compositions. Figure 22 shows the percentage equivalents of major constituents for a variety of these waters found in either springs or crater lakes at andesitic volcanoes. Paradise and Winthrop springs and simulated waters discussed below are also shown in figure 22 for comparison. The acid sulfate-chloride waters that were considered were limited to those whose magnesium, sulfate, and chloride equivalents were each greater than 10% of the major constituents; these are listed in table 25.

A geologically reasonable parent water for thermal springs on the lower flank of Mount Rainier should lie within the range of the acid sulfate-chloride compositions in figure 22. The closest example to this type of water found in the Cascade Range is at Mount Baker where increased fumarolic discharge in 1975 was accompanied by a pronounced

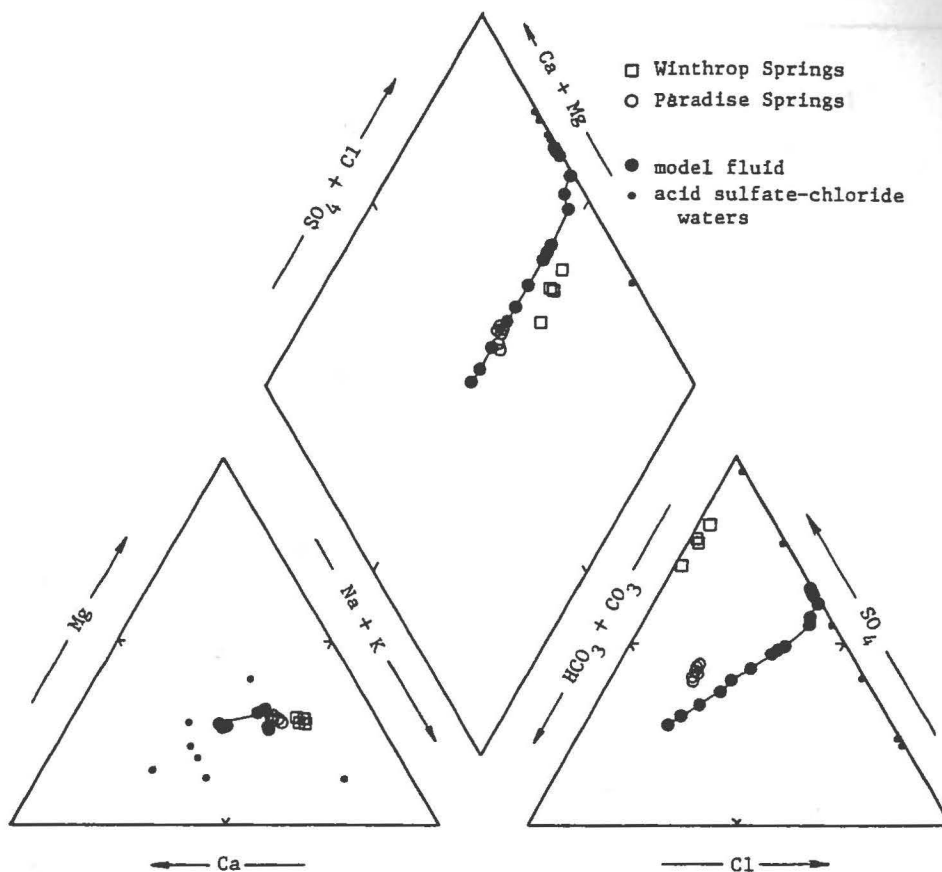


Figure 22. Trilinear diagram of percentage equivalents of major ions in acid sulfate-chloride waters, in thermal springs at Mount Rainier, and in model fluids. Winthrop and Paradise symbols are as in figure 12. A variety of acid sulfate-chloride waters from localities listed in table 25 are shown by small dots. Tie lines connect points (large dots) in the mass transfer simulation.

Table 25. Localities of high-magnesium, acid sulfate-chloride waters shown in figure 22.

LOCALITY	TEMP	PH	SO ₄ /CL	REF ¹
Arayu spring, Onikobe caldera, Honshu, Japan	70	2.0	7.7	4
Copahue volcano, crater lake, Argentina	20		4.8	3
Kawah Ijen volcano, crater lake, Java			2.5	3
Kipyashcheye crater lake, Golovnin volcano, Kunashir	35	2.6	.53	5
Lower Mendeleev volcano, spring, Kunashir		1.7	2.1	3
Mendeleev volcano, spring, Kunashir	82	1.8	.92	2
Ogama-Megama spring, Onikobe caldera, Honshu, Japan	97	2.4	.59	4
Osoreyama spring, Japan	72	2.2	.55	2
Ruapehu volcano, crater lake, New Zealand		1.2	1.2	1
Tamagawa spring, Japan	98	1.2	.41	2
Yakeyama volcano, spring Japan	88	.4	.42	3
Yan Ming Shan spring, Taiwan	81	1.6	2.5	3

¹References: 1-Ellis and Mahon (1977); 2-Weissberg and others (1979); 3-White and others (1963); 4-Yamada (1976); 5-Zotov (1967).

increase in the chloride content of an acid sulfate crater lake. A series of analyses for the lake and the creek which drained the lake basin from 1974 to 1981 (Frank, 1983, p. E21, and unpublished data) document an influx of chloride (fig. 23). Depression of the SO₄/Cl ratio in 1975 and

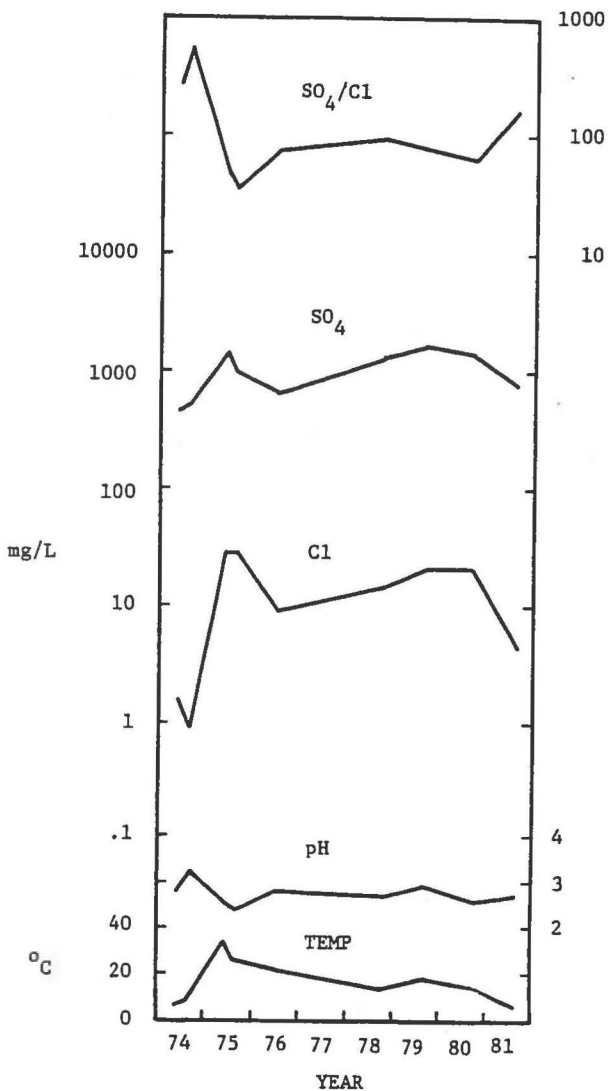


Figure 23. Selected characteristics of acid sulfate water at Sherman Crater, Mount Baker, from 1974 to 1981. An increase in chloride which accompanied the 1975 increase in heat emission indicates an influx of fluids from an underlying chloride-rich aquifer.

maintenance of relatively low values during the following five years imply a small but distinct contribution of fluids from an underlying chloride-rich aquifer. The result was formation of an acid sulfate-chloride lake, though with smaller chloride content than the examples listed in table 25.

To construct a parent water for simulation purposes at Mount Rainier, the 1975 crater lake composition at Mount Baker (table 26, A) was modified by addition of enough chloride to achieve a level consistent with that calculated for the unmixed Paradise end member (table 24). Cations were balanced primarily by sodium and a small amount of magnesium. Carbon dioxide, which was not analyzed in the initial acid water, was increased to the level in the Paradise end member (table 24). Through simulation calculations discussed below, the resulting modified water (table 26, B) was allowed to precipitate an alteration assemblage of alunite, pyrite, and chalcedony in equilibrium with a final parent water (table 26, C). The parent water is shown in figure 22 where its composition lies well within the range of the natural acid sulfate-chloride waters found at andesitic volcanoes elsewhere.

Table 26. Fluid compositions for mass-transfer simulation. Concentrations in mg/L, T in degrees Celsius, Eh in volts, IS-ionic strength.

	A ¹	B	C ²	D	E	F
	NATURAL ACID SULFATE- CHLORIDE WATER	MODIFIED ACID SULFATE-CHLORIDE WATER	PARENT WATER--B EQUILIBRATED WITH ALTERATION MINERALS	C REACTED WITH ANDESITE TO ZI=.056	D DILUTED WITH SHALLOW GROUND WATER, PS3, TO 24C	% DIFFERENCE BETWEEN E AND THERMAL SPRING, PS5
K	24	24	5	100	18	+6
Na	88	155	155	324	58	-27
Ca	130	130	130	180	32	-21
Mg	37	60	60	112	20	-29
Fe	38	38	18	.0019	5 x 10 ⁻¹²	<-100
Al	76	76	37	.012	5 x 10 ⁻⁴	<-90
Cl	28	450	450	450	79	+5
F	4.8	4.8	4.8	4.8	.83	+33
SO4	1300	1300	1140	812	144	-19
HCO3	0	0	.19	286	352	+22
CO3 TOT	ND	2700	2700	2690	508	-2
SiO2	220	220	132	132	10	-86
N	ND	.062	.062	.062	.024	-20
PH	2.5	2.5	2.3	5.5	5.4	
EH	ND	.20	.16	-.15	.48	
T	34	130	130	130	24	
IS	.053	.033	.031	.032	.008	

¹Sherman Crater lake, Mount Baker, June 6, 1975
(Frank, 1983, p. E21).

²Initial alteration minerals-kaolinite, alunite,
chalcedony, pyrite.

Reaction-Path Simulation

One scenario which might produce the lower-flank thermal springs would require neutralization of an acid sulfate-chloride parent water with subsequent cooling through dilution. This scenario was tested in a series of reaction-path simulations by which the parent water was allowed to react with andesite in a closed system. Upon reaching an appropriate point in reaction progress the solution was withdrawn from the andesite and diluted with a water having the composition of a Paradise cold spring. The reaction path simulates equilibration of an acid sulfate-chloride water with andesite in an aquifer in the upper part of the cone. No cooling occurs until the neutralized water reaches a region of mixing with cold groundwater. At this point cooling and mixing take place relatively quickly. During cooling the fluid physically moves away from the initial alteration assemblage and reequilibrates with a lower temperature assemblage.

The simulation first employs an ion-association chemical model to determine the distribution of aqueous species and the saturation state of the fluid with respect to a variety of minerals. A mass-transfer model based on methods of Helgeson (1968, 1979) is subsequently used to find the most stable assemblages of minerals which result

listed in table 26 and shown in figures 24-26. These figures are based on diagrams generated through plotting codes written for the EQ3/EQ6 package by Ghiorso (1981, unpublished). For the simulations the precipitation of quartz was suppressed because of the lack of observed macrocrystalline quartz in the alteration products at Mount Rainier; other studies (Arnorsson, 1975) in basic volcanic rocks indicate that silica solubility is likely controlled by phases other than quartz. The most common silica alteration phase at Mount Rainier is chalcedony.

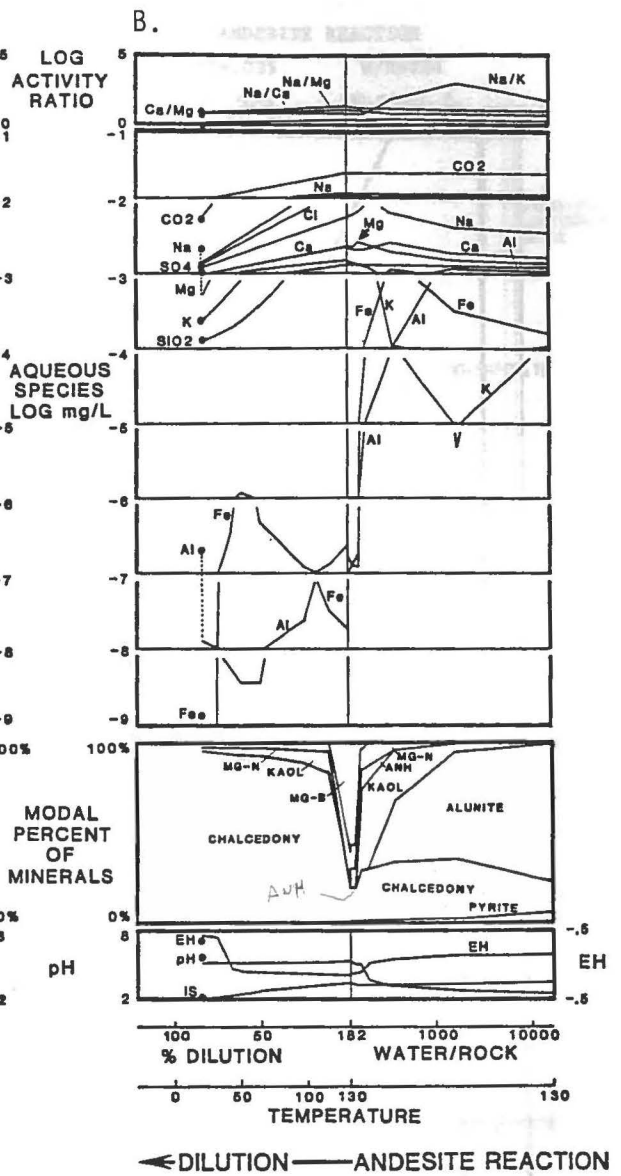
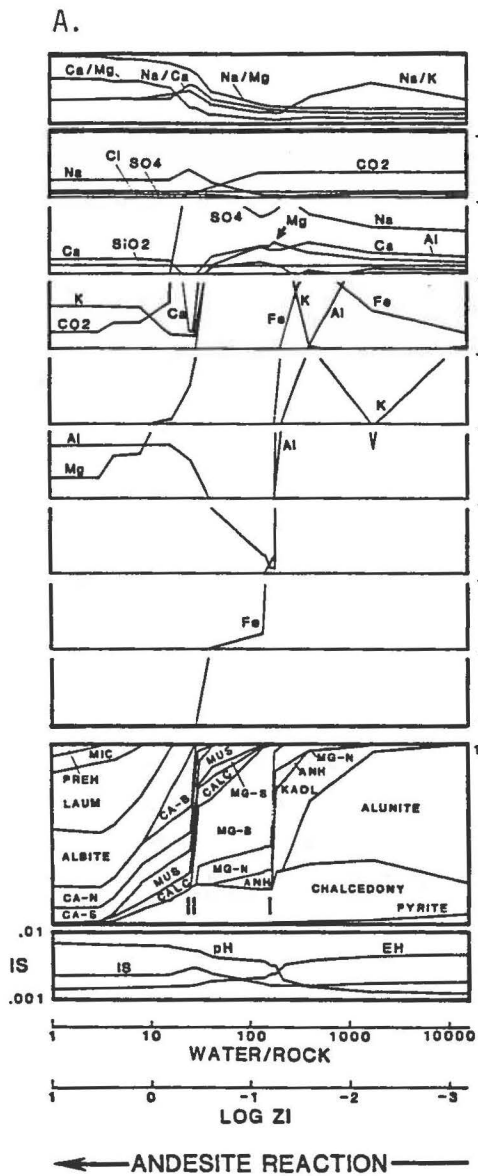
Upon initial equilibration of the 130⁰ C acid sulfate-chloride water, the solution precipitates a typical acid-alteration assemblage of alunite, chalcedony, and pyrite (fig. 24A). Reaction with andesite in a closed system in which precipitated minerals are allowed to redissolve is simulated by titration of the equilibrated solution with a glass composition equivalent to summit andesite (Fiske and others, 1963, p. 87). In figure 24A reaction progress proceeds from right to left as indicated by the decrease in water/rock ratio, W/R, from infinity to 10. With reaction the alteration assemblage goes through two major changes (I and II, fig. 24A) as the aqueous solution is neutralized. Three relatively uniform assemblages may be characterized in turn as regions of acid clay, near neutral clay, and alkaline zeolite (fig. 24A).

Figure 24. Variation in modal mineral and fluid composition during mass transfer simulation. See text for explanation. Mineral code: AB-albite, AH-anhydrite, AL-alunite, CA-calcite, CH-chalcedony, CB-ca-beidellite, CN-ca-nontronite, CS-ca-saponite, K-kaolinite, LA-laumontite, MB-mg-beidellite, MI-microcline, MN-mg-nontronite, MS-mg-saponite, MU-muscovite, PR-prehnite, PY-pyrite.

24A. Simulation of the reaction between acid sulfate-chloride water and andesite. Reaction proceeds from right to left and passes through acid-clay assemblage, reequilibration I, near-neutral clay assemblage, reequilibration II, and alkaline zeolite assemblage.

24B. Simulation of acid sulfate-chloride water that is reacted with andesite to a ZI of .056. At this point (vertical line) the resulting magnesium-rich (see arrow), near-neutral water is diluted with cold shallow ground water. Reaction proceeds from right to left.

Large dots represent composition of Paradise thermal spring, PS5, for comparison.



10-A1293-1020 system at simulation.

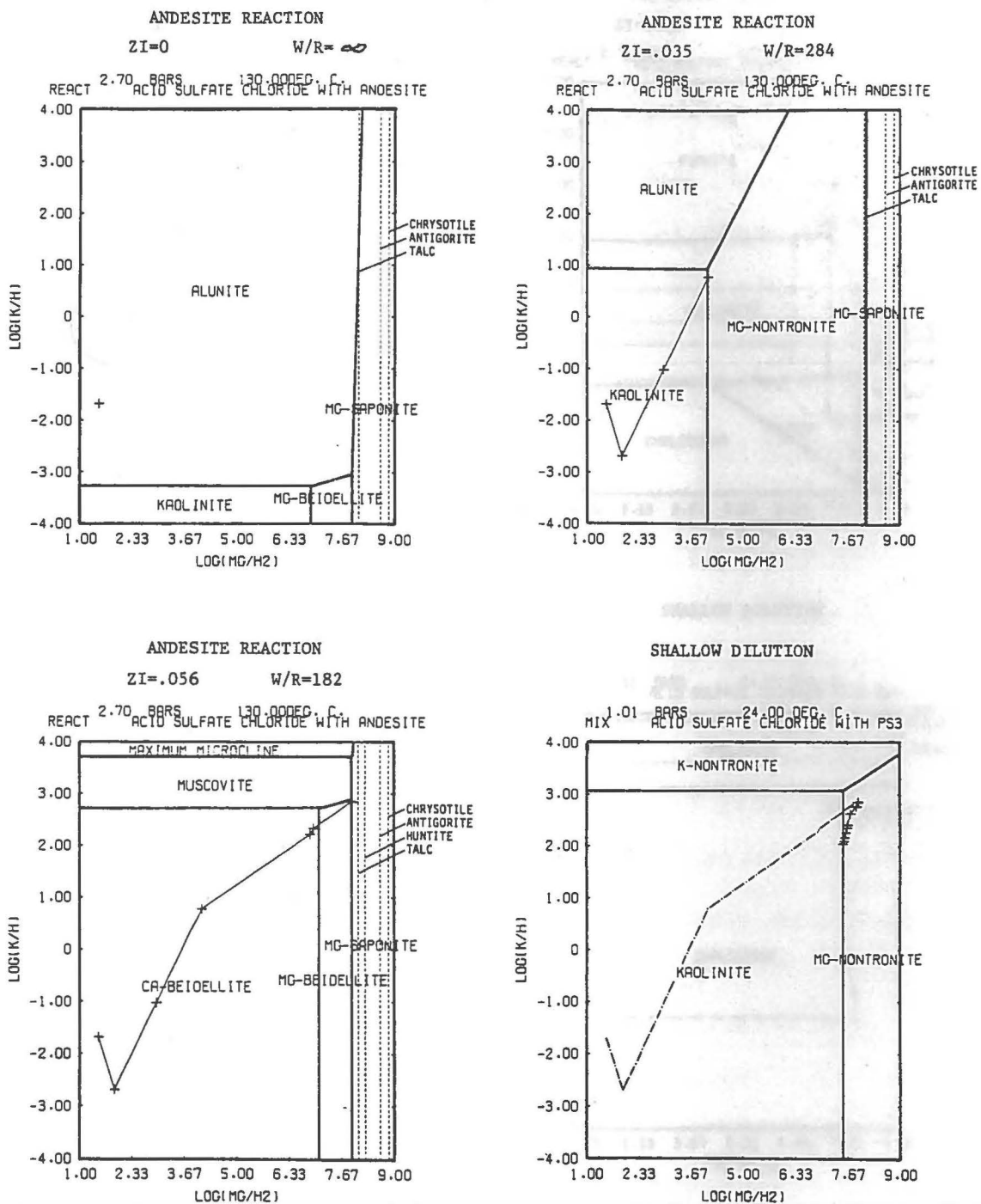


Figure 25. Activity diagram of K₂O-MgO-Al₂O₃-H₂O system at four points in the mass-transfer simulation.

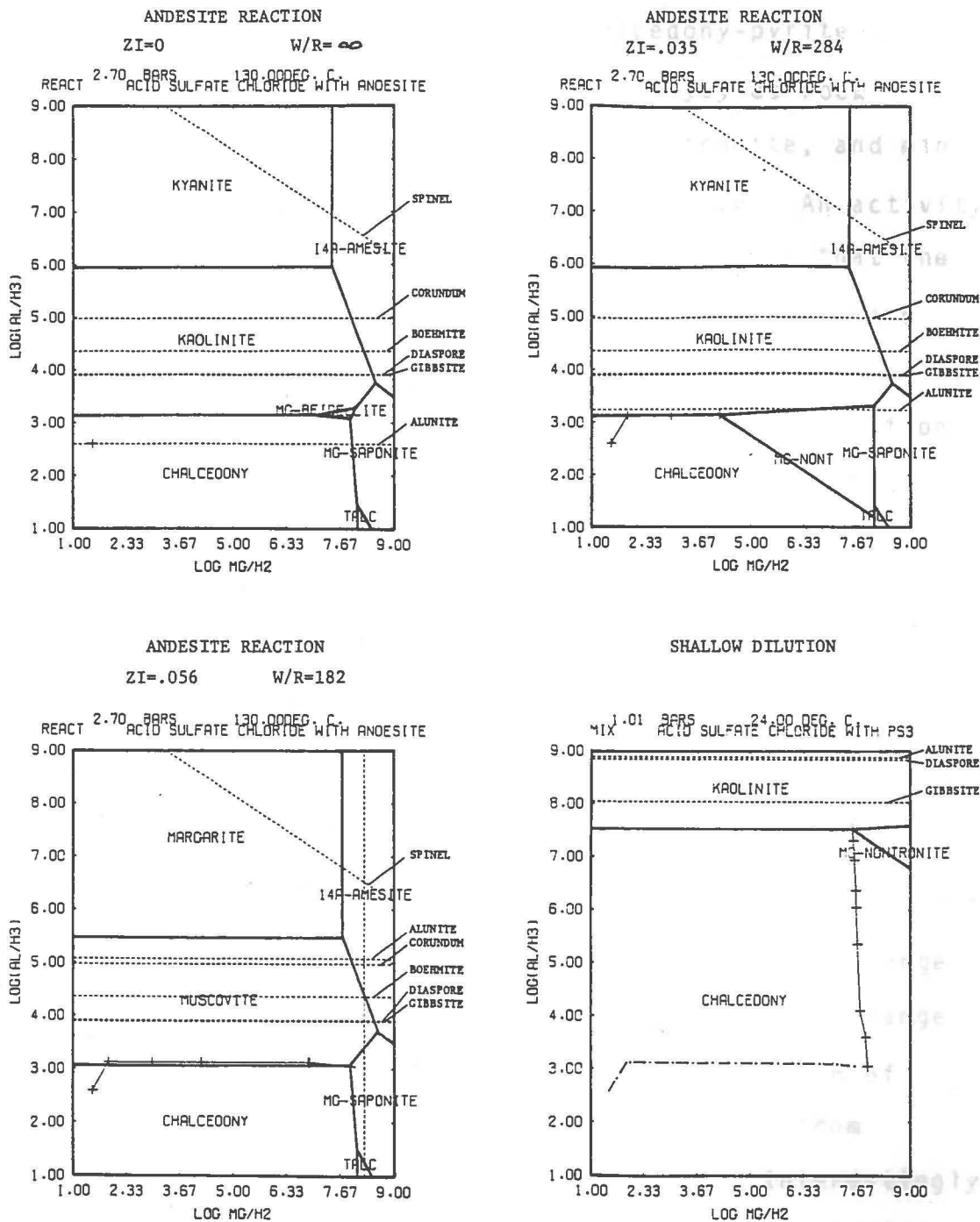


Figure 26. Activity diagram of $Al_2O_3-MgO-SiO_2-H_2O$ system at four points in the mass-transfer simulation.

At first the initial alunite-chalcedony-pyrite assemblage becomes progressively more clayey as rock dissolution occurs, and kaolinite, Mg-nontronite, and minor anhydrite are added down to a W/R of about 280. An activity diagram of $\log (K/H) - \log (Mg/H_2)$ (fig. 25) shows that the initial solution composition immediately plunges toward kaolinite saturation and then follows the kaolinite-alunite-Mg-nontronite junction as rock reaction proceeds. An activity diagram of $\log (Al/H_3) - \log (Mg/H_2)$ (fig. 26) illustrates that chalcedony controls silica activity throughout the simulation. With slowly rising pH and incorporation of aluminum into phyllosilicates, alunite dissolves and releases sulfur which is then available for anhydrite (fig. 24A).

Major features of the acid-clay region (fig. 24A) are high concentrations of all cations except potassium which is tied up in alunite. As the first major assemblage change approaches (I in fig. 24A), cation concentrations change dramatically. Potassium increases from dissolution of alunite, iron and aluminum plunge to low values from incorporation into nontronite and kaolinite. Interestingly, magnesium, the exchangeable cation in nontronite, continues to increase in concentration.

The first major assemblage change occurs at a W/R of

210 where the solution suddenly reequilibrates from an acid clay-rich assemblage to a more neutral clay-rich assemblage (fig. 24A) of a variety of smectites, chalcedony, calcite, minor anhydrite, and trace pyrite. At this point pH rises to a nearly neutral (at 130^o C) value of 5.5, both alunite and kaolinite have unsaturated, and solution composition closely follows smectite phase boundaries: first Mg-nontronite, then Mg-beidellite, and finally Mg-saponite.

The near-neutral solution has very low aluminum and iron, as these elements have entered into phyllosilicates. Although major cations remain abundant in solution, all but sodium peak in this region and slowly begin to decrease: calcium decreases after saturation with anhydrite and then calcite, magnesium after saturation with Mg-saponite, and potassium after saturation with muscovite. As the second major assemblage change (II in fig. 24A) is approached, iron continues to be incorporated into nontronite, dissolved aluminum begins to increase with slow beidellite dissolution and other major cations except sodium slowly decrease in concentration.

At the second major assemblage change at W/R of 35, the solution suddenly reequilibrates from the near-neutral Mg-rich clay assemblage to a slightly alkaline zeolite-Na-K-feldspar assemblage with Mg- and Ca-smectites.

With incorporation into alteration products after the second assemblage change, all cation concentrations drop including finally sodium after saturation of albite. Hydrogen enters into hydrated phases allowing pH to rise to 7.2 while carbon dioxide is incorporated into minor amounts of calcite.

The alkaline zeolite assemblage with laumontite and prehnite is maintained through a W/R of .001 and may be considered the final equilibrium assemblage under conditions of deep circulation or low permeability. Interestingly this assemblage has formed in the Tertiary calc-alkaline flows and volcanoclastic deposits of the Ohanapecosh Formation which underlies Mount Rainier (Fiske and others, p. 32-36). The zeolite assemblage has not been found, however, in hydrothermally altered deposits from Mount Rainier, indicating that W/R ratios are maintained above 34 and that hydrothermal fluids which feed Paradise springs do not circulate deeply. On the other hand, alunite, kaolinite, and both di- and tri-octahedral smectites are major observed alteration phases and suggest that reaction progress through the acid clay and into the nearly neutral clay assemblage is consistent with actual mineralogical observations.

For the purpose of simulating the formation of the lower-flank thermal springs, reaction with andesite is halted upon reaching the neutral smectite assemblage and

saturation with calcite at a W/R of 182 or reaction-progress value (ZI) of .056; that is after .056 moles of andesite have reacted with 1 kg of solution. At this point, magnesium concentration in the fluid has just peaked and pH has reached a plateau of 5.5. Figures 24B and 25-26 show the remainder of the simulation in which the fluid is withdrawn from the nearly neutral clay assemblage and diluted with Paradise cold-spring water along a linear mixing line from 130 to 24° C.

At 130° the cooling assemblage consists of chalcedony, Mg-beidellite, kaolinite, minor Mg-nontronite, and trace pyrite; anhydrite remains unsaturated. With cooling to 114° and 12% dilution, Mg-beidellite undersaturates. The remainder of the cooling process is dominated by chalcedony with minor kaolinite, nontronite, and trace pyrite; the latter undersaturates at 51° and 62% dilution.

Most cation concentrations decrease during the cooling process and pH remains at 5.4-5.5. Aluminum bottoms at 51° after which the amount of aluminum in the diluent exceeds that incorporated into kaolinite. Iron rises as pyrite decreases, but at the limit of pyrite saturation iron is reincorporated into nontronite and the concentration of aqueous iron again plunges. The final assemblage at 24° is chalcedony with trace kaolinite and Mg-nontronite. Activity

diagrams (fig. 25-26) show that with dilution, water composition simply follows the nontronite-kaolinite phase boundary. Throughout the simulation, both during andesite reaction and during mixing, silica is buffered by chalcedony saturation.

Figure 24B compares the composition of the final simulated solution with that actually observed at the main Paradise Spring, PS5. Final model compositions are within 30% of observed concentrations except for aluminum, iron, and silica. Gross differences in these constituents between simulated and observed water at 24⁰ might result from lack of equilibration with kaolinite, nontronite, and chalcedony at low temperature because of slow reaction rates, or perhaps from the absence of more appropriate low-temperature minerals in the thermodynamic data base. For example chalcedony should be replaced by amorphous silica as a metastably equilibrated silica phase at low temperature. The Paradise spring, PS5, is just at amorphous silica saturation at 24⁰ C and opal-A occurs as a rock coating downstream from the spring orifice. Furthermore, Fe-rich smectite formation at low temperature may be retarded by precipitation of amorphous ferric hydroxides. The presence or absence of these metastable phases, however, does not affect any other major cation concentration.

Although the model solution is somewhat more acidic and dilute than that actually observed, ratios of major cation activities are quite close (fig. 24B). The simulation is successful in demonstrating that high magnesium, low temperature thermal springs can be produced from a 130^o aquifer, and that the aquifer fluid can be derived from reaction between acid sulfate-chloride water and andesite. Minor differences between simulated and actual composition at 24^o may be reduced by optimizing the original composition of the acid sulfate-chloride water and the degree of mixing during cooling, and by incorporating appropriate metastable phases into the thermodynamic data base for the cooling reaction.

The simulation not only predicts in a general way the thermal-spring composition but it also produces equilibrium assemblages of minerals that are observed in Holocene deposits, primarily the acid clay assemblage of alunite, chalcedony, kaolinite, and pyrite, and the nearly neutral clay assemblage of smectites, chalcedony, and pyrite. Anhydrite, however, has not been found, though gypsum occurs in some deposits. The affinity for anhydrite supersaturation in the model solution at the point where cooling begins (fig. 24B) is only about 500 J/mol indicating that uncertainties in the thermodynamic data may be underestimating anhydrite solubility.

Use of clay minerals in a mass-transfer model might be considered questionable since the thermodynamic data for these minerals, particularly smectites, are not generally agreed upon and may be in error. Nonetheless, smectites are one of the main observed phases in the Mount Rainier system ^{and} need to be taken into account. The modified Tardy and Garrels (1974) approach of Wolery (1978) is considered here to be adequate since the results are consistent with observation. In this approach simple end-member smectite compositions are used. Alternative approaches, such as the site-mixing models of Aagaard and Helgeson (1983), are much more difficult to incorporate into the equilibrium calculations. Furthermore, the mixing models may be inappropriate for some clays in which physical mixtures predominate over solid solutions (Garrels, 1984). The chemical compositions of smectites in the deposits examined are unknown, but X-ray diffraction results show dioctahedral phases to be more common than trioctahedral phases. This relationship is consistent with the model results whereby dioctahedral beidellites and nontronites predominate over the trioctahedral saponites at large values of W/R.

As in any mass-transfer simulation, the results indicate one possible reaction path. If the selection of equilibrium phases is correct, the path presented is a

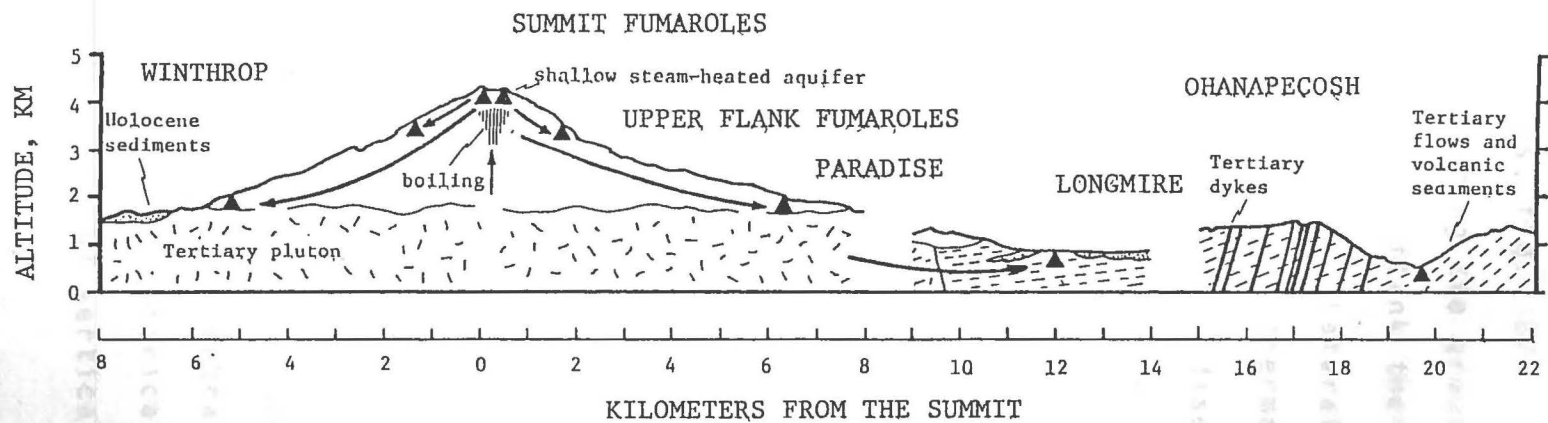
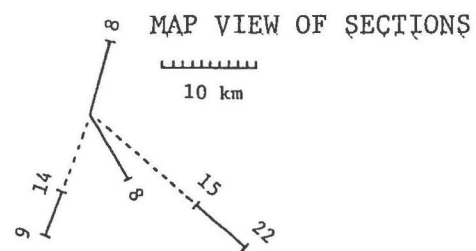
thermodynamically valid path controlled by irreversible processes. Other paths could lead to the same end result. An example that would not require andesite reaction would be oxidation and neutralization of an acidic water as a result of boiling accompanied by H_2S discharge. This would seem at first to be a geologically reasonable process, however preliminary thermodynamic calculations indicate that neutralization by removal of a reduced gas would require the presence of inordinately large amounts of a reducible mineral such as hematite or nontronite in the acid-clay assemblage.

Flow Path

Combining the simulation results with previous constraints on the characteristics of Mount Rainier's hydrothermal system allows derivation of a conceptual flow-path model as shown in figure 27. A narrow, central zone of upflowing thermal fluids, mainly hot gases (thin arrows, fig. 27), boils shallow ground water in the upper part of the cone. Condensation of steam, oxidation and hydrolysis of H_2S , and mixing with shallow recharge above the boiling zone forms a perched acid-sulfate aquifer which feeds fumaroles at the summit. Similar processes may also feed thermal activity at Sunset Amphitheater. Lateral

Figure 27. Schematic diagram of flow paths that feed flank thermal areas. Heated gas-rich fluids rise through a narrow central region of the cone and form a shallow steam-heated aquifer containing condensed gases within the upper kilometer of the cone. Secondary boiling of this water feeds fumaroles at summit. Lateral flow of gas-depleted fluids and secondary boiling feeds fumaroles on the upper flank. Lateral flow and mixing with cold shallow ground water feeds springs on the lower flank. Sulfate-chloride springs on the lower flank at Paradise have a greater input from a deeper part of the boiling zone than chloride-depleted springs at Winthrop. Chloride-rich springs at Longmire resemble the unmixed end member for Paradise and may have a similar origin but deeper flow path which allows it to surface with little appreciable shallow mixing. Chloride-rich water at Ohanapecosh probably circulates along a fracture zone beneath or to the east of the Ohanapecosh valley and originates in an aquifer at a somewhat higher temperature than the other waters.





percolation of heated water (thick arrows, fig. 27), accompanied by secondary boiling upon nearing the ground surface in headwalls, feeds most other upper flank thermal areas including that at Disappointment Cleaver. Lateral transport of heated water at deeper levels feeds thermal springs on the lower flank (fig. 27). Those at Paradise have a moderate SO_4/Cl ratio and probably are derived from through condensation near the lower part of the boiling zone. Springs at Winthrop have high SO_4/Cl and likely originate near the upper part of the boiling zone.

General Discussion

The present hydrothermal system at Mount Rainier is characterized by moderate discharge at the summit of CO_2 -enriched, slightly acidic fluid from a shallow, steam-heated boiling aquifer of snowmelt, by lesser lateral leakage of steam-heated fluids on the upper flank, and by sparse lateral leakage of neutral SO_4 -enriched, low-temperature thermal waters on the lower flank. Some 80% of the excess heat discharge occurs through the central vent, and only minor changes in the level of historical activity indicate that no effective sealing of vertical permeability has occurred.

Present heat flow of 700 W/m^2 may be compared with the thermal equivalent of the young summit cone. If one uses an average heat content and density of andesite of 1500 J/g and 2200 kg/m^3 , the cooling of the summit cone over a 1200 year period would produce 150 MW of excess heat. Discharged over the area of the summit craters, this represents a heat flow of 770 W/m^2 , comparable to present excess heat flow through the summit fumarole field. Since heat discharge from cooling lava flows should decrease with time, present heat flow clearly requires a source other than the young summit cone.

Lateral discharge on the upper flank, though not abundant in comparison to the summit activity, is much more widespread than analogous upper-flank activity on any other Cascade Range volcano. Transport paths of steam-heated fluids within the top of Mount Rainier's hydrothermal system are not confined to a central vent, but spread laterally about 2 km. The high degree of headwall erosion into the upper cone may facilitate leakage of these fluids.

The lateral extent of the hydrothermal system below the upper flank is limited as suggested by the minor discharge of SO_4 -enriched fluids. Geochemical simulation suggests that the few waters of this type that do occur may be derived by lateral transport from an acid sulfate-chloride

aquifer in the upper part of the cone. All thermal-fluid discharges appear to be greatly affected by contamination with shallow cold groundwater.

The Cl-enriched thermal water that discharges beyond the base of the volcano (fig. 27) at Longmire could conceivably originate in deeper parts of Mount Rainier's hydrothermal system, below the zone of boiling. Such a process is apparently envisioned in linking several of the scattered Cl-rich or CO₂-rich springs here and elsewhere in the Cascade Range to nearby stratovolcanoes (Korosec, 1980, 1983). The concept of Henley and Ellis (1983) for volcanic hydrothermal systems in areas of high relief and the quantitative model of Sorey and Ingebritsen (1984) for springs south of Lassen Volcanic National Park both call upon long lateral transport from beneath upflowing vapor-dominated reservoirs as the source for distant Cl-rich thermal springs. The composition of Longmire Springs (fig. 11) bears similarities to the unmixed end member for Paradise springs (fig. 21), especially in cations. Longmire Springs may have a source similar in temperature and composition but deeper than that for Paradise springs, with the notable difference that less mixing has occurred at Longmire. In any case, Longmire Springs are fed by fluids which have undergone appreciable transport through Tertiary rocks beneath Mount Rainier.

No compelling reason, however, has been found here to call upon long lateral transport as a source of thermal waters at Ohanapecosh Springs. On the contrary numerous Tertiary dykes (fig. 27) west of Ohanapecosh (Fiske and others, 1963) and the steep dip of strata beneath the springs suggest that the Ohanapecosh Springs could more easily be fed by a local, perhaps fault-controlled, hydrothermal system spatially separate from Mount Rainier. A combination of very little mixing and moderately high geothermometer temperatures for Ohanapecosh Springs (table 18) supports a local source. Nevertheless the chloride-enriched thermal water at Ohanapecosh, though not necessarily originating at Mount Rainier, may have some similarities in composition to deep water which now underlies the volcano.

Hazard Implications

The hydrothermal system within Mount Rainier formed clayey alteration products at depth 5000 years ago. The hydrothermally formed minerals, particularly the smectite, disordered kaolinite/halloysite, alunite assemblage in early to mid-Holocene deposits, are typical acid alteration products commonly found within the upper kilometer of active

hydrothermal systems. Trace amounts of clay minerals more common to somewhat deeper, hotter parts, such as well-ordered kaolinite, illite, and pyrophyllite, further indicate deep, acid alteration during the mid-Holocene. Large masses of similar material are now forming at the summit to an unknown depth, and exist in the headwall of Sunset Amphitheater. Thermal springs leaking today from the lower flank of Mount Rainier suggest that acidic fluids underlie these deposits and continue to produce deep, clayey alteration products.

Mount Rainier has a history of frequent, large destructive avalanches and mudflows. Typically, those which contain hydrothermally altered material have been the largest. The summit and Sunset Amphitheater areas are therefore potential sources for particularly hazardous avalanches, provided that appropriate slip surfaces and triggering mechanisms are also available.

Potential slip surfaces for debris avalanches are already in place at Mount Rainier. On the upper flank of the cone rubble zones within or between outward-dipping flowage deposits provide not only structurally weak surfaces but also permeable paths for fluid transport. If hydrothermal alteration produces clay minerals along these paths, rock stability can be further diminished. An extreme condition

might occur in the upper, central part of the cone in a crater basin where surficial clay formation may develop and then be buried by subsequent eruptive deposits. For example, extensive surficial alteration likely occurred in a basin at the summit during the 3000-year period between the time of the Osceola Mudflow and the formation of the young summit cone. If so, the summit cone now sits in a caldera analogous to a greased bowl. Furthermore, the bowl is likely open to the north, judging from the northward distribution of the Osceola and the northerly position of the summit cone.

Potential triggering mechanisms for avalanches include earthquakes, eruptions, or steam explosions. Steam explosions are common in hydrothermal systems when transport paths are temporarily plugged by mineral deposition, or when overburden pressures are suddenly reduced. In the case of Mount Rainier, any of the active fumarole areas could produce steam explosions. Thermal areas on the upper flank are particularly susceptible to sudden reduction of lithostatic pressures as a result of normal erosive processes that allow small, piece-meal rock avalanches. A small avalanche followed by a steam explosion could conceivably yield a much larger avalanche and produce deposits like those found in the Holocene record. The several localities of flank thermal activity make such

events possible on every side of Mount Rainier.

position
II.
mixing

ter

no. 2.

planetary

New
411 p.

[The

283 p.,

BIBLIOGRAPHY

- Stevanova, U.S. D.C., 1958, 25
- factors affecting 18, U.S. D.C., 1958, 25
- Seattle, University of Washington, 1977 p.
- Stulver, M., 1981, Oxygen isotope ratios and mean annual temperature and precipitation, *Journal of Climate*, v. 21, p. 1417-1419.
- Aagaard, Per and Helgeson, H.C., 1983, Activity/composition relations among silicates and aqueous solutions. II. Chemical and thermodynamic consequences of ideal mixing of atoms on homological sites in montmorillonites, illites, and mixed layer clays: *Clays and Clay Minerals*, v. 31, no. 3, p. 207-217.
- Arnórsson, S. 1975, Application of the silica geothermometer in low temperature hydrothermal areas in Iceland: *American Journal of Science*, v. 275, p. 763-784.
- Barry, R.G., 1981, *Mountain weather and climate*: London, Methuen and Company, 313 p.
- Bethel, J.P., 1982, An investigation of the primary and secondary mineralogy of a sequence of glacial outwash terraces along the Cowlitz River, Lewis County, Washington: Seattle, University of Washington M.S. thesis, 90 p.
- Brindley, G.W., 1980, Chapter 2. Order-disorder in clay mineral structures in Brindley, G.W. and Brown, G. (eds.), *Crystal structures of clay minerals and their X-ray identification*: Mineralogical Society Monograph no. 5, p. 125-195.
- Brindley, G.W. and Brown, G. (eds.), 1980, *Crystal structures of clay minerals and their X-ray identification*: Mineralogical Society Monograph no. 5, 495 p.
- Browne, P.R.L., 1978, Hydrothermal alteration in active geothermal fields: *Annual Review of Earth and Planetary Sciences*, v. 6, p. 229-250.
- Brunt, David, 1934, *Physical and dynamical meteorology*: New York, Cambridge, At the University Press, 411 p.
- Budyko, M.I., 1956, Teplovoi balans zemnoi poverkhnosti [The heat balance of the earth's surface]: *Hydrometeorological Press, Leningrad*, 255 p., Science.

- Translated by N. A. Stepanova, U.S. Department of Commerce, Washington D.C., 1958, 259 p.
- Burk, R.L., 1979, Factors affecting $^{18}\text{O}/^{16}\text{O}$ ratios in cellulose: Seattle, University of Washington, Ph.D. dissertation, 127 p.
- Burk, R.L. and Stuiver, M., 1981, Oxygen isotope ratios in trees reflect mean annual temperature and humidity: *Science*, v. 211, p. 1417-1419.
- Butcher, S.S. and Charlson, R.J., 1972, An introduction to air chemistry: New York, Academic Press, 241 p.
- Campbell, K.V., Miers, J.H., Nichols, B.M., Oliphant, Jerrelyn, Pytlek, Shirley, Race, R.W., Shaw, G.H., and Gresens, R.L., 1970, A survey of thermal springs in Washington State: *Northwest Science*, v. 44, no. 1, p. 1-11.
- Carmichael, I.S.E., 1970, Chemical analysis of silicate rocks: Berkeley, unpublished manual, 34 p.
- Carroll, Dorothy, 1970, Clay minerals: a guide to their X-ray identification: Geological Society of America Special Publication 126, 80 p.
- Casadevall, T.J., Cruz-Reyna, S.D.L., Rose, W.I., Jr., Bagley, Susan, Finnegan, D.L., and Zoller, W.H., 1984, Crater lake and post-eruption hydrothermal activity, El Chichon volcano, Mexico: *Journal of Volcanology and Geothermal Research*, v. 23, p. 169-191.
- Colman, S.M., 1982, Chemical weathering of basalts and andesites: evidence from weathering rinds: U.S. Geological Survey Professional Paper 1246, 51 p.
- Condie, K.C. and Swenson, D.H., 1974, Compositional variation in three Cascade volcanoes: Jefferson, Rainier, and Shasta: *Bulletin Volcanologique*, v. 37, no. 2, p. 205-230.
- Coombs, H.A., 1936, The geology of Mount Rainier National Park: University of Washington Publications in Geology, v. 3, no. 2, p. 131-212.
- Craig, Harmon, 1961a, Isotopic variations in meteoric waters: *Science*, v. 133, no. 3465, p. 1702-1703.
- Craig, Harmon, 1961b, Standard for reporting concentrations of deuterium and oxygen-18 in natural waters: *Science*,

v. 133, no. 3467, p. 1833-1834.

- Craig, Harmon, 1963, The isotopic geochemistry of water and carbon in geothermal areas in Tongiorgi, E. (ed.), Nuclear geology on geothermal areas - Spoleto, 1963: Pisa, Consiglio Nazionale Delle Ricerche, Laboratorio di Geologia Nucleare, p. 17-53.
- Crandell, D.R., 1963a, Paradise debris flow at Mount Rainier, Washington: U.S. Geological Survey Professional Paper 475-B, p. B135-B139.
- Crandell, D.R., 1963b, Surficial geology and geomorphology of the Lake Tapps quadrangle, Washington: U.S. Geological Survey Professional Paper 388-A, 84 p.
- Crandell, D.R., 1969, Surficial geology of Mount Rainier National Park, Washington: U.S. Geological Survey Bulletin 1288, 41 p.
- Crandell, D.R., 1971, Postglacial lahars from Mount Rainier volcano, Washington: U.S. Geological Survey Professional Paper 677, 73 p.
- Crandell, D.R. and Fahnestock, R.K., 1965, Rockfalls and avalanches from Little Tahoma Peak on Mount Rainier, Washington: U.S. Geological Survey Bulletin 1221-A, 30 p.
- Crandell, D.R. and Miller, 1974, Quaternary stratigraphy and extent of glaciation in the Mount Rainier region: U.S. Geological Survey Professional Paper 847, 59 p.
- Crosson, R.S., 1972, Small earthquakes, structure, and tectonics of the Puget Sound region: Bulletin of the Seismological Society of America, v. 62, no. 5, p. 1133-1171.
- Crosson, R.S. and Frank, D., 1975, The Mt. Rainier earthquake of July 18, 1973, and its tectonic significance: Bulletin of the Seismological Society of America, v. 65, no. 2, p. 393-401.
- Crosson, R.S. and Lin, J.-W., 1975, A note on the Mt. Rainier earthquake of April 20, 1974: Bulletin of the Seismological Society of America, v. 65, no. 2, p. 549-556.
- Danes, Z.F., 1965, A new steam vent on Mt. Rainier, Washington: Journal of Geophysical Research, v. 70, no. 8, p. 2003.

- Dansgaard, W., Johnsen, S.J., Clausen, H.B., and Gundestrup, N., 1973, Stable isotope glaciology: Meddeleser Om Gronland, v. 197, no. 2, p. 1-53.
- Daniels, D.L., 1968, Integrated 8-14 μ emissivities of rocks from Mono Craters region in Friedman, J.D., Thermal anomalies and geologic features of the Mono Lake area, California, as revealed by infrared imagery: National Aeronautics and Space Administration Technical Letter 82, 84 p.
- Ellis, A.J. and Mahon, W.A.J., 1977, Chemistry and geothermal systems: New York, Academic Press, 392 p.
- Ellis, A.J. and Wilson, S.H., 1961, Hot spring areas with acid-sulfate-chloride waters: Nature, v. 191, no. 4789, p. 696-697.
- Evans, Llewellyn, 1930, Preliminary studies of the Nisqually, Paradise, and Stevens Glaciers, Mount Tacoma-Rainier National Park: Tacoma, City Light of Tacoma.
- Fiske, R.S., Hopson, C.A., and Waters, A.C., 1963, Geology of Mount Rainier National Park, Washington: U.S. Geological Survey Professional Paper 444, p. 93.
- Flett, J.B., 1912, The thermal caves: The Mountaineer, v. 5, p. 58-60.
- Fontes, J. Ch., 1980, Environmental isotopes in groundwater hydrology in Fritz, P. and Fontes, J. Ch. (eds.), Handbook of environmental isotope geochemistry: Amsterdam, Elsevier Scientific Publishing Company, p. 75-140.
- Fouillac, C. and Michard, G., 1981, Sodium/lithium ratio in water applied to geothermometry of geothermal reservoirs: Geothermics, v. 10, p. 55-70.
- Fournier, R.O., 1981, Application of water geochemistry to geothermal exploration and reservoir engineering in Muffler, L.J.P. and Rybach, L. (eds.), Geothermal systems: principles and case histories: Chichester, John Wiley and Sons, p. 109-143.
- Frank, D., 1983, Origin, distribution, and rapid removal of hydrothermally formed clay at Mount Baker, Washington: U.S. Geological Survey Professional Paper 1022-E, 31 p.

- Frank, D. and Friedman, J.D., 1974, Newly detected infrared anomalies at Mount Rainier, Washington (abs.) in Symposium on applications of satellite and airplane remote sensing of natural resources in the Pacific Northwest, Tumwater, Washington, May 2, 1974: Washington Department of Natural Resources, p. 22
- Friedman, Irving and O'Neil, J.R., 1977, Chapter KK. Compilation of stable isotope fractionation factors of geochemical interest in Fleischer, Michael (ed.), Data of geochemistry, sixth edition: U.S. Geological Survey Professional Paper 440-KK, 12 p., 49 fig.
- Friedman, Irving and Smith, G.I., 1970, Deuterium content of snow cores from Sierra Nevada area: Science, v. 169, p. 467-470.
- Friedman, J.D. and Frank, D., 1977, Heat discharge from Mount St. Helens, Washington: U.S. Geological Survey Open-File Report 77-541, 29 p.
- Friedman, J.D. and Frank, D., 1978, Thermal surveillance of active volcanoes using Landsat-1 Data Collection System: Part 4, Lassen volcanic region: National Technical Information Services, NTIS N78 23499/LL, 46 p.
- Friedman, J.D. and Frank, D., 1980, Infrared surveys, radiant flux, and total heat discharge at Mount Baker volcano, Washington, between 1970 and 1975: U.S. Geological Survey Professional Paper 1022-D, 33 p.
- Friedman, J.D., Frank, D., and Kieffer, H.H., 1981, Thermal infrared surveys of the May 18 crater, subsequent lava domes, and associated volcanic deposits in Lipman, P.W. and Mullineaux, D.R., The 1980 eruptions of Mount St. Helens, Washington: U.S. Geological Survey Professional Paper 1250, p. 279-293.
- Friedman, J.D., Frank, D.G., Preble, Duane, and Painter, J.E., 1973, Thermal surveillance of Cascade Range volcanoes using ERTS-1 multispectral scanner, aircraft imaging systems, and ground-based data communication platforms in Symposium on significant results from the Earth Resources Technology Satellite-1, New Carrollton, Maryland, March 5-9, 1973: NASA SP-327, p. 1549-1560.
- Friedman, J.D., Williams, D.L., and Frank, D., 1982, Structural and heat-flow implications of infrared anomalies at Mount Hood, Oregon, 1972-1977: Journal of

- Geophysical Research, v. 87, no. B4, p. 2793-2803.
- Garrels, R.M., 1984, Montmorillonite/illite stability diagrams: Clays and Clay Minerals, v. 32, no. 3, p. 161-166.
- Giggenbach, W.F. and Stewart, M.K., 1982, Processes controlling the isotopic composition of steam and water discharges from steam vents and steam-heated pools in geothermal areas: Geothermics, v. 11, no. 2, p. 71-80.
- Haines, A.L., 1962, Mountain fever, historic conquests of Rainier: Portland, Oregon Historical Society, 255 p.
- Helgeson, H.C., 1968, Evaluation of irreversible reactions in geochemical processes involving minerals and aqueous solutions-I. Thermodynamic relations: Geochimica Cosmochimica Acta, v. 32, p. 853-877.
- Helgeson, H.C., 1979, Mass transfer among minerals and hydrothermal solutions in Barnes, H.L. (ed.), Geochemistry of hydrothermal ore deposits: New York, John Wiley and Sons, p. 568-610.
- Helgeson, H.C., Delaney, J.M., Nesbitt, H.W., and Bird, D.K., 1978, Summary and critique of the thermodynamic properties of the rock forming minerals: American Journal of Science, v. 278A, 229 p.
- Helgeson, H.C. and Kirkham, D.H., 1974a, Theoretical prediction of the thermodynamic behaviour of aqueous electrolytes at high pressures and temperatures: I. Summary of the thermodynamic/electrostatic properties of the solvent: American Journal of Science, v. 274, p. 1089-1198.
- Helgeson, H.C. and Kirkham, D.H., 1974b, Theoretical prediction of the thermodynamic behaviour of aqueous electrolytes at high pressures and temperatures: II. Debye-Huckel parameters for activity coefficients and relative partial molal properties: American Journal of Science, v. 274, p. 1199-1261.
- Helgeson, H.C. and Kirkham, D.H., 1976, Theoretical prediction of the thermodynamic properties of aqueous electrolytes at high pressures and temperatures: III. Equation of state for aqueous species at infinite dilution: American Journal of Science, v. 276, p. 97-240.

- Hemley, J.J., Hostetler, P.B., Gude, A.J., and Mountjoy, W.T., 1969, Some stability relations of alunite: *Economic Geology*, v. 64, p. 599-612.
- Henley, R.W. and Ellis, A.J., 1983, Geothermal systems: ancient and modern: a geochemical review: *Earth-Science Reviews*, v. 19, p. 1-50.
- Hoblitt, R.P., Crandell, D.R., and Mullineaux, D.R., 1980, Mount St. Helens eruptive behaviour during the past 1,500 years: *Geology*, v. 8, no. 11, p. 555-559.
- Hodge, S.M., 1972, The movement and basal sliding of the Nisqually Glacier, Mount Rainier: Seattle, University of Washington Ph.D. dissertation, 409 p.
- Ingraham, E.S., 1895, The Pacific Forest Reserve and Mt. Rainier: Seattle, The Calvert Company, 48 p.
- Jackson, M.L., 1969, Soil chemical analysis - advanced course: published by the author, Department of Soil Science, University of Wisconsin, Madison, 2nd edition, 8th printing, 895 p.
- Jones, J.B. and Segnit, E.R., 1971, The nature of opal. I. Nomenclature and constituent phases: *Geological Society of Australia Journal*, v. 18, pt. 1, p. 57-67.
- Kharaka, Y.K., Specht, D.J., and Carothers, W.W., 1985, Low to intermediate subsurface temperatures calculated by chemical geothermometry (abs.): *AAPG Bulletin*, v. 69, no. 2, p. 273.
- Kieffer, H.H., Frank, D., and Friedman, J.D., 1981, Thermal infrared surveys at Mount St. Helens - observations prior to the eruption of May 18 in Lipman, P.W. and Mullineaux, D.R. (eds.), *The 1980 eruptions of Mount St. Helens*, Washington: U.S. Geological Survey Professional Paper 1250, p. 257-277.
- Kieffer, H.H., Frank, D., and Friedman, J.D., 1982, Calibrated airborne thermal infrared survey of the Cascade Range volcanoes (abs.): *Proceedings, International Association of Volcanology and Chemistry of the Earth's Interior (IAVCEI)*, Reykjavik, August 1982.
- Kittrick, J.A. and Hope, E.W., 1963, A procedure for the particle-size separation of soils for X-ray diffraction analysis: *Soil Science*, v. 96, p. 319-325.

- Kiver, E.P. and Mumma, M.D., 1971, Summit firn caves, Mount Rainier, Washington: *Science*, v. 173, p. 320-322.
- Kiver, E.P. and Steele, W.K., 1972, Summit firn cave research, August 1971, Mount Rainier Nat. Pk., Wash. (abs.): *Geological Society of America Abstracts with Programs*, v. 4, no. 6, p. 385.
- Kiyosu, Yasuhiro and Kurahashi, Makoto, 1983, Origin of sulfur species in acid sulfate-chloride thermal waters, northeastern Japan: *Geochimica et Cosmochimica Acta*, v. 47, p. 1237-1245.
- Korosec, M.A., 1980, IV. Thermal and mineral spring investigations (surveys and analyses, 1978-1979) in Korosec, M.A. and Schuster, J.E., The 1979-1980 geothermal resource assessment program in Washington: Washington Department of Natural Resources Open File Report 81-3, p. 42-92.
- Korosec, M.A., 1983, 11. Geothermal resource targets: progress and proposals in Korosec, M.A., Phillips, W.M., and Schuster, J.E., The 1980-1982 geothermal resource assessment program in Washington: Washington Department of Natural Resources Open File Report 83-7, p. 268-293.
- Lange, I.M. and Avent, J.C., 1973, Ground-based thermal infrared surveys as an aid in predicting volcanic eruptions in the Cascade Range: *Science*, v. 182, p. 279-281.
- Lange, I.M. and Avent, J.C., 1975, Ground-based thermal infrared surveys of Mount Rainier volcano, Washington: *Bulletin Volcanologique*, v. 38, no. 4, p. 929-943.
- LeDrew, E.F., 1975a, The energy balance of a mid-latitude alpine site during the growing season, 1973: *Arctic and Alpine Research*, v. 7, no. 4, p. 301-314.
- LeDrew, E.F., 1975b, The estimation of clear sky atmospheric emittance at high altitudes: *Arctic and Alpine Research*, v. 7, no. 3, p. 227-236.
- Lokey, W.M., 1973, Crater studies at a sleeping volcano: *Explorers Journal*, v. 51, no. 3, p. 167-170.
- Lokey, W.M., Mack, R., Miller, M.M., Prather, B.W., and Kiver, E.P., 1972, Project Crater: Mt. Rainier glacio-volcanological research, 1970-72 (abs.): *Arctic and Mountain Environments Symposium*, Michigan State

- University, April 22-28, 1972.
- Majors, H.M., 1962, The springs of Lassen Volcanic National Park, Mount Rainier National Park, and Olympic National Park: Seattle, March, 1962, unpublished, 88 p.
- Majors, H.M. and McCollum, R.C. (eds.), 1981a, First winter expedition to Mount Rainier, 1894: Northwest Discovery, v. 2, no. 7, p. 406-465.
- Majors, H.M. and McCollum, R.C. (eds.), 1981b, Mount Rainier, the tephra eruption of 1894: Northwest Discovery, v. 2, no. 6, p. 334-381.
- Mariner, R.H., Presser, T.S., and Evans, W.C., 1982, Chemical and isotopic composition of water from thermal and mineral springs of Washington: U.S. Geological Survey Open-File Report 82-0098, 20 p.
- Mattinson, J.M., 1977, Emplacement history of the Tatoosh volcanic-plutonic complex, Washington: ages of zircons: Geological Society of America Bulletin, v. 88, p. 1509-1514.
- Mazor, E. and Wasserburg, G.J., 1965, Helium, neon, argon, krypton and xenon in gas emanations from Lassen Volcanic and Jellystone National Parks: Geochimica et Cosmochimica Acta, v. 29, p. 443-454.
- McClatchey, R.A., Fenn, R.W., Selby, J.E.A., Volz, F.E., and Garry, J.S., 1972, Optical properties of the atmosphere (third edition): Air Force Cambridge Research Laboratories, AFCRL-72-0497, Environmental Research Paper No. 411, 110 p.
- Miller, M.M., 1970, Wind, sky, and ice: Explorers Journal, v. 48, no. 3, p. 192-197.
- Minikami, T., 1960, Fundamental research for predicting volcanic eruption: Part 1: Bulletin of the Earthquake Research Institute, v. 38, p. 497-544.
- Molenaar, Dee, 1979, The challenge of Rainier: Seattle, The Mountaineers, 364 p.
- Moser, H. and Stichler, W., 1970, Deuterium measurements on snow samples from the Alps in Isotope hydrology: Vienna, IAEA (International Atomic Energy Agency), p. 43-57.
- Moxham, R.M., 1970, Thermal features at volcanoes in the

- Cascade Range, as observed by aerial infrared surveys: Bulletin Volcanologique, v. 34, no. 1, p. 77-106.
- Moxham, R.M., 1972, Thermal surveillance of volcanoes in The surveillance and prediction of volcanic activity: Paris, UNESCO, p. 103-124.
- Moxham, R.M., Boynton, G.R., and Cote, C.E., 1972, Satellite telemetry of fumarole temperatures, Mount Rainier, Washington: Bulletin Volcanologique, v. 36, no. 1, p. 191-199.
- Moxham, R.M., Crandell, D.R., and Marlatt, W.E., 1965, Thermal features at Mount Rainier, Washington, as revealed by infrared surveys: U.S. Geological Survey Professional Paper 525-D, p. D93-D100.
- Mullineaux, D.R., 1974, Pumice and other pyroclastic deposits in Mount Rainier National Park, Washington: U.S. Geological Survey Bulletin 1326, 83 p.
- Mullineaux, D.R., Sigafos, R.S., and Hendricks, E.L., 1969, A historic eruption of Mount Rainier, Washington in Geological Survey research 1969: U.S. Geological Survey Professional Paper 650-B, p. B15-B18.
- National Climatic Center, 1972, Northern hemisphere data tabulations, November 1972 (microfilm): Asheville, National Oceanographic and Atmospheric Administration, Environmental Data Service.
- National Climatic Center, 1983, Monthly normals of temperature, precipitation, and heating and cooling degree days, 1951-1980 (Washington): Asheville, National Oceanographic and Atmospheric Administration, National Climatic Center.
- Nehring, N.L., Mariner, R.H., White, L.D., Heubner, M.A., Roberts, E.D., Harmon, Karen, Bowen, P.A., and Tanner, Lane, 1979, Sulfate geothermometry of thermal waters in the western United States: U.S. Geological Survey Open-File Report 79-1135, 11 p.
- Nehring, N.L., Wollenberg, H.A., and Johnston, D.A., 1981, Gas analyses of fumaroles from Mt. Hood, Oregon: U.S. Geological Survey Open-File Report 81-236, 9 p.
- Pevear, D.R., Dethier, D.P., and Frank, D., 1982, Clay minerals in the 1980 deposits from Mount St. Helens: Clays and Clay Minerals, v. 30, no. 4, p. 241-252.

- Ozima, Minoru and Podosek, F.A., 1983, Noble gas geochemistry: Cambridge, Cambridge University Press, 367 p.
- Piper, A.M., 1944, A graphic procedure in the geochemical interpretation of water analyses: Transactions of the American Geophysical Union, v. 25, p. 914-923.
- Porter, S.C., 1977, Present and past glaciation threshold in the Cascade Range, Washington, U.S.A.: topographic and climatic controls, and paleoclimatic implications: Journal of Glaciology, v. 18, no. 78, p. 101-116.
- Rasmussen, Norman, 1967, Washington State earthquakes, 1840 through 1865: Bulletin of the Seismological Society of America, v. 57, no. 3, p. 463-476.
- Richardson, Donald, 1968, Glacier outburst floods in the Pacific Northwest: U.S. Geological Survey Professional Paper 600-D, p. D79-D86.
- Riddihough, R.P., 1977, A model for recent plate interactions off Canada's west coast: Canadian Journal of Earth Science, v. 14, p. 383-396.
- Riddihough, R.P. and Hyndman, R.D., 1976, Canada's active west margin - the case for subduction: Geoscience Canada, v. 3, no. 4, p. 269-278.
- Robin, G. de Q., 1983, The climatic record of polar ice sheets: Cambridge, Cambridge University Press, 212 p.
- Russell, I.C., 1898, Glaciers of Mount Rainier: U.S. Geological Survey 18th Annual Report, 1896-97, pt. 2, p. 349-415.
- Saunders, P.M., 1970, Correction for airborne radiation thermometry: Journal of Geophysical Research, v. 75, no. 36, p. 7596-7601.
- Schoen, Robert, White, D.E., and Hemley, J.J., 1974, Argillization by descending acid at Steamboat Springs, Nevada: Clays and Clay Minerals, v. 22, p. 1-22.
- Sekioka, Mitsuru and Yuhara, Kozo, 1974, Heat flux estimation in geothermal areas based on the heat balance of the ground surface: Journal of Geophysical Research, v. 79, no. 14, p. 2053-2058.
- Sellers, W.D., 1965, Physical Climatology: Chicago, University of Chicago Press, 272 p.

- Sharp, R.P., Epstein, Samuel, and Vidizianas, Irene, 1960, Oxygen isotope ratios in the Blue Glacier, Olympic Mountains, Washington, U.S.A.: *Journal of Geophysical Research*, v. 65, no. 12, p. 4043-4059.
- Skougstad, M.W., Fishman, M.J., Friedman, L.C., Erdmann, D.E., and Duncan, S.S. (eds.), 1979, Methods for and determination of inorganic substances in water and fluvial sediments: U.S. Geological Survey Techniques of Water-Resources Investigations, TWRI Book 5, Chapter A1, 626 p.
- Sorey, M.L. and Ingebritsen, S.E., 1984, Quantitative analysis of the hydrothermal system in Lassen Volcanic National Park and Lassen Known Geothermal Resource Area: U.S. Geological Survey Water Resources Investigations Report 84-4278, 80 p.
- Stearns, N.D., Stearns, H.T., and Waring, G.A., 1937, Thermal springs in the United States: U.S. Geological Survey Water-Supply Paper 679-B, 206 p.
- Stevens, Hazard, 1876, The ascent of Mount Tahoma: *Atlantic Monthly*, Nov., p. 511-530.
- Sumi, Kiyoshi, 1969, Zonal distribution of clay minerals in the Matsukawa geothermal area, Japan: *International Clay Conference, Tokyo, Proceedings*, v. 1, p. 501-512.
- Tardy, Y. and Garrels, R.M., 1974, A method of estimating the Gibbs energies of formation of layer silicates: *Geochimica Cosmochimica Acta*, v. 38, p. 1101-1116.
- Truesdell, A.H. and Hulston, 1980, Isotopic evidence on environments of geothermal systems in Fritz, P. and Fontes, J. Ch. (eds.), *Handbook of environmental isotope geochemistry*: Amsterdam, Elsevier Scientific Publishing Company, p. 178-226.
- Unger, J.D. and Decker, R.W., 1970, The microearthquake activity of Mt. Rainier, Washington: *Bulletin of the Seismological Society of America*, v. 60, no. 6, p. 2023-2035.
- Unger, J.D. and Mills, K.F., 1972, Microearthquakes at Mt. Rainier - 1969: *Bulletin of the Seismological Society of America*, v. 62, p. 1079-1081.
- Weaver, C.S. and Malone, S.D., 1976, Mt. St. Helens seismic

- events: volcanic earthquakes or glacial noises?:
Geophysical Research Letters, v. 3, p. 197-200.
- Weaver, C.S. and Malone, S.D., 1979, Seismic evidence for discrete glacier motion at the rock-ice interface: Journal of Glaciology, v. 23, no. 89, p. 171-184.
- Weaver, C.S. and Smith, S.W., 1983, Regional tectonic and earthquake hazard implications of a crustal fault zone in southwestern Washington: Journal of Geophysical Research, v. 88, no. B12, p. 10371-10383.
- Weissberg, B.G., Browne, P.R.L., and Seward, T.M., 1979, Ore metals in active geothermal systems in Barnes, H.L., Geochemistry of hydrothermal ore deposits: New York, John Wiley and Sons, p. 738-780.
- White, D.C., 1959, The titrimetric micro determination of sulphate using lead nitrate as titrant and dithizone as indicator: Mikrochimica Acta, v. 2, p. 254-269.
- White, D.C., 1960, A note on the micro determination of sulphate using lead nitrate as titrant and dithizone as indicator: Mikrochimica Acta, v. 2, p. 282-285.
- White, D.E., 1957, Thermal waters of volcanic origin: Geological Society of America Bulletin, v. 68, p. 1637-1657.
- White, D.E., Muffler, L.J.P., and Truesdell, A.H., 1971, Vapor-dominated hydrothermal systems compared with hot-water systems: Economic Geology, v. 66, no. 1, p. 75-97.
- White, D.E. and Waring, G.A., 1963, Chapter K. Volcanic emanations in Fleischer, Michael (ed.), Data of geochemistry: U.S. Geological Survey Professional Paper 440-K, 29 p.
- Wildrick, L.L., 1976, Geochemical equilibria in Pleistocene sediments of the southeast Puget Sound drainage basin: Seattle, University of Washington MS thesis, 77 p.
- Wolery, T.J., 1978, Some chemical aspects of hydrothermal processes at mid-oceanic ridges - a theoretical study. I. Basalt-sea water reaction and chemical cycling between the oceanic crust and the oceans. II. Calculation of chemical equilibrium between aqueous solutions and minerals: Evanston, Northwestern University, PhD dissertation, 263 p.

- Wolery, T.J., 1979, Calculation of chemical equilibrium between aqueous solution and minerals: the EQ3/6 software package: Lawrence Livermore Laboratory report UCRL-52658, 41 p.
- Wood, W.W., 1976, Guidelines for collection and field analysis of ground-water samples for selected unstable constituents: U.S. Geological Survey Techniques of Water-Resources Investigations, Book 1, Chapter D2, 24 p.
- Yamada, Eizo, 1976, Geological development of the Onikobe caldera and its hydrothermal system: Proceedings, 2nd Symposium on the Development and Use of Geothermal Resources, San Francisco, May 20-29, 1975, v. 1, p. 665-672.
- Yamasaki, T, Matsumoto, Y., and Hayashi, M., 1970, The geology and hydrothermal alterations of Otake geothermal area, Kujyo volcano group, Kyushu, Japan: Geothermics, special issue 2, v. 2, pt. 1, p. 197-207.
- Zachara, J.M., 1979, Clay genesis and alteration in two tephritic subalpine podzols of the Central Cascades, Washington: Seattle, University of Washington M.S. thesis, 81 p.
- Zotov, A.V., 1967, Recent formation of alunite in the Kipyashcheye ("Boiling") Crater Lake, Golovnin volcano, Kunashir Island: Akademiya Nauk Armyanskoy SSR Doklady, v. 174, p. 124-127.

VITA

David Gerard Frank

Born: September 14, 1947
Giessen, Germany

Education: Fayetteville High School, 1965
Fayetteville, North Carolina

B.S. in Geology, 1969
North Carolina State University
Raleigh, North Carolina

M.S. in Geological Sciences, 1977
University of Washington
Seattle, Washington

Ph.D. in Geological Sciences, 1985
University of Washington
Seattle, Washington